INVESTIGATION OF MICROWAVE ANTENNAS IN LOSSY MEDIA FOR MEDICAL APPLICATIONS

MICHAEL JOYSTON A JOSEPHRAJ FDO

PhD

2012

INVESTIGATION OF MICROWAVE ANTENNAS IN LOSSY MEDIA FOR MEDICAL APPLICATIONS

MICHAEL JOYSTON A JOSEPHRAJ FDO

A thesis submitted in partial fulfilment of the requirements of the University of Northumbria at Newcastle for the degree of Doctor of Philosophy

Research undertaken in the School of Computing, Engineering & Information Sciences

January 2012

Abstract

For several years, microwave engineers have dreamed of using non-ionising electromagnetic waves in medical imaging applications. The rate of evolution of microwave techniques for medical application has been immense and shows no signs of relenting. Since the limitations of X-ray mammography are well reported, alternative techniques using microwaves for breast cancer detection are developed. Some of these techniques have progressed to the point where positive clinical experience has emerged.

The most important factor in medical imaging applications is the ability of the system to work in different dielectric media. Microwave antennas, as one of the fundamental building blocks of microwave imaging systems, must be capable of working efficiently in these environments. Microwave antennas have been previously designed for use in medical applications, but the criterion for the design specifications has been narrowed down to a specific microwave imaging technique. At present, little investigation exists to support the general behaviour of microwave antennas in lossy media for medical applications and research in this field is empirical. This necessitates a requirement to address this knowledge gap.

To facilitate this, a novel mathematical model is developed to predict the characteristics of a Monopole. The new model reduces the computational time for predicting the antenna characteristics in comparison with the traditional integral equation method. The new technique has also been developed to take account of the conductivity property of the surrounding medium. This helps to predict the antenna fields and input impedance in

different dielectric media. Results are obtained in freespace and dielectric media of high & low conductivities. Practical verification has been performed, with comparisons made between the results obtained from the novel model, experimental results and simulation done in electromagnetic software.

The comparison shows the new model is valid and the study shows the different behaviour of the Monopole pattern with respect to the different dielectric media. In conclusion, this thesis addresses a major knowledge gap in the field of antenna behaviour in dielectric media. This research will enable microwave engineers in medical fields to comprehend the antenna characteristics in dielectric media and develop a more clinically viable system for medical applications.

Table of Contents

List of Figures

Acknowledgements

First and foremost, I would like to thank my Principle Supervisor Prof. David Smith for all of his time, energy and patience throughout the entirety of this research work. Without his support, valuable contributions and insights this work would not have been possible. I will be forever grateful and indebted to him.

I would also like to thank other members of the academic team at Northumbria University, especially Dr Krishna Busawon for being my second supervisor and tirelessly sharing his maths expertise with me and Dr. Michael Elsdon for offering support in times of need. Thanks must also go to Stephen Foti whose constant interest was always an encouragement and inspiration. I'm grateful to all the technicians who patiently helped me with everything I asked for.

Thank you to my co-researchers and for your unfaltering support and encouragement, I couldn't have done this without you. Thank you to my family and friends, who always took an interest in my work as well as providing a sometimes necessary rest from my work.

Last but not least, I need to thank my lovely wife Mel for her proof reading, for always being there for me, listening to me and trying to understand my work.

Most of all I thank God for giving me this opportunity and for guiding me through it. Without the perspective on this life he gives and hope and assurance for the next, these past few years would have been meaningless.

Declaration

I declare that the work contained in this thesis has not been submitted for any other award and that it is all my own work. I also confirm that this work fully acknowledges opinions, ideas and contributions from the work of others.

Name: Michael Joyston A Josephraj Fdo

Signature: 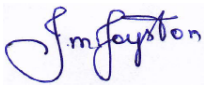

Date: 20.01.2012

Chapter 1 Introduction

1.1 Introduction

The use of microwaves for imaging purposes is currently receiving much attention for a variety of applications. The spectrum of applications for microwave imaging is highly diverse: terrestrial imaging [1], radio astronomy [2], antenna measurements systems [3], security imaging [4] and medical imaging [5] are some of the applications in which microwaves are currently employed. Depending on the nature of the source or target imaged, the microwave imaging system can be classified into two basic types: passive and active. An example of passive microwave imaging system is radio astronomy applications, in which the target is an energy source that generates and radiates energy in the microwave region, thereby avoiding the use of active transmitters [2]. Terrestrial and security imaging applications are examples of an active microwave imaging system, as they require active transmitters.

In radio astronomy, microwave radiation is received from cosmological sources using huge antenna arrays and produces images that display the distribution of sky brightness [6]. The different techniques used in radio astronomy are Radio Telescopes, Radio Interferometry [2], and Very Long Baseline Interferometry. Images obtained through these techniques possess much higher angular resolution and image quality compared to those of optical astronomy. In terrestrial imaging applications microwaves are used to collect pictures at long distance on or near the Earth surface[1]. The objective is to obtain images of

sufficient quality to determine the nature of the target, their relative positions, their deployment and targets may be counted. Different terrestrial imaging systems are Radio Camera[7], Synthetic Aperture Radar (SAR), Inverse Synthetic Aperture Radar (ISAR)[8] and Inverse Synthetic Radio Camera (ISRC)[1].

In the area of security the use of microwave and millimetre wave imaging systems offers the potential for providing a non-ionising technique capable of producing high quality images of concealed objects in a fast and inexpensive manner. One important security application is in security screening at transport terminals to detect concealed objects or weapons[9]. For safety reasons X-rays cannot be used for this application as they produce ionising radiation and hence microwave imaging methods are increasingly used[4]. In the antenna measurement area microwaves are used to determine antenna far field radiation pattern in a cost effective manner at the expense of the vector network analyser[10]. Microwave indirect holographic technique is used to predict antenna fields from intensity-only patterns, thereby allowing 3D images to be reconstructed from the measured 2D patterns[11].

In the medical area the ability of microwaves to penetrate to considerable depths beneath the skin in a non-ionising, safe manner coupled with the large differences in electrical properties between healthy and malignant tissues[12] has also stimulated much research interest. Detection of cancer tissue using microwave imaging is based on this contrast in electrical properties. The typical relative permittivities of normal and malignant tissues are 10 and 50 respectively, it is this difference in relative permittivity that is identified using microwaves[13]. A growing interest exists among medical engineers in microwave

imaging for breast cancer detection. The current golden standard for breast cancer detection is mammography, an X-ray based image of a compressed breast.

The main disadvantages of mammography are that the patients are exposed to ionisation and breast compression[14]. Microwaves do not have any ionisation properties, as their level of energy used is low compared to X-rays and hence this technology is ideal for breast imaging resulting in safer and more comfortable examination[15]. It is also less expensive than Magnetic Resonance Imaging (MRI) and Nuclear Medicine Methods. The advantage of the microwave imaging system is that the process is very rapid, sensitive and specific[13].

However, the microwave imaging technique for medical applications requires the whole microwave arrangement to be within a lossy medium in order to avoid reflections from the air-skin interface and thereby achieving greater depth of penetration[14]. When using microwaves in a lossy medium one of the important parameters which determines the suitability of any system is the antennas used in the imaging procedure[16]. This work aims to develop a novel mathematical model to predict the characteristics of a Monopole antenna taking account of the conductivity property of the surrounding medium.

1.2 Scope of Work and Contribution

'Synthetic Reference Beam Holography' is a patented technique developed at Northumbria University for 3D imaging of antenna fields [3, 10, 17, 18]. This technique allows the indirect holographic approach to be adapted at microwave frequencies. The basis of this

technique is that a planar offset radiated reference signal, which consists of a constant amplitude and linearly varying phase shift, can be synthesised electronically by applying a linear phase shift to a signal which is fed forward to be combined with the measured near field signal[3].

At each measurement position the complex near field is combined with the electronically synthesised reference wave and the resultant intensity is recorded at each position. The recorded intensity pattern is Fourier transformed and after eliminating the unwanted terms and centralising the required component the far field radiation pattern of the Antenna Under Test (AUT) can be determined[19]. Along with antenna radiation pattern measurements, this Novel Indirect Holographic Technique has been used in several other applications such as security screening for concealed weapons and plastic explosives[9, 20, 21], imaging of dielectric objects[19] and Microwave Medical Imaging, in particular breast tumour imaging [22, 23].

The experimental arrangement for medical imaging involves microwave components being immersed in lossy media to reduce the reflections at the air-skin interface. Initial results have shown that this technique is capable of locating a simulated tumour buried within a breast phantom[23]. The refinement of the results obtained through this technique and further advancement of this system towards viable clinical setup was severely challenged by the lossy media involved in the measurement system.

One of the major challenges facing the experimental arrangement is the characteristics of the microwave antenna employed. Because of the lossy media the microwave antenna

behaves differently when compared to operation in freespace environment. The challenges posed by the lossy media are detailed in the Chapter 2. Waveguide antennas were used for all the applications involving Indirect Holographic Technique at Northumbria University.

Microwave medical imaging groups around the world employ different types of antennas for their medical imaging system. Some of the antennas used are detailed in Chapter 2 along with their specifications. So far there hasn't been a comprehensive study of microwave antennas and their behaviour in different lossy media. This study aims to fill that knowledge gap in understanding the behaviour of microwave antenna in lossy media. For this research purpose the Monopole has been chosen and the study will involve comparing the input impedance and radiation pattern in freespace and also in different lossy media.

It is proposed here to develop a novel mathematical model for the calculation of Monopole fields theoretically. This new model is compared with a traditional approach involving Pocklington Integral Equation to check its validity and also to highlight its advantages. The new model relies on only three key quantities to predict the antenna characteristic which significantly reduces the computational time. The antenna behaviour is studied under different lossy media: low and high conductivity. Theoretical measurements are validated by measurements using Finite Difference Time Domain simulation and experimental results.

1.3 Aims and Objectives

The main aim of this research is to study the characteristics of a microwave antenna in different dielectric media which will enable microwave engineers in the medical field to comprehend the antenna characteristics in dielectric media and develop more clinically viable systems for medical applications. This main aim is expressed in terms of eight objectives to provide a structured approach to the research:

1. To develop a theoretical base for microwave antennas employed in medical imaging applications and the challenges faced in this area, by means of researching previous works and the current developments in these research areas: Chapter 2.

2. To follow a traditional approach to analytically calculate the radiation pattern and input impedance of a Monopole in freespace and study its limitations: Chapter 3.

3. To develop a novel mathematical model approach for the Monopole to calculate the antenna characteristics and to the compare the results for freespace with those for traditional approach as verification of the new approach: Chapter 3 and Chapter 4.

4. Experimental arrangement is setup to measure antenna characteristics in freespace and results obtained are compared with both traditional and Novel approach and also with the simulated data: Chapter 4.

5. The novel approach is extended to lossy media environment and antenna characteristics are calculated for different conductivity levels: Chapter 4.

6. To develop an experimental system for obtaining Monopole fields and impedances in lossy media including vegetable oil and water. Results obtained are compared with simulated values: Chapter 4.

7. To compare the results obtained using the novel approach for freespace and lossy media with results obtained in a traditional manner using Pocklington's integral equation: Chapter 4.

8. To critically analyse the results and study the effects of complex permittivities on microwave antennas and provide suggestions for improvements: Chapter 4 and Chapter 5.

1.4 Outline of Thesis

Chapter 2 – Presents an overview of medical imaging and the challenges faced by microwave antennas in medical imaging applications. This is followed by a review of the various microwave antennas currently used in medical imaging applications.

Chapter 3 – Pocklington's integral equation approach is used to calculate the Monopole characteristics. The complex integral equation is explained along the method of moment

technique. Methods involved in calculating the input impedance and radiation patterns of a Monopole using the Pocklington integral equation are also presented. The chapter also presents the limitations of this traditional approach. A novel mathematical model approach is adapted and analytical results of different lengths of antenna are presented. Advantages of the new model are also listed.

Chapter 4 – The new mathematical model is validated by comparing the results obtained by using it with the results from Tsai's [24]. Measurement parameters and an experimental design for freespace calculation for a Monopole are detailed, along with the theory to calculate the input impedance from the measured return loss values. S-Parameters, input impedance and radiation patterns of the Monopole in freespace are presented. Finite Difference Time Domain (FDTD) simulation software procedures are explained. The results obtained for input impedance and radiation patterns using simulation method are compared with the predicted results from the new mathematical model and with experimental results. The theory behind antenna characteristics in lossy media is presented. Experimental arrangements for lossy media measurements are discussed. Lossy media and their effects on Monopole characteristics are provided. Water and vegetable oil are the two lossy media considered. Results are measured through experimental procedure; simulation results are presented alongside data obtained from the analytical approach. Antenna characteristics such as radiation patterns, input impedance and return loss are compared and discussed.

Chapter 5 – Provides a summary of the conclusions that have been made during the course of the work and also presents ideas for the future development of the new model for

microwave antennas working under dielectric media. Also highlights some of the applications where the findings of this research can be employed directly.

1.5 Published Works

The following is a list of publications arising as a result of the work carried out in this thesis:

- D. Smith, M. Leach, M. Elsdon, **M. J. Fernando** and S. J. Foti, 'Imaging Of Dielectric Objects Reconstructed Using Indirect Holographic Intensity Patterns', 9th International Conference on Electromagnetics in Advanced Applications (ICEAA 05), pp401-404, Sept. 12-16, 2005, Torino, Italy

- **M. J. Fdo**, M. Elsdon, M. Leach, D. Smith, S.J. Foti, "Breast Cancer Detection using Microwave Holographic Imaging", Britain's Top Young Engineers Competition, House of Commons, London, December 2005.

- **M. J. Fdo**, M. Elsdon, M. Leach, D. Smith, S.J. Foti, "Early Breast Cancer Detection using Microwave Holographic Imaging", School of CEIS, Northumbria University, Research Forum, Poster Competition, January 2006.

- M. Elsdon, M. Leach, **M. J. Fdo**, S. J. Foti, D. Smith, "Early Stage Breast Cancer Detection using Indirect Microwave Holography" 9th European Microwave Week 2006 (EuMW2006), Manchester, UK, September 2006

- **M. J. Fdo**, M. Elsdon, M. Leach, S. J. Foti, D. Smith, "A Holographic Solution for Concealed Object Detection," The Mediterranean Journal of Computers and Networks (MJCN), Vol. 2, No. 4, pp 84-89, 2006

- D. Smith, M. Elsdon, M. Leach, **M. J. Fdo,** S. J. Foti , "Medical Imaging using a Microwave Indirect Holographic Technique," Mediterranean microwave Symposium(MMS) 2006- Genova, Italy

- D. Smith, M. Elsdon, M. Leach, **M. J. Fdo**, S. J. Foti, " 3D Microwave Imaging for Medical and Security Applications", International RF and Microwave Conference, Malaysia, Sept. 2006

- D. Smith, M. Elsdon, M. Leach, **M. J. Fdo**, S. J. Foti, "A Method for 3D Breast Cancer Imaging Using Microwave Holography", International Symposium on Antennas and Propagation, Singapore, November 2006

- D. Smith, M. Elsdon, M. Leach, **M. J. Fdo**, S. J. Foti, "A Microwave Indirect Holographic System for Security and Medical Imaging Applications", European Conference on Antennas and Propagation, France, November 2006

- M. Leach, S. Skobelev, M. Elsdon, **M. J. Fdo** and D. Smith, "A Modified Holographic Technique for Antenna Measurements and Object Imaging", International Symposium on Antennas and Propagation, Niigata, Japan, pp 77-80, 20th-24th August 2007

- M. Leach, S. Skobelev, M. Elsdon, **M. J. Fdo** and D. Smith, "An improved Holographic Technique for Medium Gain Antenna Near Field Measurements ",

European Conference on Antennas and Propagation, Edinburgh, Scotland UK, November 2007

- **M J Fernando**, K Busawon and D Smith, "A Novel Simplified Mathematical model for Antennas used in Medical Imaging Applications", Electrical Impedance and Electromagnetic Inverse Problems Conference Proceedings, Manchester, UK, June 2009

- **M Fernando,** K Busawon and D Smith, "Fundamental Issues with Antennas in Microwave Medical Imaging", 7th IEEE,IET International Symposium on Communication Systems , Networks and Digital Signal Processing, Newcastle, UK, July 2010

Chapter 2 Microwave Antennas and Medical Imaging Applications

2.1 Microwave Medical Imaging Overview

Microwave imaging for medical applications has been of interest for many years. In the last decade, microwave-based imaging techniques have shown potential as a viable and advantageous approach for many medical applications. Microwave images are maps of electrical property distributions in the body. The changes in electrical property indicate the differences in relative permittivity in the tissues and in other cases the changes are caused by disease[15].

Cancer detection using microwave imaging is based on this contrast in electrical properties. Recently, microwave imaging for breast cancer detection has gained attention due to advances in imaging algorithms, microwave hardware and computational power[12]. Microwave breast cancer detection is based on differences in electrical properties between healthy and malignant tissues at microwave frequencies[25, 26]. Breast cancer is a significant health issue for women and affects one in every seven women and early detection and timely medical intervention is the key to successful treatment, long-term survival and quality of life for patients[27].

Currently, X-ray mammography is the most effective detection technique, and women are encouraged to participate in breast cancer screening programs that involve regular

mammograms[28, 29]. A mammogram is the map of the densities of the breast, and has proven to be quite sensitive to the presence of lesions in the breast. According to the reports published on the X-ray mammography reviews by the U.S. Institute of Medicine (IOM)[29], the limitations of the mammography include missing up to 15% of breast cancers together with false negative rates ranging from 4% to 34%[30]. Mammography has a recall rate of 11%[31] and the diagnosis of suspicious lesions identified on mammograms often involves waiting for further imaging or biopsies. From a patient viewpoint, this modality also involves uncomfortable compression of the breast. X-rays are also ionising and this poses limitations on the frequency of screening[32].

The concerns related to mammography have generated interest in alternative approaches to breast imaging. The application of various medical imaging techniques to breast imaging has met with some success. One example is ultrasound, which uses acoustical impedance differences to create images[33]. Ultrasound has found success clinically to identify whether the lesion detected on a mammogram is a liquid cyst or a solid tumour, as well as in determining whether a lesion is located in or below the skin. Other applications include guided aspiration and biopsy; however ultrasound is not currently used as a screening technology[34].

Magnetic Resonance Imaging (MRI) is also used for diagnostic breast imaging. However MRI requires the use of contrast medium that is taken up differently by benign and malignant lesions[35], which results in complex image interpretation. MRI is useful for examining women with implants. However, it is expensive and is currently in the testing stage as a breast screening tool. Alternative imaging methods for detecting breast cancer have been proposed. The success of any medical imaging approach for reliable detection of

small malignant tumours hinges on the presence of a significant and consistent contrast between malignant and other breast tissues. This physical basis is present for methods relying on electromagnetic fields including microwave imaging[15].

Microwave imaging of breast tumours offers an alternate approach to mammography. X-rays detect density changes in tissue cells whilst microwaves detect changes in dielectric properties. Also, microwaves do not have any ionisation properties and hence this technology is ideal for breast imaging and could result in safer and more comfortable examinations[15]. It is also less expensive than MRI and nuclear medicine methods. The advantages of the microwave imaging system are that the process is very rapid, sensitive and specific. It has the ability to detect small tumours by measuring the difference in the electrical permittivity of malignant and normal tissues. The typical difference in the permittivity values between the normal and malignant tissues can range between 300% and 500% depending on the stage of the cancer cells[13].

Different techniques are employed by different microwave research groups around the world in the hope of developing an efficient tool for early breast cancer detection. The three different methods of microwave breast imaging methods are discussed briefly below.

1. *Passive Microwave Imaging*: Passive methods incorporate radiometers to measure temperature differences in the breast, detecting tumours based on their increased temperature compared to normal tissue. Microwave radiometry has been explored for breast cancer detection as an adjuvant to mammography[36-38]. Images display the temperature measured over a quadrant of the breast. Two examples of microwave radiometers are Oncoscan[38] and the system reported by S. Mouty et

al.[39]. Clinical results suggest that microwave radiometry has the potential to assist in the diagnosis of suspicious areas on mammograms.

2. *Hybrid Microwave - Acoustic Imaging*: Hybrid methods use microwave energy to select and rapidly heat tumours and ultrasound transducers to detect pressure waves generated by the expansion of the heated tissues. Hybrid microwave acoustic imaging uses microwaves to illuminate the breast. Due to higher conductivity of malignant breast tissue, more energy is deposited in tumours, resulting in selective heating of these lesions. The tumours expand and generate pressure waves which are detected by ultrasound transducers. Two methods of image reconstruction proposed are Computed Thermo-acoustic Tomography (CTT)[40, 41] and Scanning Thermo-acoustic Tomography (STT)[42, 43]. Clinical results have been obtained with CTT that show tissue structure in the breast. STT has successfully imaged phantoms and clearly indicates interfaces between materials.

3. *Active Microwave Imaging*: Active methods involve illuminating the breast with microwaves and then measuring transmitted or reflected microwave signals, and forming images with this data. Active microwave methods for breast imaging can be classified as tomography and radar based. In tomographic approaches maps of the electrical property distributions in the breast are created using sophisticated algorithms. It is a spatial based approach, which involves continuous waves. Several research groups are involved in tomographic approaches to imaging the breast. Meaney et al.[5, 14] at Dartmouth college are the only group currently to have successfully implemented a clinical prototype for active microwave imaging of the breast. Another example of active imaging using tomographic approaches is

the Microwave Holography technique[23, 44]. This approach has yielded successful initial results; more information on this particular system is given in Section 2.2. Radar based approaches for breast cancer detection work on the principle of identifying the location of strongly scattering objects, rather than plotting the distributions of electrical properties. It is a time based approach involving Microwave pulses. Hagness et al.[45] proposed the first radar based breast cancer detection in 1998. Since then two systems have been developed, Microwave Imaging via Space Time beamforming (MIST) by Hagness et al.[46, 47] in 2003 and Tissue Sensitive Adaptive Radar (TSAR) by Fear et al.[25, 48] also in 2003.

So far in this section the evolvement of microwave medical imaging for breast cancer detection has been presented along with the different imaging approaches. In the following section the initial research carried out as part of thesis is outlined. One of the active imaging approaches, the Microwave Holography technique, has been explained and results obtained for breast phantom and animal tissues are presented.

2.2 Initial Research & Outcome

Microwave Holography technique is a novel, inexpensive holographic technique used in the early detection of breast cancer. Synthetic Reference Beam Holography technique is the patent technology behind the Microwave Holography system. The patented technique enables the simple and inexpensive indirect holographic method, usually employed at optical frequencies, can be adapted to image breast tumours at microwave frequencies[18,

49]. Figure 2-1 shows the breast imaging system using the Microwave Holography system. The experimental setup, shown in Figure 2-2, emulates a system configuration where a patient is lying in a prone position[50] with transmit and receive antennas placed near the surface of the naturally flattened breast.

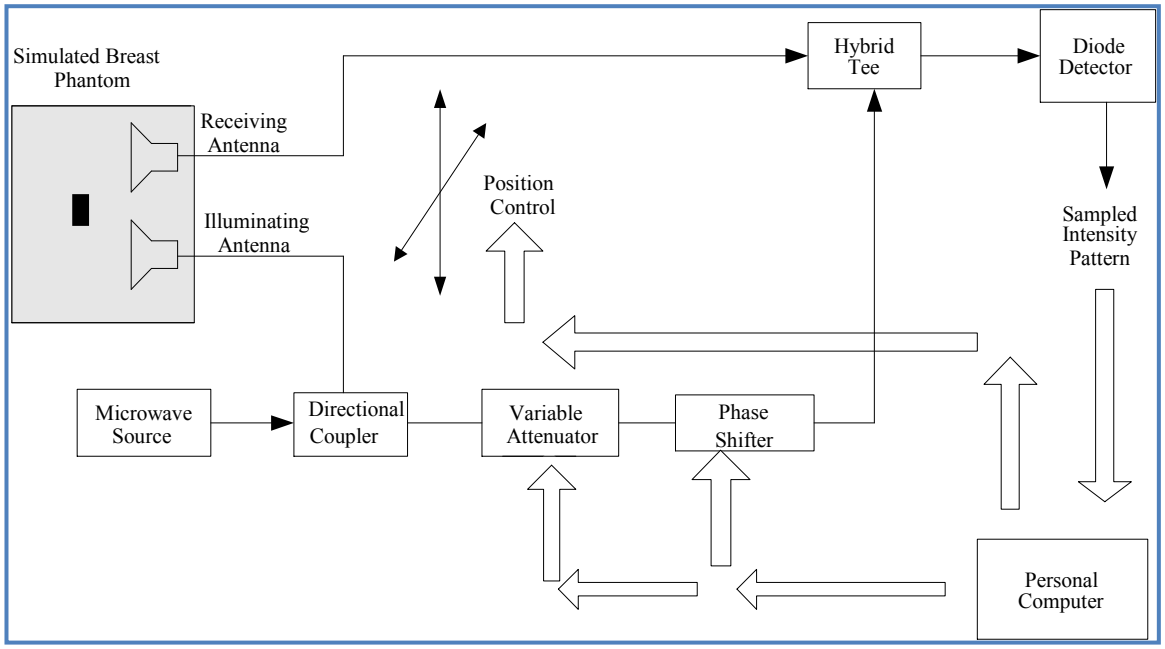

Figure 2-1 Breast Imaging System using Microwave Holography System

The breast phantom consists of a container filled with a liquid with similar properties to a normal tissue. To demonstrate the ability for the proposed system to distinguish between normal and malignant tumours, an object with a different dielectric constant to that of the liquid was also placed inside the phantom[51].

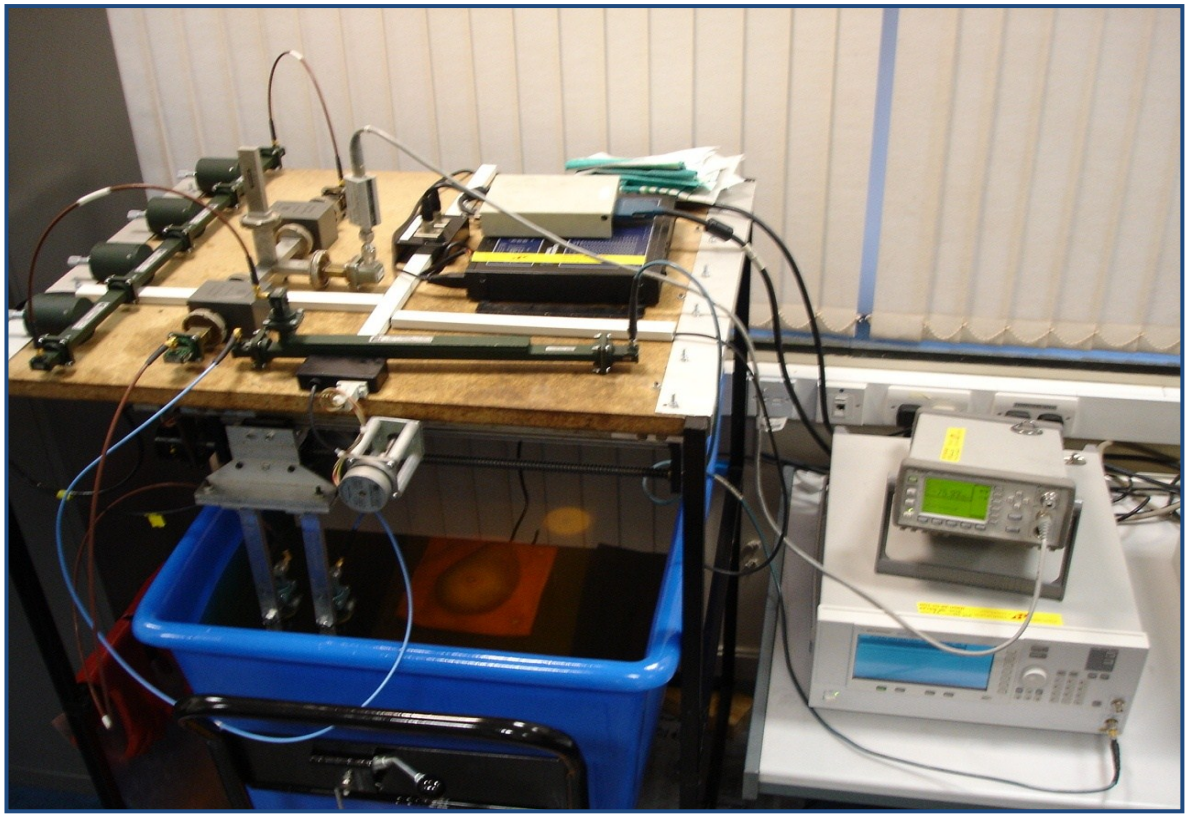

Figure 2-2 Photography of Breast Phantom Imaging System

Figure 2-3 presents a detailed image of the human breast. A to G represent the different types of tissues within the human breast. The detected tumour image shows the ability of the Microwave Holography system to image the dielectric object inside the breast phantom. One advantage of this technique over the X-ray mammography technique is the ability to present the results in 3D. As shown in Figure 2-3 the tissues in the breast are situated all along from the nipples to the chest. This technique provides the advantage of knowing the exact location of the cancer tissue due to its capabilities in presenting the results in 3D. This means the medical practitioner will be able to identify the cancer tissue's location as being closer to the chest or to the nipple without the need for a biopsy.

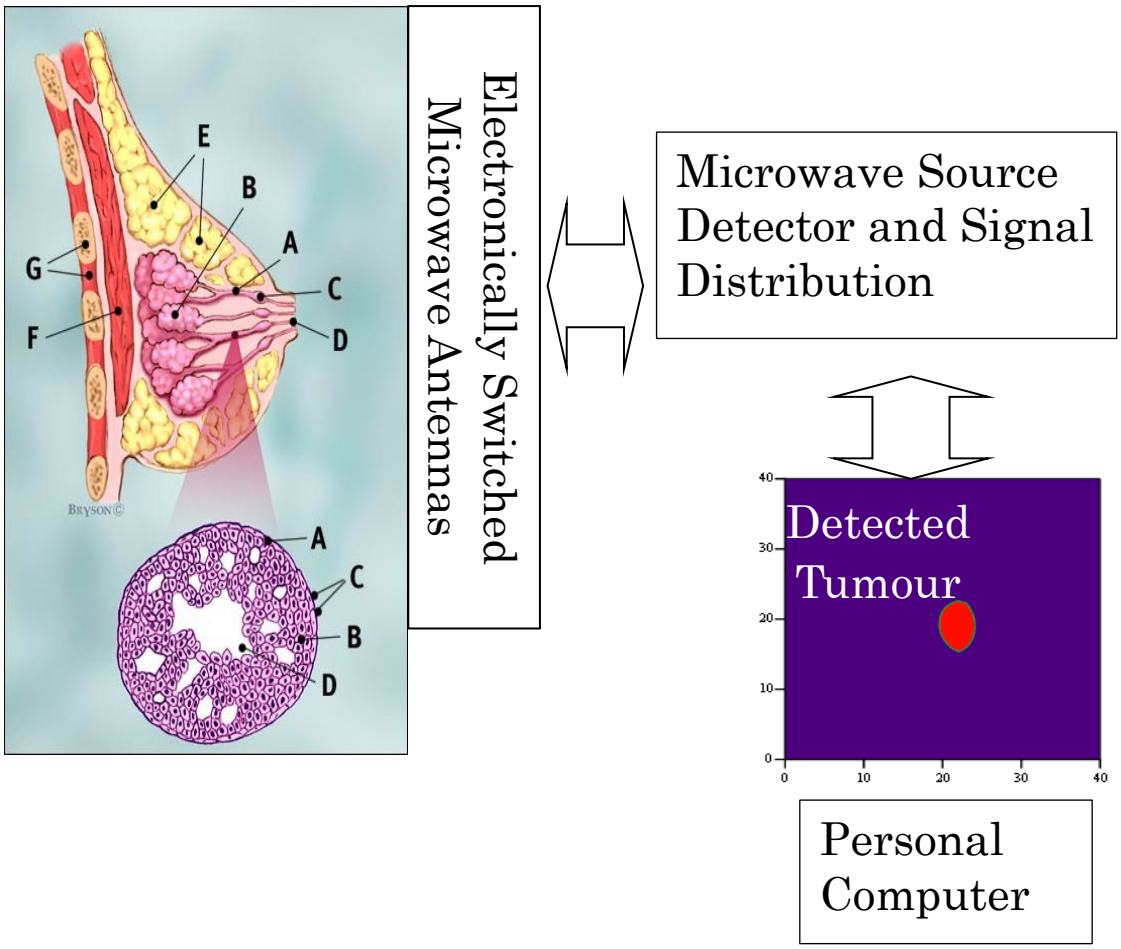

Figure 2-3 Human Breast Tissue

Given the initial success in imaging the breast phantom using the Microwave Holographic technique; the imaging technique was employed in imaging animal tissues. Figure 2-4 shows the pork chop used for imaging along with the different size metal cuts placed underneath the tissue. The metal cuts in the experiment replicate the presence of cancer tissues, in the same way the dielectric object does within the breast phantom. Figure 2-5 shows the results of the pork chop imaging. The overall shape of the pork chop is shown clearly in Figure 2-5, also there is a clear distinction between the pork chop and the metal cuts underneath them. It also shows the capabilities of the system to image clearly the difference in size of the metal cuts.

Figure 2-4 Pork Chop with different Metal cuts underneath

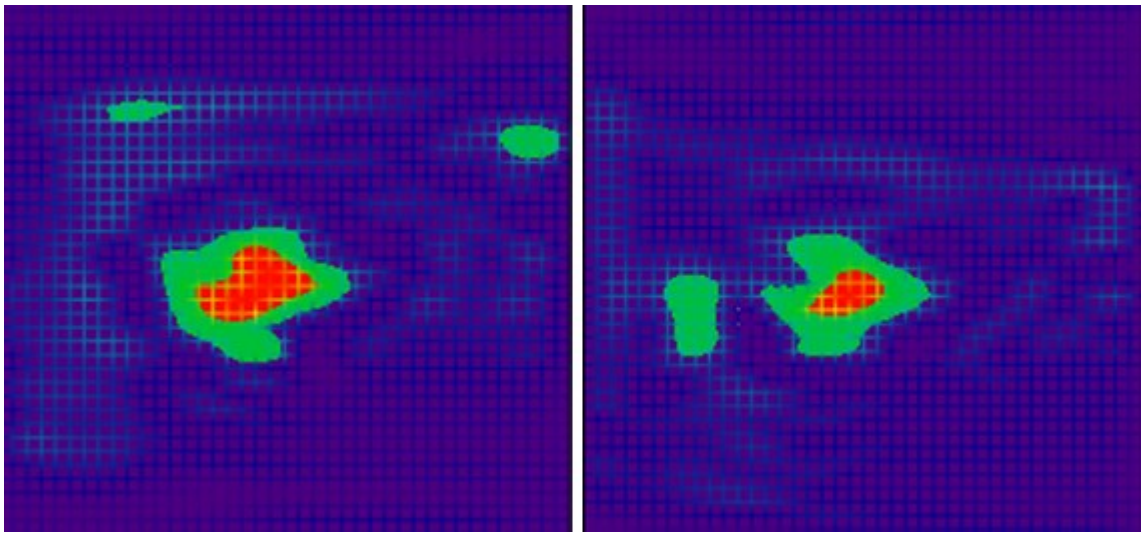

Figure 2-5 Pork Chop image showing the metal cuts

The next step in the initial research is to use the technique to identify the differences in tissue. For this purpose, a pig kidney covered in two layers of fat is used in the imaging setup. Figure 2-6 shows the arrangement of the tissues before and after the imaging process. Figure 2-7 shows the image of the results of imaging the pig kidney covered in fat layers using Microwave Holography system. As seen from the figure the technique has the ability to distinguish between two different tissues as it works on the principle of

exploiting the differences in dielectric property among various tissues, including cancerous cells.

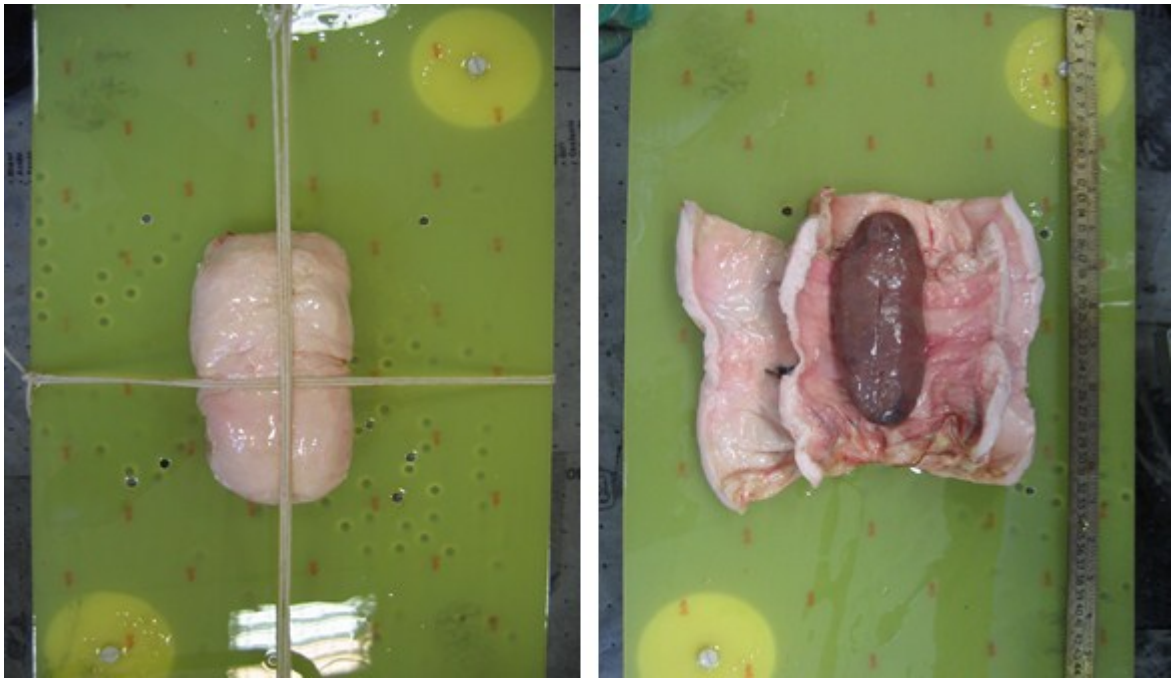

Figure 2-6 Pig Kidney covered in Fat layers

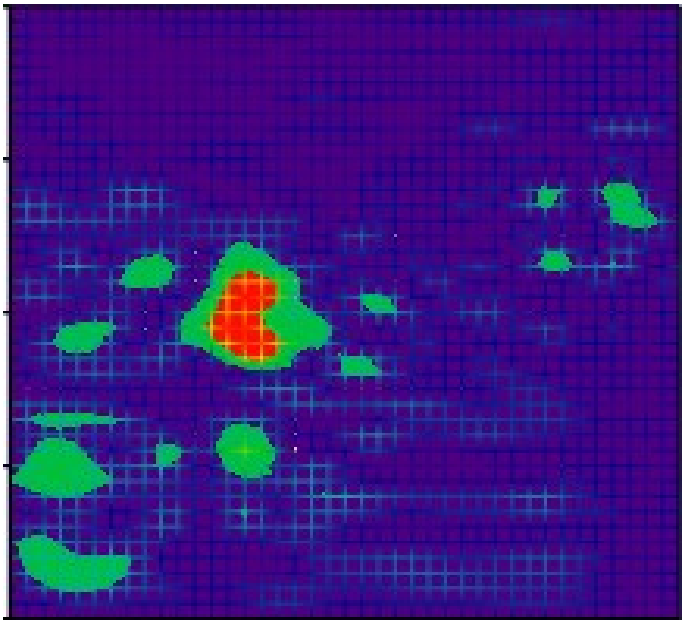

Figure 2-7 Pig Kidney Image

Imaging results clearly indicate the ability of the Microwave Holography system in imaging phantoms and tissues. Although initial results have clearly shown the potential of Microwave Holography system to be used in early breast cancer detection, during the course of this research one of the limitations of this system was identified. Figure 2-3 shows the image of the breast phantom under study. The image shows the dielectric object very clearly, however the size of the dielectric object was 4 cm. In order for this system to be used in medical imaging applications, the technique needs to be capable of imaging objects of sizes in the range of mm. This limitation has made the focus of the remainder of this research to identify ways to improve the ability of the current technique. One important aspect of the experimental setup for microwave imaging is the antennas employed and their ability under lossy medium.

All microwave medical imaging approaches including the above mentioned Microwave Holography system use microwave antennas to transmit and receive signals/energy. The characteristics of the microwave antenna differ considerably in freespace and lossy media. Most of the imaging techniques employ dielectric media to nullify the reflections at the air-skin interface. So it is paramount to study the behaviour of the antenna used in relation to that of the lossy medium employed. The following section details the challenges facing the microwave antenna used in medical imaging application.

2.3 Microwave Antennas & Challenges

In order to develop a clinically viable medical imaging system, it is important to understand the characteristics of the microwave antenna under lossy media. One of the

major requirements of the microwave medical imaging is for the whole arrangement to be immersed in a lossy medium in order to minimise reflections at the air-skin interface[23]. It is essential that the system designers take into consideration all the changes to the antenna characteristics used in comparison to its freespace behaviour. As stated in the previous section, all active imaging systems work on the principle of transmitting and receiving signal or energy to and from the object.

The signal propagation from the microwave antenna to the object and the reflected signal to the receiving antenna will be altered depending on the medium it propagates in relation with freespace propagation. The microwave signal propagation is characterised by a constant *k*, often quoted as the propagation constant. In freespace the propagation constant *k* is related to the angular frequency ω, the permeability μ_o and permittivity ε_o of freespace and it is given as

$$k_0 = \frac{2\pi}{\lambda} = \omega\sqrt{\mu_0\varepsilon_0} \qquad \textbf{2-1}$$

The permittivity of a lossy medium ε_r is given as $\varepsilon_r = \varepsilon_r' - j\varepsilon_r''$

$$\varepsilon_r = \varepsilon_r' - j\varepsilon_r''$$

where ε_r' is the real part and ε_r'' is the imaginary part of the dielectric constant. The conductivity σ σ of the lossy medium is given as

$$\sigma = \omega\varepsilon_o\varepsilon_r''$$

Ideally for medical applications lossy media with no losses are preferred, i.e., the imaginary part in the permittivity equation will be zero and the propagation constant k_r will be given as

$$k_r = \omega\sqrt{\mu_o \varepsilon_o \varepsilon_r}$$

But practically it is impossible to have a lossy medium without any losses. Because of the conductivity values of the lossy medium the propagation constant k_r' will be a complex value and this will change the wavelength λ to λ_r in lossy medium. The propagation constant k_r for a lossy media is given as

$$k_r = k_r' + jk_r'' \qquad \textbf{2-2}$$

Equation 2-2 will give rise to a negative real constant, corresponding to a decaying signal, and, if the propagation constant k_r is given as

$$k_r = k_r' - jk_r''$$

Then the above equation will give rise to a positive real constant, corresponding to an exponentially increasing signal which is not realistic.

Generally in microwave antenna design, the size of the antenna *l* will always be specified in terms of wavelength, for example *l* can be λ/4 long (quarter wavelength). This relationship between the wavelength and size of the length will affect the length of the antenna in lossy medium when compared with freespace length. Input impedance of the antenna will also be affected by the lossy medium. Input impedance *Z* is normally derived as the ratio between the voltage and current at the input. The current distribution of the

antenna in the lossy medium will depend on the new wavelength λ_r and thereby altering the input impedance of the antenna.

In order to match the antenna properly in the lossy medium the designer needs to accounts for the input impedance in the lossy medium. This variation caused by the conductivity values in the radiation pattern of the microwave antenna will affect the performance of the imaging system. In freespace the power decay in far field is proportional to $1/R^2$ where R is the distance between the origin and the observation point. However, in a lossy medium this decay factor will be increased by a factor $e^{-jk_z'}$. This exponential term accounts for the additional loss in the system because of the lossy medium. Thereby, the radiated signal from the antenna cannot illuminate the whole object or reach the required depth of penetration. Figure 2-8 shows the difference in the power loss in freespace and lossy media.

This presents the designer with the challenge to fully understand the antenna behaviour in lossy media and comprehend the situation by introducing the effect of complex permittivities to accommodate these changes or to modify the design parameters of the antenna to enhance its performances. Until now there has not been any comprehensive study on antenna behaviour in different lossy media for medical applications. Given the improvement in the microwave medical imaging field in recent years, it is vital to bridge this knowledge gap. This research aims to conduct an extensive study on the Monopole similar to the one used by Meaney et al. at Dartmouth college for their clinical trials[14].

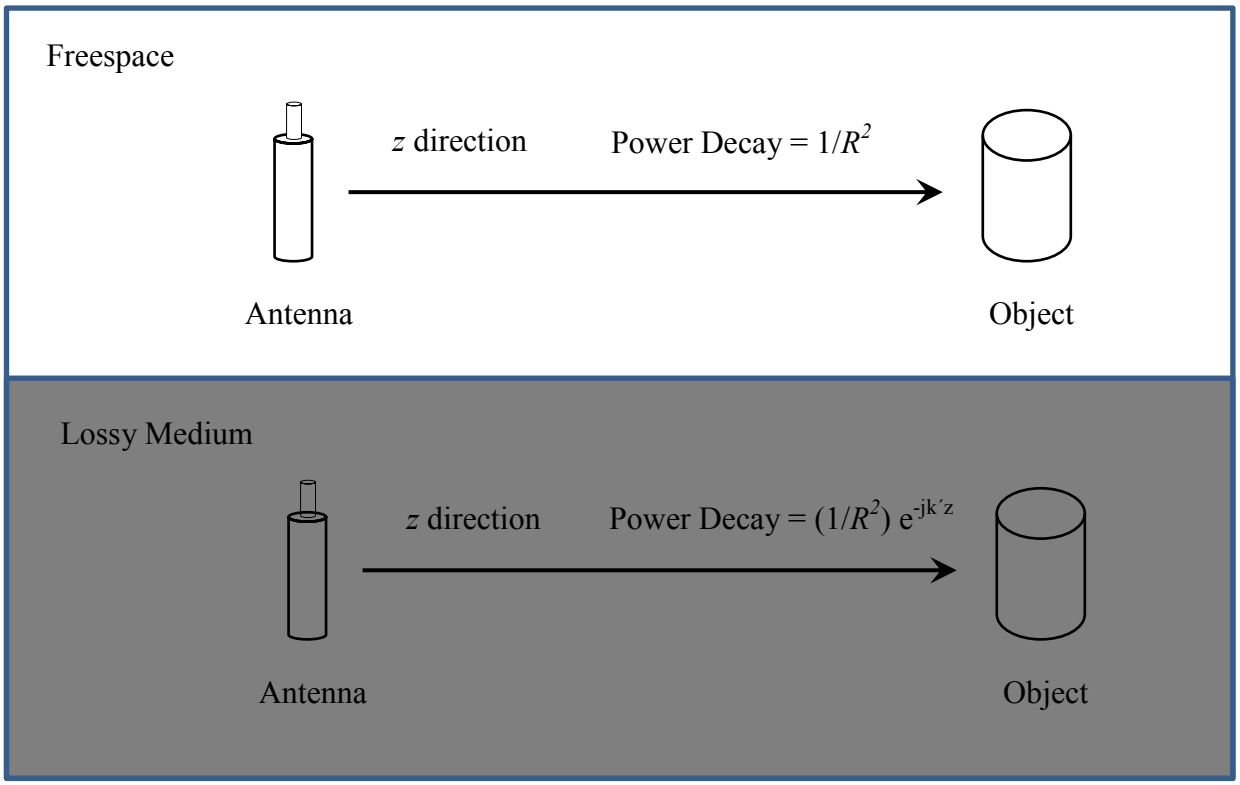

Figure 2-8 Illustration of the power decay component difference in Freespace and Lossy Medium

2.4 Different Microwave Antennas Used in Medical Imaging

Ever since engineers started using microwaves for medical applications, the search for suitable microwave antennas was underway. Various microwave antennas are used across the globe by different microwave medical imaging groups. This section details four such antennas which are either used in medical imaging applications or are identified as having the potential to be used. The four antennas are:

- Monopole
- Bow-tie Antenna
- Vivaldi Antenna

- Pyramidal Horn Antenna

These antennas will now be discussed.

2.4.1 Monopole

Several prototype active microwave imaging systems have been reported in the literature[52, 53]. In these systems, waveguide-type radiators or Monopoles are used as transmitters and receivers[53, 54]. Using Monopoles the entire imaging region can be illuminated by placing them close to the target, whereas in waveguide antennas the distance has to be greater in order for its main lobe to provide sufficient illumination coverage[16]. Furthermore, the space advantage offered by the Monopole transmitters can prove to be very useful for systems using multiple transmit/receive channels.

Meaney et al.[16] has designed a configuration which utilizes the Monopoles as both transmit and receive elements. The Monopoles were constructed by having the centre conductor of a semi rigid cable of quarter wavelength (physical length was 2.5 cm) exposed in a medium at 500 MHz. A typical Monopole constructed using semi rigid coax is shown in Figure 2-9. In a medium such as air or deionised water this type of antenna is notorious for producing exciting currents. Due to the lack of any Balun arrangement, the characteristic impedance of the Monopole in deionised water is uneven[16]. Meaney et al. capitalised on the high attenuation of the surrounding saline solution to limit this effect. The characteristic impedance of the Monopole in the saline solution (0.9%) is considerably different; it exhibits a nominal return loss of 9dB for the frequency range of 300–1100 MHz[16].

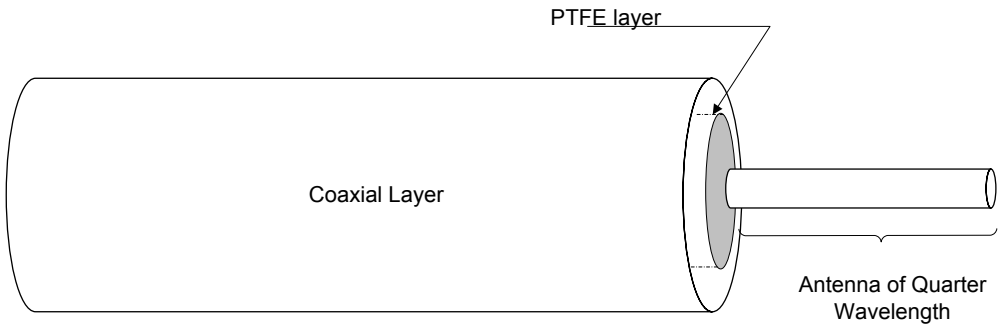

Figure 2-9 Monopole constructed using Semi Rigid Coax

Because of the better impedance match between the Monopole and the surrounding saline solution the images obtained with this system show a systematic improvement over the images obtained with their waveguide counterparts. Through this finding Meaney et al. demonstrate that the isotropic radiation pattern of the Monopole does not serve to degrade imaging performance in the near field context, rather it actually increases the image quality obtained. In order to realise a clinically viable system a fixed array data acquisition design may be desired[16]. Because of the physical advantages offered by the Monopole transceiver arrangement, by eliminating the more bulky waveguides, they can be conducive to a fixed array design thereby making this arrangement more suitable for medical applications.

Apart from the above specified Monopole design there are other Monopole designs presented in the literature with wide bandwidth properties and different geometrical shapes. Some of the Monopole designs from the literature are listed below:

- Wideband Planar Monopoles[55]
- Printed Circular disc Monopole for ultra wideband application[56]
- Novel Top Sleeve Monopole in two Parallel planes[57]

- Wideband Double-Fed Planar Monopole[58]
- Broadband Roll Monopole[59]

Although the literature presents us with different wideband Monopole designs, very few of them account for Monopole study in lossy media. This overall inadequacy of detailed studies on microwave antennas used for medical applications lead this research to study the antenna behaviour in response to different conductivity media. Chapter 3 details Monopole theory; their performance in different lossy media are explained with results in Chapter 4.

2.4.2 Bow-tie Antenna

G. Bindu et al. designed an efficient wideband coplanar stripline fed bow-tie antenna with improved bandwidth, low cross polarization and reduced back radiation. The new antenna is constructed by structurally modifying the conventional microstrip bow-tie antenna design; this is achieved by attaching an image plane[60]. The antenna is designed as a patch on a single layered substrate with $\varepsilon_r = 4.28$ and thickness of 1.6 mm. The coplanar stripline is designed to have an input impedance of 50Ω in order to couple the antenna effectively with the measurement system. The parameters, such as the distance to the image plane, flare angle of the bow, and dimensions of the antenna, are found to affect the bandwidth. These parameters are optimised to enhance the performance. An optimum distance of 2 cm for the image plane is selected to obtain good bandwidth and maximum forward radiation in the operating feed.

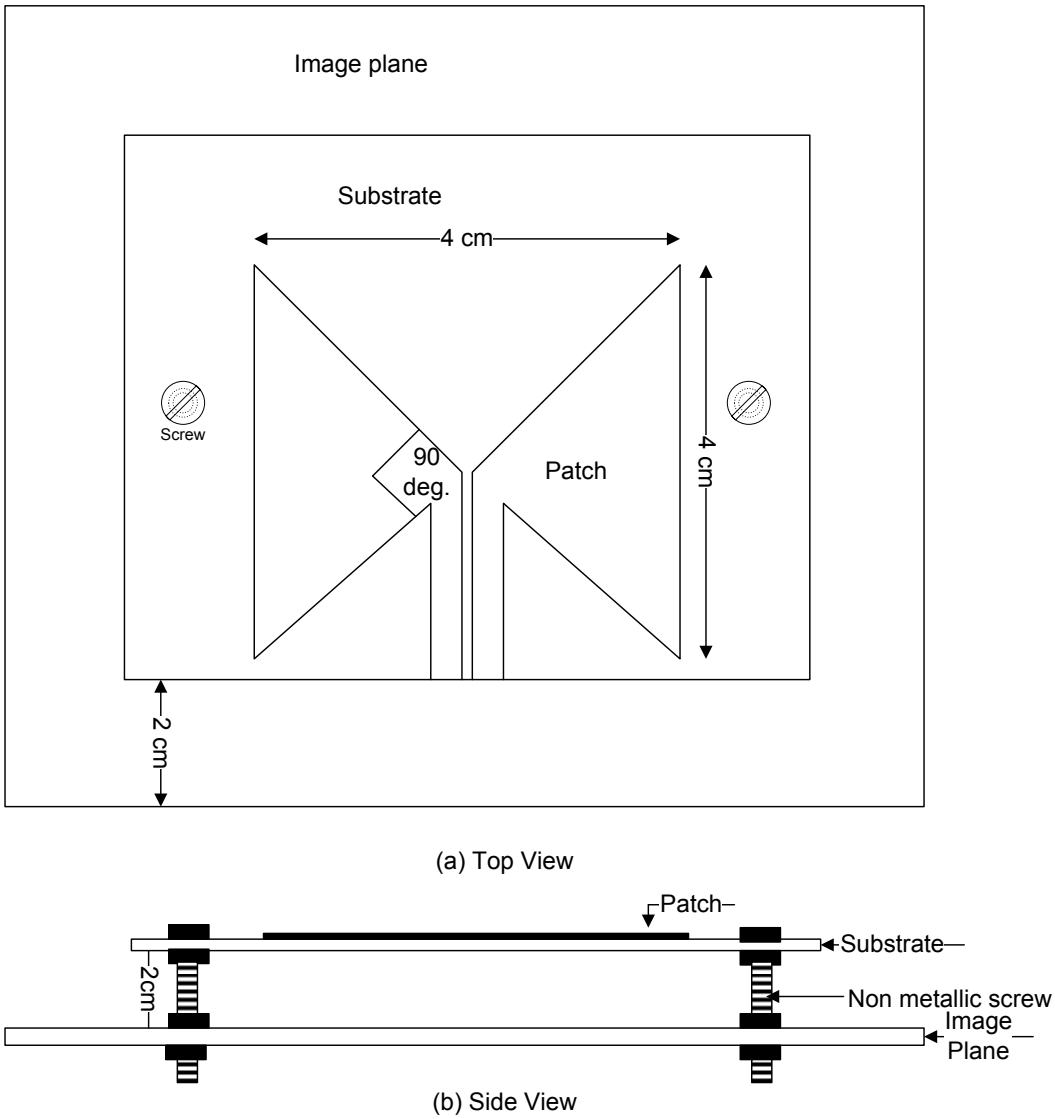

Figure 2-10 Wideband bow-tie antenna

The antenna exhibits a unidirectional radiation pattern with enhanced bandwidth reduced back radiation and low cross polarization in the operational band and thus making it suitable for Confocal Microwave Imaging (CMI). A typical wideband bow-tie antenna with coplanar stripline feed for CMI is shown in Figure 2-10. CMI employs back scattering to locate breast cancer tumours, so the antenna employed is required to focus the microwave signal towards the target and collect the back scattered energy[26]. A 2:1 Standing Wave Ratio (SWR) bandwidth of 45.9% is obtained for the designed 4x4 cm

bow-tie antenna in air, which has a flare angle of 90˚. The antenna operates in the band of 1850 - 3425 MHz with a return loss of -53 dB. It is reported in corn syrup, the bandwidth is enhanced to 91% in the range of 1215 – 3810 MHz with resonant frequency of 2855 MHz and return loss of -41 dB[61].

2.4.3 Vivaldi Antenna

The Vivaldi antenna, a form of the tapered slot radiator, has been shown to produce performance over a wide bandwidth limited only by the traditionally used slotline to microstrip transition[62]. Langley et al. designed a Vivaldi antenna that satisfies the requirements for imaging systems in terms of bandwidth, gain and impulse response, albeit at the expense of significant volumetric size[63]. In addition to the bandwidth requirement, the antenna supports the sub nanosecond pulse transmission with negligible distortion to achieve precision imaging without ghost targets.

Later in 2006, Abbosh et al. designed a Vivaldi antenna that reduced its physical dimensions such that it can be incorporated in a compact microwave imaging detection system whilst maintaining its distortionless performance[64]. A typical Ultrawideband Antipodal Vivaldi antenna is shown in Figure 2-11. The antenna operates over an Ultrawideband (UWB) from 3.1 to 10.6 GHz with a peak gain of 10.2 dBi at 8 GHz. This type of antenna has proved to have the potential to be used in medical applications.

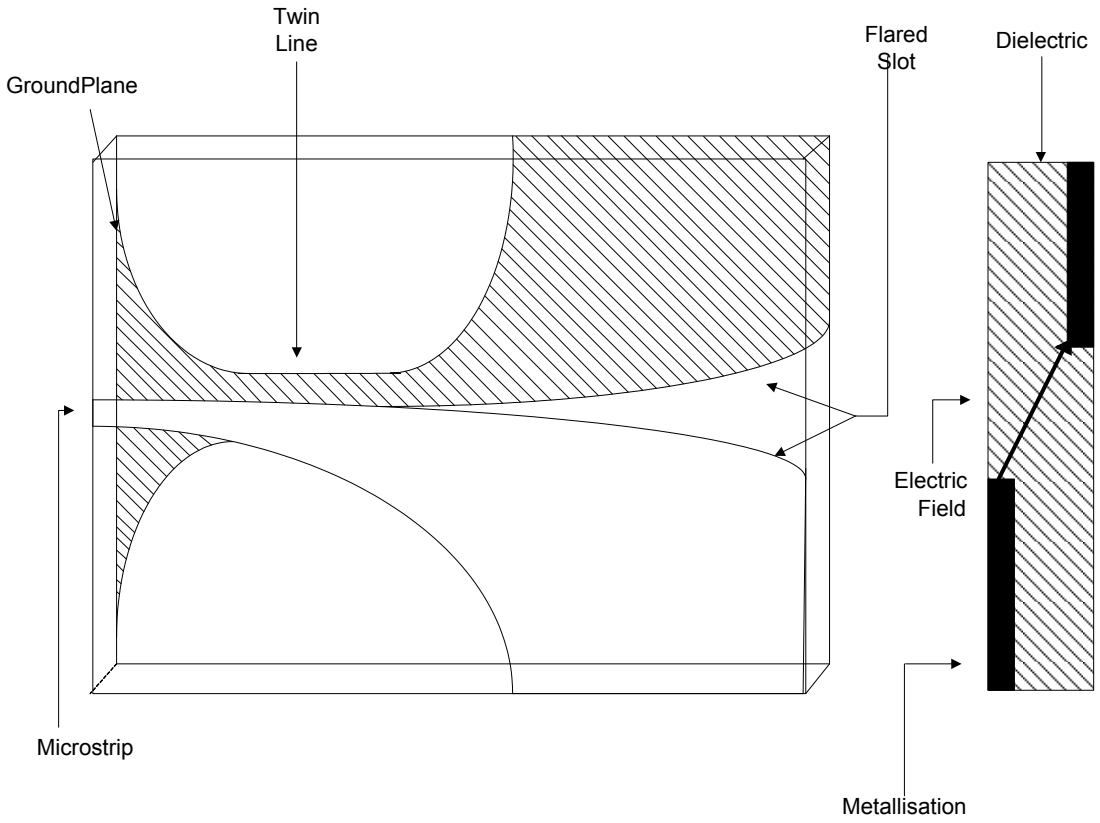

Figure 2-11 Antipodal Vivaldi antenna

2.4.4 Pyramidal Horn Antenna

Horn antennas are known for their higher aperture efficiencies but are constrained to certain applications due to their limited bandwidths. However the bandwidth of the Horn antennas can be increased significantly by adding metallic ridges to the waveguide and flared sections[65]. Numerical and experimental investigations of Pyramidal Horn antennas with double ridges have been reported[66]. This type of antenna is commercially available with an operational frequency band of 1–18 GHz.

However, the large dimensions and high cost of these antennas make them unsuitable for medical imaging applications. E.T. Rosenbury et al.[67] designed a modified version of the Ridged Horn antenna in which the waveguide section is eliminated and one of the two ridges is replaced by a curved metallic plane terminated by resistors. Later in 2003 Susan C. Hagness and her team presented a complete numerical and experimental study of a specific realisation of this design, wherein the antenna is customized to centimetre scale dimensions for operation in the microwave frequency range 1 to 11 GHz[68].

The antenna consists of a Pyramidal Horn radiation cavity, a metallic ridge, and a curved metallic launching plane terminated with resistors. The Pyramidal Horn is connected to the outer conductor of the coaxial feed and serves as the ground plane, providing a current return path. Because of the coaxial feed, the ground plane configuration eliminated the need for a UWB Balun. The launching plane is a curved plane structure connected to the central conductor of the coaxial feed. Termination resistors are attached between the end of the launching plane and the side wall of the Pyramidal Horn.

Microwave energy is directed and launched by this curved plane into the surrounding medium. The termination resistors suppress reflections from the end of the launching plane. The top surface of the ridge curves toward the antenna aperture. The dimensions of the Horn antenna are chosen according to the physical size required and operating frequency range. A typical Ridged Pyramidal Horn antenna is shown in Figure 2-12. The curvature and shape of the launching plane, the thickness and the contour of the curved side of the ridge and the termination resistors are the main factors influencing the input impedance of the antenna. In order to match the 50Ω input impedance of the feeding coaxial cable, two 100Ω termination resistors are connected in parallel near opposite

corners of the launching plane. The Pyramidal Horn has a depth of 13 mm with a 25 mm x 20 mm aperture.

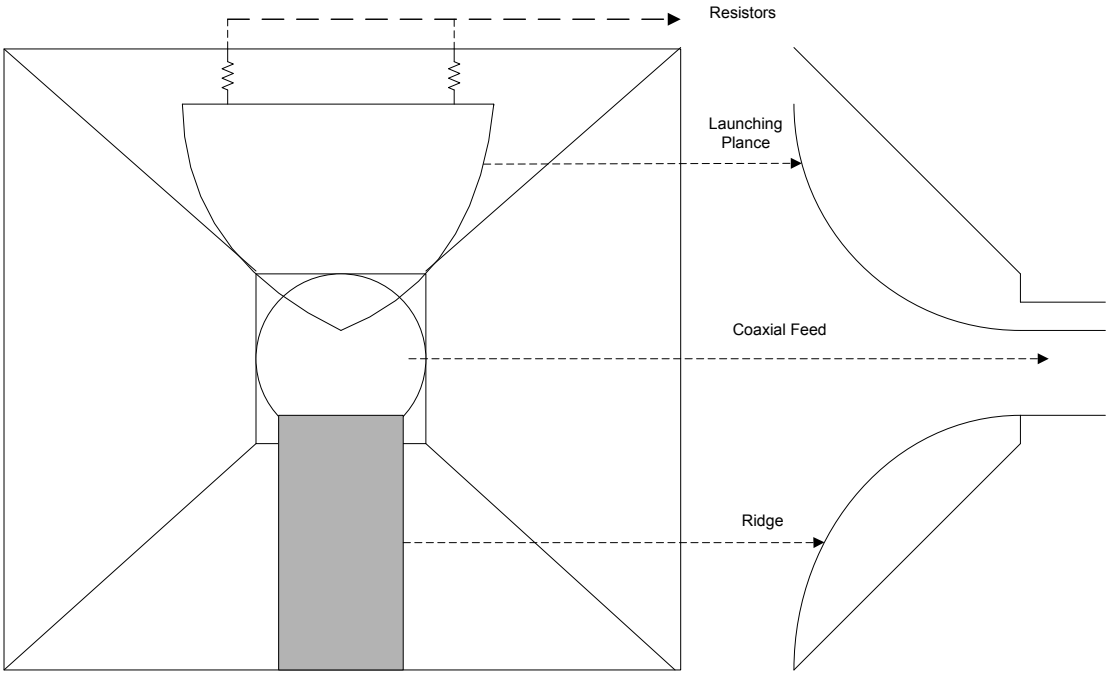

Figure 2-12 Ridged Pyramidal Horn Antenna

The maximum width of the launching plane is 12 mm and the thickness of the ridge is 2 mm. The UWB performance of the antenna can be characterized in the time domain by the fidelity, which is a measure of how accurately the transmitted waveform reproduces the time derivative of the voltage applied to the antenna terminals[69]. This antenna yields VSWR of less than 1.5 over the frequency range and fidelity of approximately 0.96 in both the simulation and experiment[68]. The antenna has been tested under a low loss immersion medium and achieved similar VSWR and fidelity. Overall it is evident that this type of antenna can be useful for biological sensing and imaging applications.

2.5 Summary

The main methods available for microwave medical imaging have been discussed along with initial research and outcomes. Microwave antennas currently used in medical imaging and Vivaldi antennas with a potential to be used in medical imaging are presented along with their design specification and published results. The body of this work is concerned with the extensive study of the Monopole used by Meaney et al. in media of low and high conductivity levels[14].

A novel mathematical model approach is developed to predict the Monopole fields and impedances. To achieve this goal of the thesis, the theoretical analysis behind the Monopole using the traditional Pocklington Integral Equation approach and development of the novel mathematical model approach and its advantages will be presented in the next chapter, as this is fundamental to the comprehensive study of the Monopole in different lossy media.

Chapter 3 Analysis of Monopole Antennas: Traditional and New Mathematical Method

3.1 Introduction

Having examined the development of currently used medical imaging methods, different antennas employed and highlighted the direction in which this research will move, it is now necessary to focus in detail on the theory behind the Monopole model and procedures involved in calculating the input impedance and radiation pattern as this forms the foundation for the novel mathematical model discussed later.

An introduction to the Monopole model is given in Section 3.2. The Method of Moment (MOM) technique is used in predicting the current calculation for a wire antenna and discussed in Section 3.2.1. The general approach to convert integral equations using basis and testing functions to a discrete matrix equation is known as Method of Moments (MOM). This procedure is also called the "weighted-residual" method, as the matrix equations are obtained by forcing the residuals to be orthogonal to the testing functions. The applicability of Pocklington integral equation to calculate the input impedance and radiation pattern calculation is shown in Section 3.3. This section ends with the limitations of these traditional methods and the need for a new model is raised.

The outline of the novel mathematical model is given in Section 3.4, detailing the need for the new model and the expression to predict the current across the Monopole. The new expression depends only on three parameters which are explained and also reasoned in this section. The current distribution along a wire of λ/2 length predicted using the new model is presented. Results from the traditional model for wire length of λ/4 and 3λ/4 are also compared with the predicted results of the new model and shown in Section 3.4.1. The final section of this chapter lists the advantages of this new model compared to that of the traditional model and its usability in workspaces comprising complex permittivities.

3.2 Monopole Model

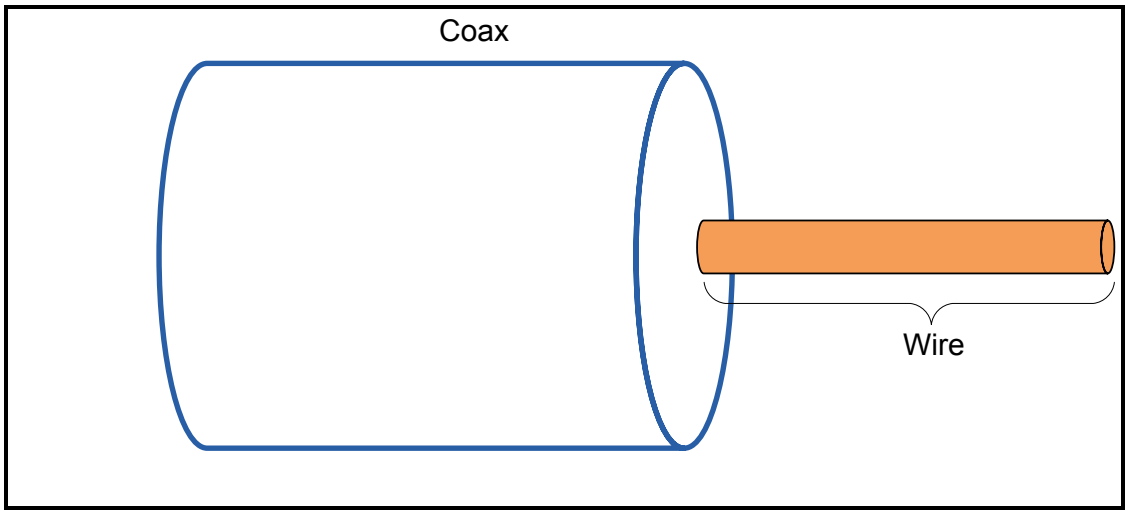

Figure 3-1 Simple Monopole Model

A simple Monopole model is shown in Figure 3-1. The model has taken account of the feed system employed; in this case the coaxial aperture acts as the feed. Thus the evaluation of current distribution involves not only the wire but also the effect of the coaxial aperture on the current distribution[70]. The basics of predicting the Monopole

characteristic is very simple; if the current distribution along the Monopole is known then the radiation pattern can be determined and if the voltage and current at the start of the Monopole are known, then the input impedance can be calculated.

Section 3.3 details the effect of this consideration of the coaxial feed on the current distribution. This model of evaluation gives rise to two problems; interior and exterior. The exterior problem is associated with the field across the aperture and hence input impedance and the interior is due to the current along the wire of the Monopole and radiation pattern. The next section explains the Method of Moment technique which is used to solve the interior problem, i.e. current across the wire.

3.2.1 Current along the wire using Method of Moment technique

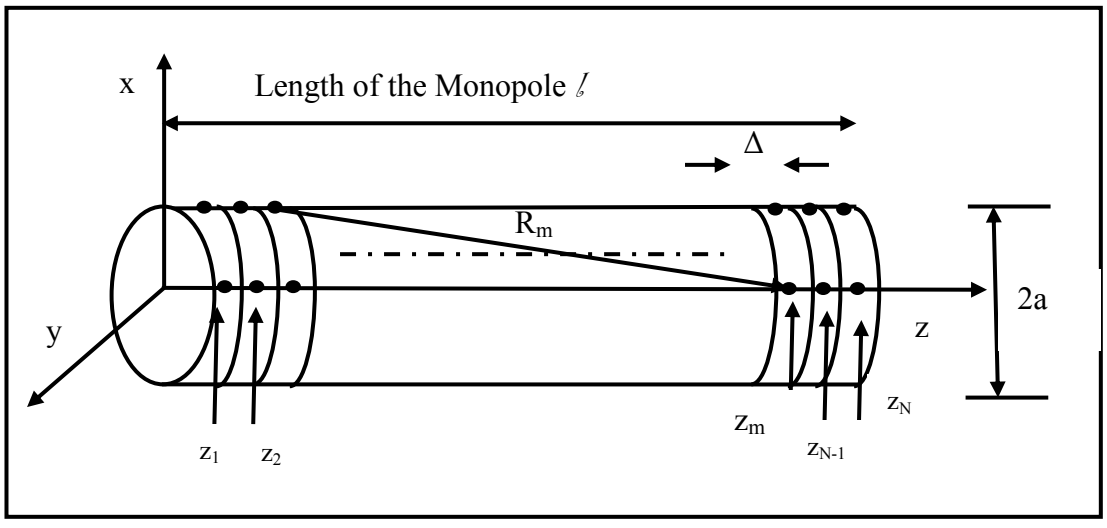

Figure 3-2 Segmented wire

A straight wire of length *l* and radius *a* is placed along the *z* axis as shown in Figure 3-2. Across the wire an electric potential *V(r)* is created using a linear charge distribution *ρ(r)* [71] which is given by

$$V(r) = \frac{1}{4\pi\varepsilon_0}\int \frac{\rho(r')}{R} dl' \qquad \textbf{3-1}$$

Where *r′(x′, y′, z′)* denotes the source coordinates, *dl′* is the path of integration, the observation coordinates is *r(x, y, z)* and the *R* is the distance from any point on the source to the observation point, which is given by

$$R(r - r') = |r - r'| \qquad \textbf{3-2}$$
$$= \sqrt{(x - x')^2 + (y - y')^2 + (z - z')^2}$$

The normalised constant electric potential of *1V* is given to the wire. The charge density on the surface wire can be expressed as (considering the observation point along the wire axis *x = y = 0*)

$$1 = \frac{1}{4\pi\varepsilon_0}\int_0^l \frac{\rho(z')}{R(z,z')} dz', 0 \le z \le l \qquad \textbf{3-3}$$

Where

$$R(z,z') = R(r,r') = \sqrt{(z - z')^2 + [(x)^2 + (y)^2]}$$
$$= \sqrt{(z - z')^2 + a^2}$$

R(z, z′) = 0 is avoided by chosing the observation point along the wire and the charge density is represented along the surface of the wire. The solution for equation 3-3 can be

obtained by the MOM technique. $\rho(z')$, the unknown charge distribution, can be expressed as the product of N known terms with constant but unknown coefficients (refer Appendix I: Method of Moment) , that is,

$$\rho(z') = \sum_{n=1}^{N} \alpha_n \mathrm{g_n}\,(z') \qquad \textbf{3-4}$$

Thus, equation 3-3 may be written using equation 3-4 as,

$$4\pi\varepsilon_0 = \int_0^l \frac{1}{R(z,z')} \left(\sum_{n=1}^{N} \alpha_n \mathrm{g_n}\,(z') \right) dz' \qquad \textbf{3-5}$$

Since equation 3-5 is a non-singular integrand, its integration and summation can be interchanged and it can be written as

$$4\pi\varepsilon_0 = \sum_{n=1}^{N} a_n \int_0^l \frac{\mathrm{g}_n(z')}{\sqrt{(z-z')^2 + a^2}} dz' \qquad \textbf{3-6}$$

The wire is now divided into *N* uniform segments, each of length $\Delta = {}^{l}/_{N}$. The $\mathrm{g}_n(z')$ function is referred to as basis functions and is given by

$$\mathrm{g}_n(z') = \begin{cases} 0 & z' < (n-1)\Delta \\ 1 & (n-1)\Delta \le z' \le n\Delta \\ 0 & n\Delta < z' \end{cases} \qquad \textbf{3-7}$$

Let z_m be a fixed point on the surface on the wire. If z in Equation 3-6 is replaced by the fixed point z_m then Equation 3-6 becomes

$$4\pi\varepsilon_0 = a_1 \int_0^{\Delta} \frac{g_1(z')}{R(z_m, z')} dz' + a_2 \int_{\Delta}^{2\Delta} \frac{g_2(z')}{R(z_m, z')} dz' + \cdots$$

$$+ a_n \int_{(n-1)\Delta}^{n\Delta} \frac{g_n(z')}{R(z_m, z')} dz' + \cdots \qquad \textbf{3-8}$$

$$+ a_N \int_{(N-1)\Delta}^{l} \frac{g_N(z')}{R(z_m, z')} dz'$$

N linearly independent equations are necessary to obtain a solution for $a_1,\ldots,a_N$. By choosing N observation points $z_1,\ldots,z_N$ on the surface of the wire each at the centre of each Δ length element a set of linearly independent equations can be obtained. This yields

$$\begin{pmatrix} 4\pi\varepsilon_0 = a_1 \int_0^{\Delta} \frac{g_1(z')}{R(z_1, z')} dz' + \cdots + a_N \int_{(N-1)\Delta}^{l} \frac{g_N(z')}{R(z_1, z')} dz' \\ \vdots \qquad\qquad \ddots \qquad\qquad \vdots \\ 4\pi\varepsilon_0 = a_1 \int_0^{\Delta} \frac{g_1(z')}{R(z_N, z')} dz' + \cdots + a_N \int_{(N-1)\Delta}^{l} \frac{g_N(z')}{R(z_N, z')} dz' \end{pmatrix} \qquad \textbf{3-9}$$

Equation 3-9 can be given in matrix notation as

$$[V_m] = [Z_{mn}][I_n] \qquad \textbf{3-10}$$

Where,

$$[V_m] = \begin{pmatrix} 4\pi\varepsilon_0 \\ \vdots \\ 4\pi\varepsilon_0 \end{pmatrix}, [I_n] = \begin{pmatrix} a_1 \\ \vdots \\ a_1 \end{pmatrix}$$

And,

$$[Z_{mn}] = \begin{pmatrix} \int_0^{\Delta} \frac{g_1(z')}{R(z_1, z')} dz' & \cdots & \int_{(N-1)\Delta}^{l} \frac{g_N(z')}{R(z_1, z')} dz' \\ \vdots & \ddots & \vdots \\ \int_0^{\Delta} \frac{g_1(z')}{R(z_N, z')} dz' & \cdots & \int_{(N-1)\Delta}^{l} \frac{g_N(z')}{R(z_N, z')} dz' \end{pmatrix} \quad \textbf{3-11}$$

Note that the entries Z_{mn} of term [Z] is equal to

$$Z_{mn} = \int_0^l \frac{\mathrm{g}_n(z')}{\sqrt{(z_m - z')^2 + a^2}} dz' = \int_{(n-1)\Delta}^{n\Delta} \frac{1}{\sqrt{(z_m - z')^2 + a^2}} dz'$$

Solving (Z) for [I] gives

$$[I_n] = [Z_{mn}]^{-1}[V_m] \quad \textbf{3-12}$$

Equation 3-12 gives the current across the wire of length *l* and radius *a* using the MOM technique. Thus the Method of Moment technique is used to solve the interior problem of the Monopole model. In the next subsection the Pocklington Integral equation will be employed to calculate the field due to the aperture and its effect on the current across the wire, thereby solving the exterior problem.

3.3 Input Impedance and Radiation Pattern Calculation using Pocklington Integral Equation

In the case of the Monopole constructed by stripping the outer conductor of the semi rigid coaxial cable and exposing the centre conductor, the wire exposed will experience an

incident field across the surface caused by the coaxial aperture of the outer conductor. This evaluation is similar to the exterior problem of the Monopole model stated earlier.

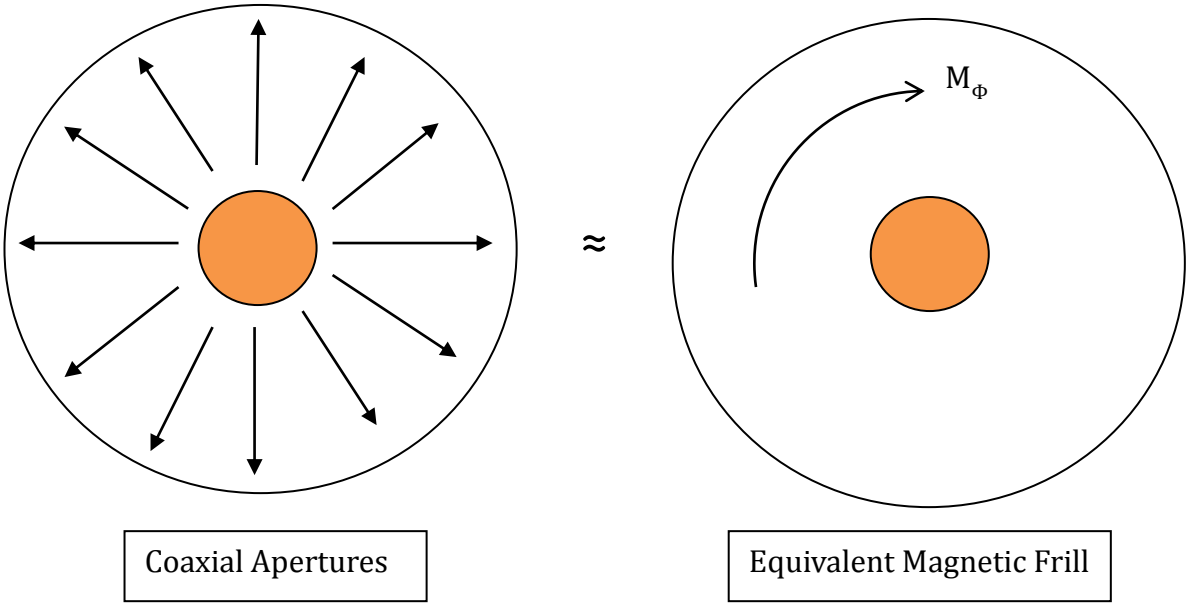

Figure 3-3 Equivalence Principle

Figure 3-3 shows the coaxial apertures and its equivalent magnetic frill given by the equivalence principle which states *"two sources producing the same field within a region of space are said to be equivalent within that region"[72]*. Thereby the coaxial aperture is replaced by an equivalent magnetic frill to calculate the fields from coaxial apertures. The magnetic frill consists of a circumferentially directed magnetic current density that exists over an annular aperture with inner radius *a*, which is usually chosen to be the radius of the wire, and an outer radius *b*. Figure 3-4 shows the segmented wire with the magnetic frill. Pocklington Integral equation 3-13[73] can be used to determine the equivalent filamentary line source current of a thin wire, by knowing the incident field on the surface of the wire[74].

$$\int_0^l I_z(z')\frac{e^{-jkR}}{4\pi R^5}[(1+jkR)(2R^2-3a^2)+(kaR)^2]dz' = -j\omega\varepsilon E_z^i(\rho=a) \quad \textbf{3-13}$$

Where for observations along the centre of the wire *(ρ=0)*

$$R = \sqrt{a^2+(z-z')^2}$$

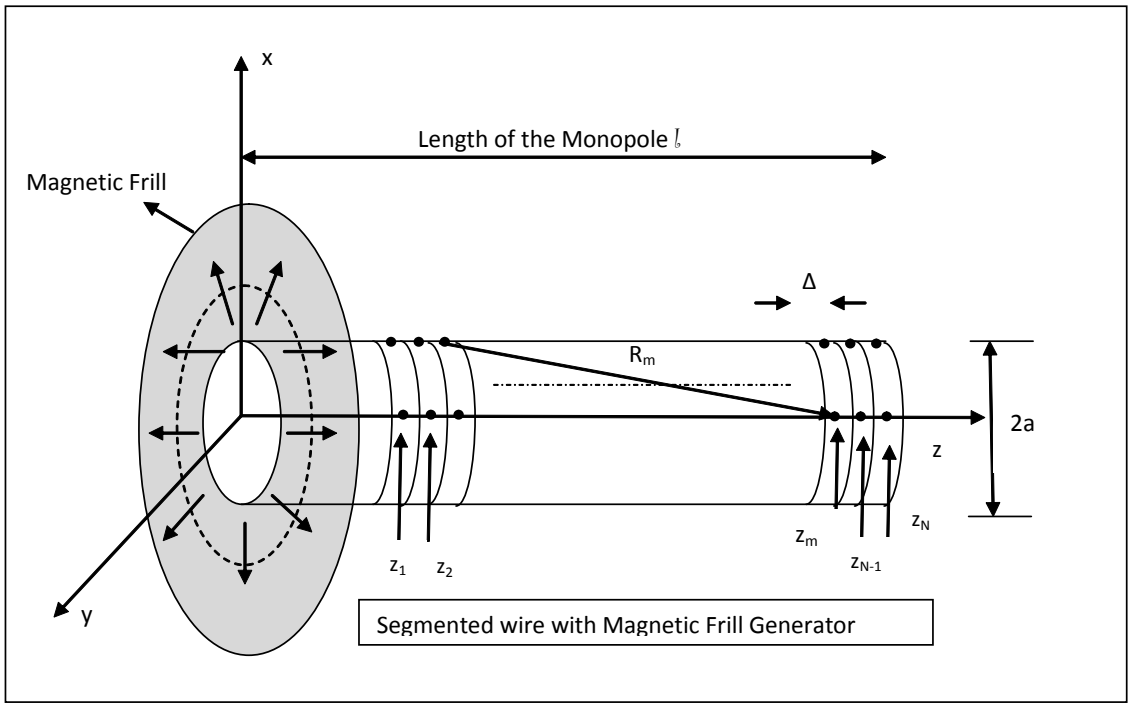

Figure 3-4 Segmented wire with Magnetic Frill

Over the annular aperture of the magnetic frill generator, the electric field is represented by the TEM mode field distribution of a coaxial transmission line and is given by

$$E_f = \widehat{a_\rho}\frac{V_i}{\ln(b/a)} \quad a \le \rho' \le b$$

Therefore the corresponding equivalent magnetic current density M_F for the magnetic frill generator used to represent the aperture is equal to

$$M_F = -2\hat{n}\, x\, E_f = -2\hat{a}_z\, x\, \hat{a}_\rho E_\rho = -\hat{a}_\phi \frac{V_i}{\rho' \ln(b/a)}\ a \leq \rho' \leq b \qquad \textbf{3-14}$$

The field generated by the magnetic frill generator of 3-14 on the surface of the wire along the axis *(ρ=0)* is given by [24]

$$E_z^i(\rho = 0, 0 \leq z \leq l) = -\frac{V_i}{2\ln(b/a)}\left[\frac{e^{-jkR_1}}{R_1} - \frac{e^{-jkR_2}}{R_2}\right] \qquad \textbf{3-15}$$

Where

$$R_1 = \sqrt{z^2 + a^2}\ R_2 = \sqrt{z^2 + b^2}$$

Knowing the incident field, the current across the wire can be calculated using equation 3-13. Using MOM the current $I_z(z')$ can be given by

$$I_z(z') = \sum_{n=1}^{N} \alpha_n\, g_n(z')$$

Replacing $I_z(z')$ in equation 3-13

$$\int_0^l \sum_{n=1}^{N} \alpha_n\, g_n(z') \frac{e^{-jkR}}{4\pi R^5}[(1 + jkR)(2R^2 - 3a^2) + (kaR)^2]dz' = -j\omega\varepsilon E_z^i \qquad \textbf{3-16}$$

Interchanging the integration and summation in equation 3-16

$$\sum_{n=1}^{N} \alpha_n \int_0^l g_n(z') \frac{e^{-jkR}}{4\pi R^5} [(1 + jkR)(2R^2 - 3a^2) + (kaR)^2] dz' \quad \textbf{3-17}$$

$$= -j\omega\varepsilon E_z^i$$

Where $g_n(z')$ is the basis function given as in equation 3-7. Replacing *z* in equation 3-17 by a fixed point on the surface of the wire, such as z_m and *R* is given as

$$R = \sqrt{a^2 + (z - z')^2}$$

Now by using piecewise integration over the N segments, equation3-17 becomes

$$-j\omega\varepsilon E_z^i = \alpha_1\beta_1(z_m) + \alpha_2\beta_2(z_m) + \cdots + \alpha_N\beta_N(z_m), m$$

$$= 1, \cdots, N$$

Where

$$\beta_n(z_m) = \int_{(n-1)\Delta}^{n\Delta} g_n(z') \frac{e^{-jkR(z_m,z')}}{4\pi R^5(z_m,z')} [(1 + jkR(z_m,z'))(2R^2(z_m,z') - 3a^2)$$

$$+ (kaR(z_m,z'))^2] dz'$$

By varying, *m* from *1* to *N* we obtain *N* equations of the above form, which can be written in matrix form as:

$$\begin{pmatrix} -j\omega\varepsilon E_{z'}^i \\ \vdots \\ -j\omega\varepsilon E_{z'}^i \end{pmatrix} = \begin{pmatrix} \beta_1(z_1)\beta_2(z_1) & \dots & \beta_N(z_1) \\ \vdots & \vdots & \vdots \\ \beta_1(z_N)\ \beta_2(z_N) & \cdots & \beta_N(z_N) \end{pmatrix} \begin{pmatrix} \alpha_1 \\ \vdots \\ \alpha_N \end{pmatrix} \quad \textbf{3-18}$$

Equation 3-18 can be written using matrix notation as,

$$[V_m] = [Z_{mn}][I_n]$$

Where voltage at the m^{th} segment is given by

$$V_m = E_z^m \Delta$$

And the current across the n segments is given by

$$[I_n] = [Z_{mn}]^{-1}[V_m] \qquad \textbf{3-19}$$

And $[Z_{mn}]$ is given by

$$[Z_{mn}] = \int_{n\Delta}^{(n+1)\Delta} \frac{e^{-jkR(z_m,z_n')}}{4\pi R^5(z_m,z_n')}[(1+jkR(z_m,z_n'))(2R^2(z_m,z_n') - 3a^2) + (kaR(z_m,z_n'))^2]dz'$$

Knowing the impedance $[Z_{mn}]$ and the voltage $[V_m]$ across the segment, the current across the wire $[I_n]$ can be calculated using equation 3-19. The input impedance of the Monopole is calculated by using the input voltage V_i and the current at segment zero I_0. The following expression is used to calculate the input impedance of the Monopole.

$$[Z] = \frac{[V_i]}{[I_0]} \qquad \textbf{3-20}$$

3.3.1 Radiation Pattern

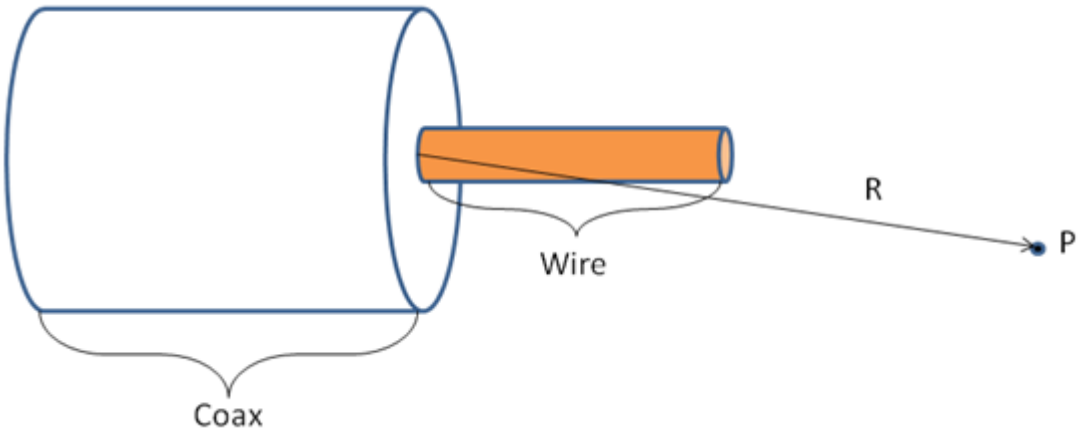

Figure 3-5 Far Field at point P at distance R

As shown in Figure 3-5, the radiation pattern for the Monopole is calculated at a point *P*. To calculate the fields radiated by this current element wire, it is essential to evaluate the magnetic vector potential *A* due to the electric current I_n across the wire. The Vector Potential *A* is related to I_n by

$$A(x,y,z) = \frac{\mu}{4\pi}\int_0^l I_n(x',y',z')\frac{e^{-jkR}}{R}dl' \qquad \textbf{3-21}$$

Equation 3-21 gives the vector potential at a distance *R* caused by the current across the wire whereas earlier *(x, y, z)* represent the observation point coordinates, *(x', y', z')* represent the coordinates of the source. The next step of the field calculation is to find the magnetic field intensity *H* using the following expression

$$H = \frac{1}{\mu}\nabla \times A \qquad \textbf{3-22}$$

In order to make the calculation simpler, it is often easier to transform from rectangular to spherical components. The transformation between rectangular and spherical components is given by

$$\begin{bmatrix} A_r \\ A_\theta \\ A_\varphi \end{bmatrix} = \begin{bmatrix} \sin\theta\cos\varphi & \sin\theta\sin\varphi & \cos\theta \\ \cos\theta\cos\varphi & \cos\theta\sin\varphi & -\sin\theta \\ -\sin\varphi & \cos\varphi & 0 \end{bmatrix} \begin{bmatrix} A_x \\ A_y \\ A_z \end{bmatrix} \qquad \textbf{3-23}$$

For the Monopole structure, $A_x = A_y = 0,$ so equation 3-23 reduces to

$$A_r = A_z \cos\theta \ , \qquad A_\theta = -A_z \sin\theta \ , \quad A_\varphi = 0$$

And using the Monopole symmetry (no variations in φ), equation 3-22 can be expanded in spherical coordinates and written as

$$H = \widehat{a_\varphi} \frac{1}{\mu r}\left[\frac{\partial}{\partial \mathrm{x}}(\mathrm{r}A_\theta) - \frac{\partial A_r}{\partial \mathrm{x}}\right] \qquad \textbf{3-24}$$

Using the above equation, the radiation pattern (field) of the Monopole can be calculated as

$$E = \eta \, . H \qquad \textbf{3-25}$$

3.3.2 Limitation of MOM and Pocklington Integral Equation Technique

The above section details the calculation of input impedance and electric field from Pocklington integral equation of wire length *l* and radius *a* using the MOM technique. One

of the fundamental problems in predicting the electromagnetic field generated by a semi rigid co-axial wire "Monopole" at a particular point in space using the conventional MOM technique is that it requires[71, 75] a large amount of computation *(N x N)* as the accuracy of the numerical result is directly proportional to the number of basis functions *N* involved[76]. In addition, the MOM technique cannot be easily employed for applications involving media other than freespace, such as medical imaging application which require the use of lossy medium[44, 51]. Because of the conductive nature of the lossy medium the current prediction along the wire using the MOM technique becomes very laborious. More specifically $(N \times N)^2$ computations are required.

The extent of the limitation of the traditional MOM technique is directly proportional to the number of basis functions involved. In antenna field calculations this limitation is related to the segmentation of the wire. As the segment length Δ decreases, the number of segments *N* increases. As *N* increases, the accuracy of the current distribution along the wire increases, however this also increases the complex nature of the matrix equation involved, and this will in turn increase the computational time from $N \times N$ to $(N \times N)^2$ thereby increasing the computational time. This limitation of the MOM technique increases as we address the issue of field calculation of antenna in conducting media. In a conducting medium the dielectric property of the medium is complex[77] and it takes into account the loss tangent of the medium. Thereby the propagation constant *k* will be of complex nature, normally

$$k = k' + jk''$$

In order to address the limitations of the MOM technique for current distribution calculation, a new mathematical model is proposed. A new technique has been proposed to

model the current across a Monopole antenna. The proposed model requires only the knowledge of three parameters for the prediction of the current along the wire, hence reducing the computational time drastically as its results do not depend on the number of functions involved. Also, the new model will be useful to predict the antenna fields and impedance in different lossy media easily. Consequently this technique can be used in field prediction for antennas employed in medical imaging applications.

3.4 New Mathematical Model

The new model aims to reduce the computational time and the tedious nature of the MOM equations explained in the previous section. The expression for the new model is given below in equation 3-26

$$I(z) = I_0 e^{-\alpha z} \sin(k(l-z)) + f(z,\tau) \qquad \textbf{3-26}$$

Equation 3-26 consists of two parts; the first part,

$$I_0 e^{-\alpha z} \sin(k(l-z))$$

accounts for the damping in the current distribution curve of Figure 3-6. This characterises the effect of the surrounding medium of the wire. The current distribution curve in Figure 3-6 is of the wire of length λ/2 in freespace. In this case the damping coefficient α is zero and its value changes as the surrounding medium changes. This is very effective for applications involving lossy media with complex dielectric properties, such as medical imaging applications.

This part also provides the overall shape of the current distribution curve in Figure 3-6. This part of the equation is similar to that of the current distribution expression given in[71]. The final part of the expression is given as,

$$f(z,\tau) = \begin{cases} d_0 + \frac{\tau}{4}\sin\big(2k(l-z)\big)\,, & for\ l = (2w+1)\,\frac{\lambda}{4} \\ d_0 + 2\tau\sin\big(2k(l-z)\big), & for\ l = 2w(\lambda/4) \end{cases}$$

Where d_0 is the dc component and w is a positive integer. This part accounts for the variation due to the radius of the wire; it acts like the dc term in the expression. It also provides the delay element in the current distribution curve in Figure 3-6.

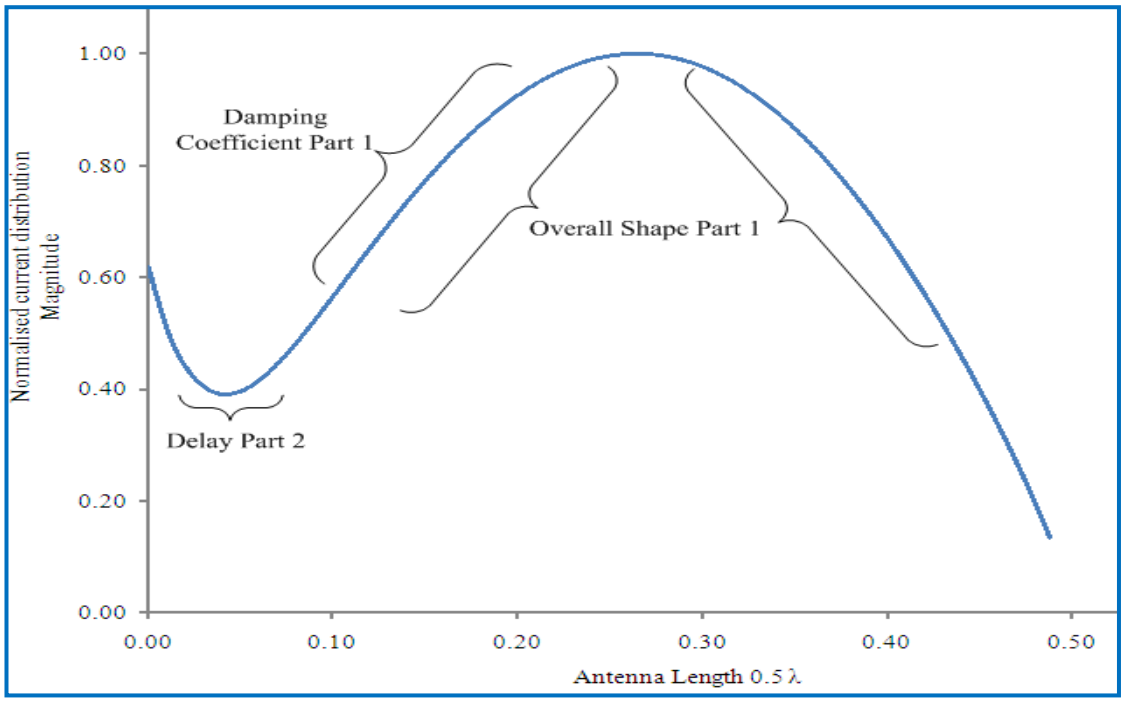

Figure 3-6 Current distribution curve of the semi rigid coaxial wire of length λ/2

This new mathematical model decreases the computational time as it depends on only three parameters; Initial current I_0, damping coefficient α and radial parameter τ. The initial current I_0 is the current at the first segment of the wire, the damping coefficient α

characterises the conductivity of the surrounding medium. It is this parameter of the expression which makes this model suitable for the predicting the current distribution of the wire in different surrounding media other than freespace. And finally, τ is a parameter related to the radius of the wire.

3.4.1 Input Impedance and Radiation Pattern Calculation using New Model

The ability to predict the current across the Monopole using this new mathematical model has been analysed by predicting the current distribution of two different lengths of wire. Lengths of one quarter wavelength (λ/4) and three quarter wavelength (3λ/4) Monopoles are considered.

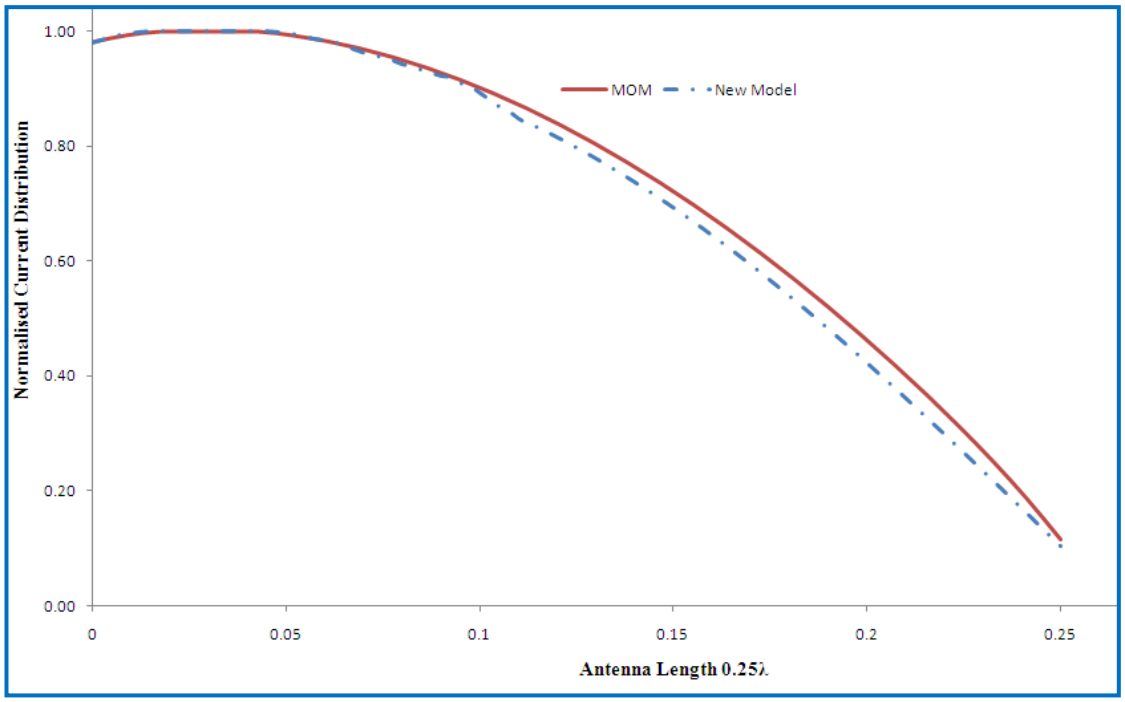

Figure 3-7 Current distribution curve of the semi rigid coaxial wire of length λ/4

The predicted current distributions of the above lengths of wire using conventional techniques were available to compare with the results from the new mathematical model. Antenna radius *a* is given as 0.005λ and the outer radius *b* is related to the inner radius by *b = 2.3a,* and the wire is considered along the *z* axis. For the conventional method the number of basis function is kept at 80, i.e. the wire along the *z* axis is discretised to 80 segments.

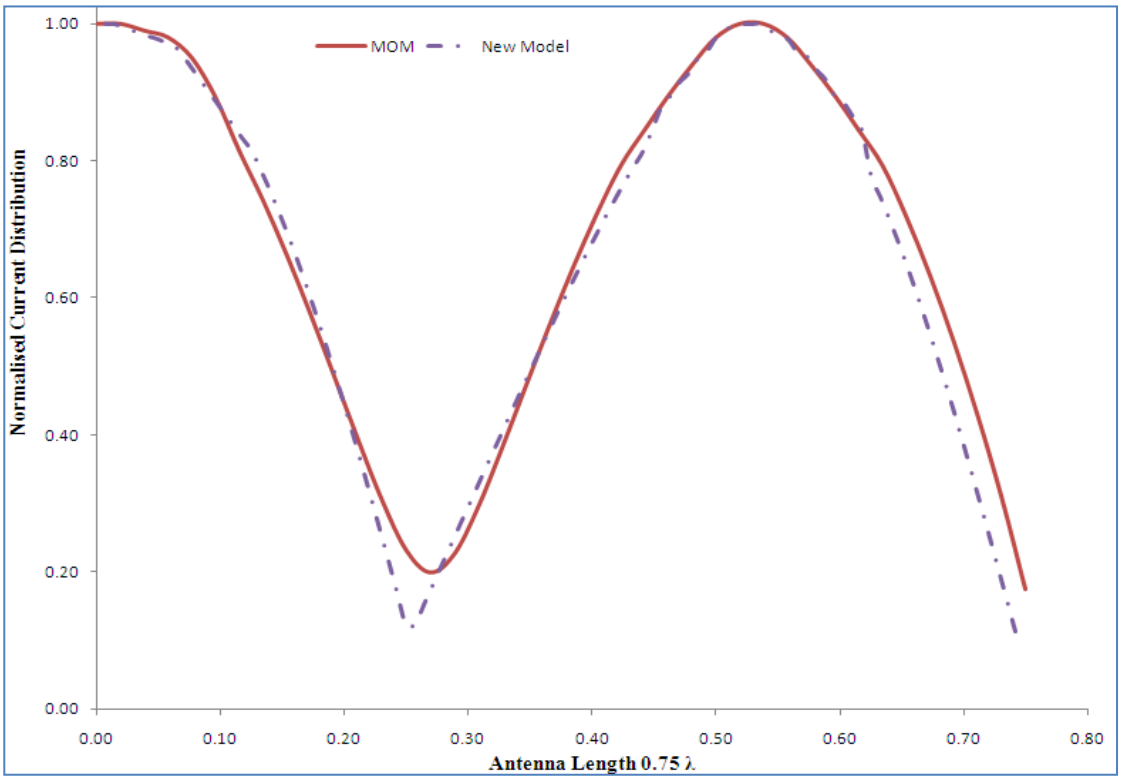

Figure 3-8 Current distribution curve of the semi rigid coaxial wire of length 3λ/4

The specific discretization places a limit on the accuracy of a numerical result for a fixed number of basis and testing functions and determines whether or not the numerical result will converge to the exact solution as the number of basis and testing functions is increased. For antenna length of quarter wavelength (λ/4) and three quarter wavelength (3λ/4), discretizing the antenna into 80 segments begins the convergence of the numerical

results to the exact solution. This is achieved by the small discontinuity between segments as the phase shifts between segments will be only 4° (360/80) for 80 segments per wavelength model. The initial current parameter I_0 of the new model is measured for different lengths of the antenna. Using these initial current values the other two parameters, damping coefficient α and radial parameter τ are calculated by optimization.

Figure 3-7 and Figure 3-8 show the result of both MOM and the new model. As it shows there is a good correlation between the two techniques for the two different lengths of wire. From the current values across the wire, input impedance and the electric field at point *P* in Figure 3-5 can be calculated using the same equations as for the Pocklington integral equation technique. Thus the electric field of a Monopole can be calculated using our new model; because of the less complex nature of the new model and its flexibility to predict the current distribution in media other than freespace (damping coefficient α), this can be extended to surroundings involving lossy medium.

3.5 Advantages of Proposed New Model

This new model offers several advantages compared to that of the MOM technique. As the limitations of the traditional method discussed in Section 3.3.2, the computational time is very high as the accuracy of the model depends on the number of basis functions used. However this limitation is eliminated in the new model as the model accuracy does not depend on the number of basis function which in turn reduces the computational time.

For the traditional method consisting of 80 basis functions the time to predict the antenna characteristics is 20 minutes in freespace and this time increases considerably when the workspace is different to that of freespace, such as vegetable oil and water. Using the new model the antenna characteristics are predicted in less than one minute. The new model only depends on three parameters the initial current I_0, α the damping coefficient and τ the wire radius parameter. This allows the new model to be easier to calculate and predict the current across the wire in comparison with the old model. Another advantage of this model is the ease at which it can be used for applications involving complex media like medical imaging applications.

As discussed in Section 2.2, the dielectric constant for a lossy medium is complex in comparison to a purely real dielectric constant in freespace. In the traditional method this increases the computational time from $N \times N$ to $(N \times N)^2$. However the new model only needs to adjust the damping coefficient in order to accommodate the complex dielectric constant. This makes the new model very effective in predicting the current across the wire in application involving complex media. The above advantages make the new model very effective in comparison with the traditional approach.

3.6 Summary

In this chapter the existing MOM technique is used to predict the current across the Monopole which has been discussed in the initial section. The Pocklington Integral equation, with the use of equivalence principle is used to take into consideration the effects of the coax in the current distribution. Using the current distribution across the Monopole,

expressions to predict input impedance and radiation pattern are also calculated and presented. The limitation on the old model is also well documented.

Section 3.4 begins with the problem statement associated with the limitation of the traditional approach to predict the current across the Monopole and thereby the complications involved in calculation of input impedance and radiation pattern values. The novel mathematical model for current prediction across the Monopole has been presented. The new model aims to reduce the computational time and the tedious nature of the MOM equations from 20 minutes to one minute. The expression for the current across the wire using the new model only depends on three parameters; the initial current I_0, α the damping coefficient and τ the wire radius parameter. This allows the new model to be easier to calculate and predict the current across the wire in comparison with the old model.

The predicted results for current across the Monopole for different antenna length are presented and compared with the results obtained from the traditional approach. The graphs show a high degree of agreement between the two methods. The advantage of the new model in comparison with the old model is also presented.

In the following chapter the application of the new model to predict the input impedance and radiation pattern of the Monopole is presented, together with a comparison of the simulation of the mathematical procedure involved and the experimental results. Furthermore the challenge facing the complex lossy medium is highlighted and the new model is extended to antenna characteristics prediction in workspace of complex permittivities.

Chapter 4 Validation and Applications of New Model for Monopole Measurements in Freespace and Complex Permittivities

4.1 Introduction

In Chapter 3 the traditional technique for calculating the current across the wire using the MOM technique and Pocklington integral equation was presented. It was shown how the input impedance and radiation pattern could be calculated from the current distribution along the Monopole. In Section 3.4 the novel mathematical model to predict the current across the wire was also presented. The results were then verified by comparison with the standard MOM technique. The model has been shown to produce results to the same standard as the traditional complex Pocklington integral equation method but with significantly reduced computational time. This signifies that the novel technique developed can be used to replace the complex and extensive MOM required for predicting Monopole measurements.

This chapter begins with the validation of the new model. In Section 4.2 the results predicted for a dipole antenna by the new model are compared for validation purposes with the results from Tsai's experiment. This chapter focuses on Monopole measurement system, the measurement of the antenna input impedance and radiation patterns in freespace and complex permittivities environments. The outline of the Monopole measurement system is given in Section 4.3, detailing the component structure and the

methodology used for measurement. The initial system is constructed for measuring antenna patterns in freespace. The input impedance and radiation patterns in a freespace environment are also discussed. Section 4.4 details the Finite Difference Time Domain (FDTD) simulation software used to simulate the antenna measurements in freespace, along with its advantages. The results from the theoretical method from Chapter 3 and the experimental and simulation results from this chapter are compared and analysed in Section 4.5.

The effective use of the Monopole in applications such as medical imaging and subsea engineering highly depends on the ability of the Monopole to function within environments of complex permittivities. The parameter which controlled this, ε_r, is the relative permittivity of the lossy media. The relative permittivity of the freespace environment is 1; however, the relative permittivity of the lossy media used in medical and subsea applications will be different and is often a complex permittivity as discussed in Section 4.6.

Sections 4.6 to 4.9 detail the efficient use of the new model by employing it in surroundings different to that of freespace. Monopole measurements are predicted using the new model in two different media: vegetable oil and water. Vegetable oil and water are chosen for this investigation as they exhibit properties of low and high conductivities respectively. Broadly speaking, conductivity σ of the lossy media is related to the permittivity ε of the media by the following expression

$$\sigma = \omega\varepsilon$$

where ω is the angular frequency. Detailed properties of the two different medium is discussed in Section 4.6. Monopole measurements predicted in vegetable oil, which has low conductivity values, are presented in Section 4.7.

The experimental arrangement for the vegetable oil measurements is detailed in Section 4.7.2. The predicted values are then compared with the simulated and experimentally measured data and presented in Section 4.8. The next section of this chapter discusses the effect of a high conductivity medium, such as water, on the Monopole measurements. Again, the predicted results are compared with the simulated and experimental values in Section 4.9. Finally, a summary of the results obtained for the Monopole employed in freespace and complex permittivities is provided in Section 4.10.

4.2 Validation of the New Model

The new mathematical model is validated by comparing it with results obtained from Tsai's experiments[78]. Tsai conducted the experiments on measuring the dipole characteristics which was mounted symmetrically on a conducting sphere. The new model is validated by comparing the predicted values with the experimentally obtained results from Tsai's paper[78]. As we can see from Figure 4-1, the measured values correlate well with Tsai's result. The new model values on the graph have been predicted from equation 3-26 using the input impedance. The conductance and susceptance values are calculated by inversing the resistance (real) part and reactance (imaginary) part of the input impedance. Tsai's measurement has been conducted with the antenna above a conducting sphere; however, the numerical model assumes the ideal antenna condition i.e., antenna above a

flat ground plane. This attributes to the differences in the conductance values at 0.25 *h/λ*. This validates the new model used in measuring the input impedance and it provides a confidence in the model used and the results obtained using it. In the following sections the new model is used in predicting the Monopole characteristics in freespace and in complex permittivities.

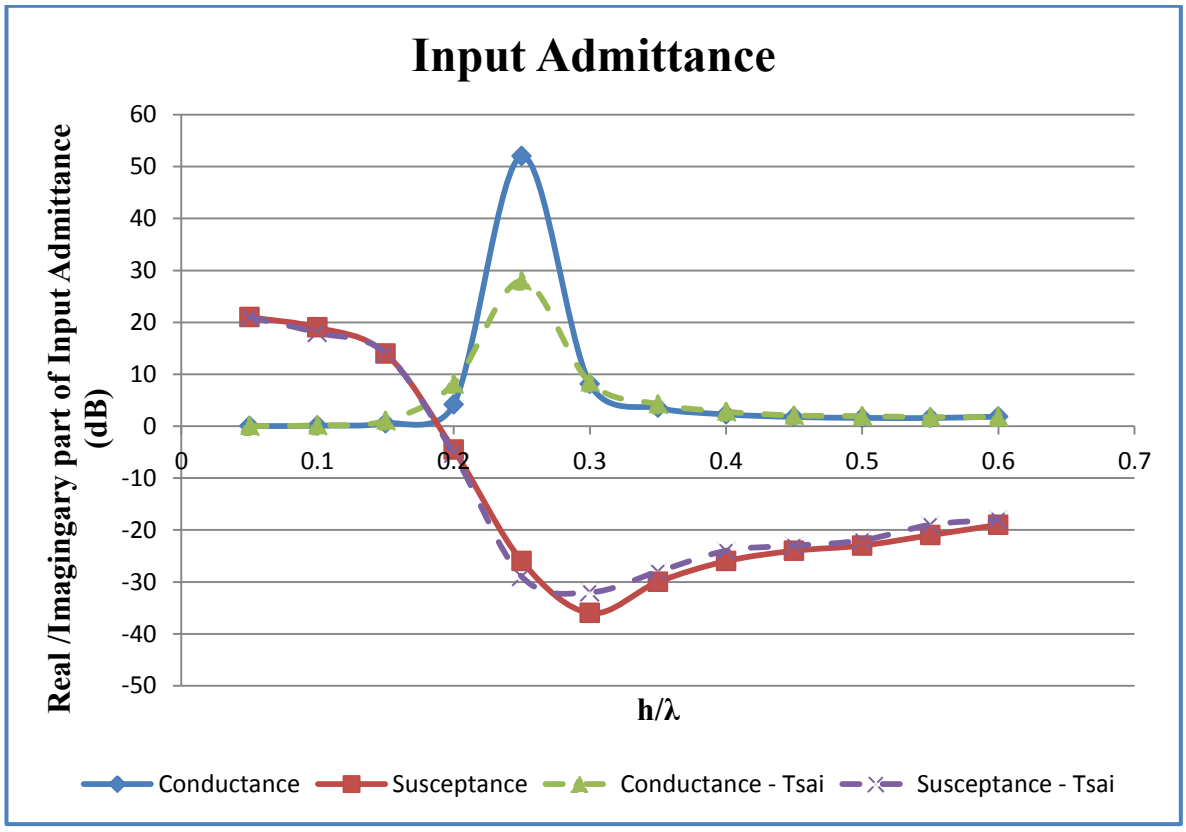

Figure 4-1 Comparison with Predicted and Tsai's Experimental Results

4.3 Monopole Measurement System Design and Results

This section details the design setup of the Monopole measurement system and the parameters associated with the setup are listed and reasoned. The results obtained in

freespace using this arrangement are also presented. Measurements such as radiation patterns and input impedance for the Monopole in freespace are carried out in an experimental setup enclosed by an anechoic chamber. The anechoic chamber is lined with microwave absorber material; this absorbs the microwave energy when radiated at it, thereby avoiding reflections. This helps in obtaining results which are free from reflections and background radiation.

4.3.1 Design Parameters and Setup

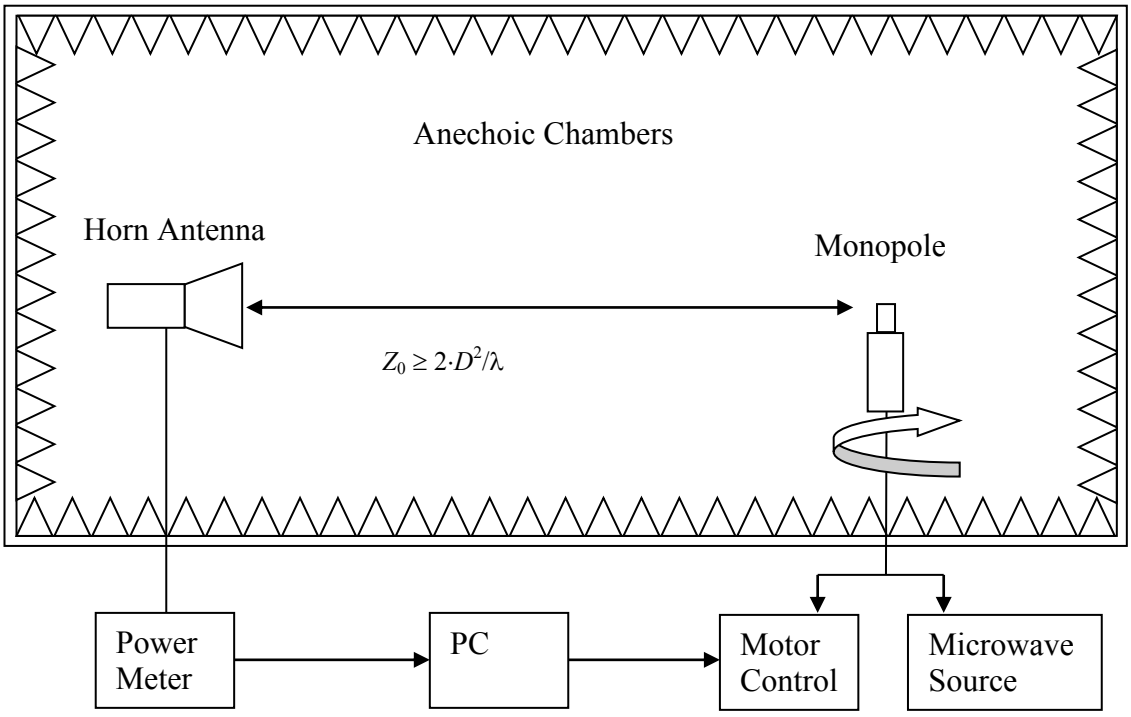

Figure 4-2 Experimental arrangement of the Monopole measurement system (Azimuth)

Figure 4-2 shows the experimental arrangement of the Monopole measurement system. The radiated fields from the Monopole are received by a Pyramidal Horn antenna, which is

used as the receiving antenna. The Pyramidal Horn antenna should be mounted such that the E-plane is parallel to the Monopole, with the antennas perpendicular to each other. The tip of the Monopole is positioned at the same height as the aperture centre of the Pyramidal Horn antenna. The separation distance between the Monopole and the receiving antenna is determined by the frequency of operation. To ensure being in the far radiation field of the Monopole a minimum of $2D^2/\lambda$ is used[68]. The values for the Pyramidal Horn antenna are taken from the data supplied by the manufacturer. Table 1 lists out some of the properties of this Pyramidal Horn antenna.

The Monopole is constructed by removing the outer conductor of the semi rigid coaxial cable and leaving quarter wavelength of the inner conductor to as the Monopole for experimental purposes; the inner conductor was of length 7 mm and frequency 10.5 GHz. A photo of the Monopole antennas constructed using the semi rigid coaxial cable is shown in Figure 4-3.

Antenna	Flann Microwave Pyramidal Horn Model 16240	
Plane	E-Plane	H-Plane
Aperture Size (m)	0.079	0.109
Frequency Band	X-Band 8.2-12.5 GHz	
Frequency of Operation	10.5 GHz	

Table 1: Antenna properties

Figure 4-3 Photo of the Monopoles constructed using the semi rigid cable

The radiation pattern measurements for the Monopole are conducted in both azimuth and elevation planes. The Monopole arrangements shown in Figure 4-4 is used for elevation and azimuth pattern measurements. The antenna structure is rotated 360˚ around the longitudinal axis for azimuth and 180˚ around the aperture plane for elevation rotation. The rotating is computer controlled using LabVIEW v7.2. The software controls the stepper motor via the motor control unit, which in turn rotates the Monopole.

The azimuth and elevation plane measurements were taken at 10˚ intervals. At the receiving end of the measurement system the Pyramidal Horn antenna receives the transmitted signal and the power meter connected to the Horn antenna displays the energy level recorded. The same LabVIEW software is also programmed to collect the

measurements through a General Purpose Interface Bus (GPIB) cable and store the data for analysis purposes. A picture of the measurement system along with each component labelled is shown in Figure 4-5.

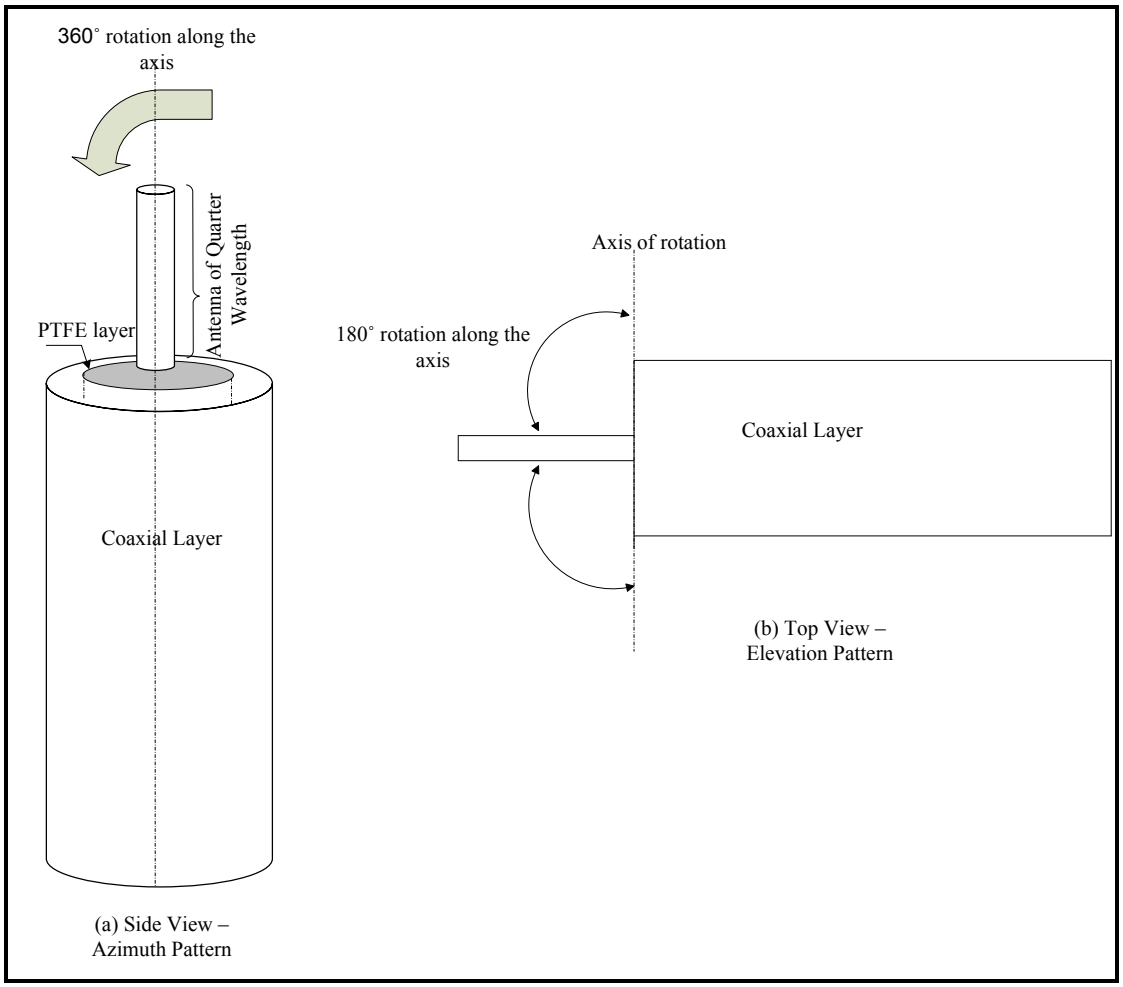

Figure 4-4 Antenna position for azimuth and elevation pattern measurements

Figure 4-6 shows the difference in setup when measuring the elevation pattern in comparison with Figure 4-2 of azimuth pattern. In this case the antennas are parallel to each other, with the Monopole in line with the aperture centre of the Horn antenna. In this case the E field of the antenna is horizontal to align with the field of the Monopole. Table 2 provides a summary of the measurement parameters that have been defined above.

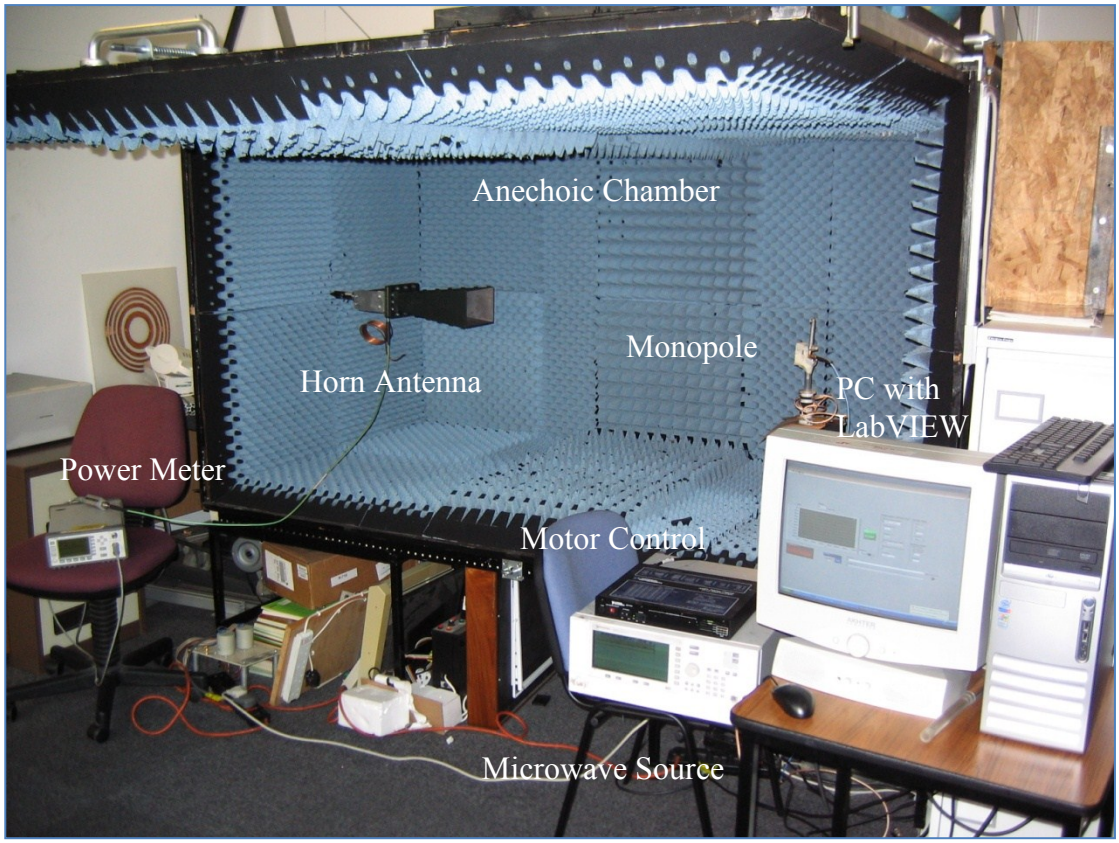

Figure 4-5 Photograph of the measurement system

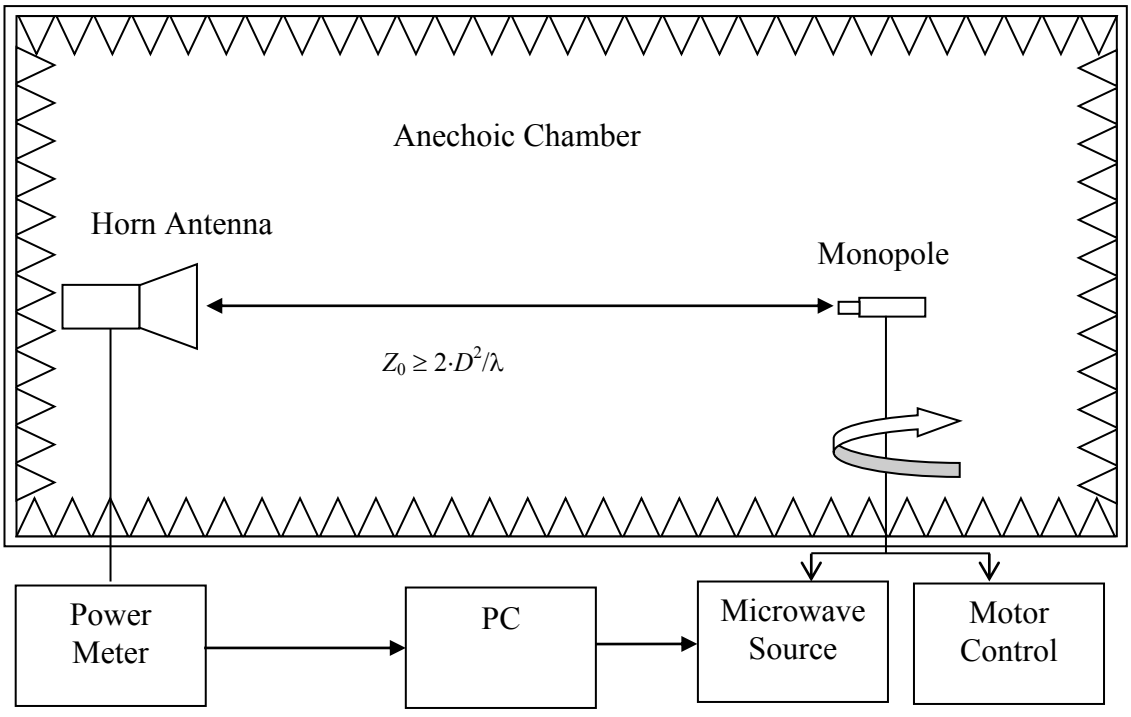

Figure 4-6 Elevation pattern arrangement

Parameter	Specification
Transmitting Antenna	Monopole
Receiving Antenna	Flann Microwave Pyramidal Horn Model 16240
Outer Conductor of Monopole	Quarter Wavelength
Frequency	10.5 GHz
Elevation Pattern measurement	180˚
Azimuth Pattern measurement	360˚

Table 2: Parameters for Monopole Freespace measurement

4.3.2 S-Parameter Measurement

S-Parameters are vector quantities which represent reflection and transmission coefficients. Reflection coefficients relate to quantities such as Voltage Standing Wave Ratios (VSWRs) and impedances, whereas transmission coefficients are generally referred to as gains and attenuations. S-Parameters are vector quantities which relate to the power associated with the inputs and outputs of a black box. For a 2 port network, there are four possible S-Parameter quantities that can be derived. They are: S_{11}, S_{12}, S_{21} and S_{22}. $|S_{11}|^2$ indicates the fraction of the input power at port 1 that is reflected at port 1, also known as reflection coefficient. And the fraction of input power at port 1 that is transmitted is $|S_{21}|^2$. Similarly, the fraction of incident power at port 2 that is reflected at port 2 is $|S_{22}|^2$ and the fraction $|S_{12}|^2$ is transmitted at port 2[79].

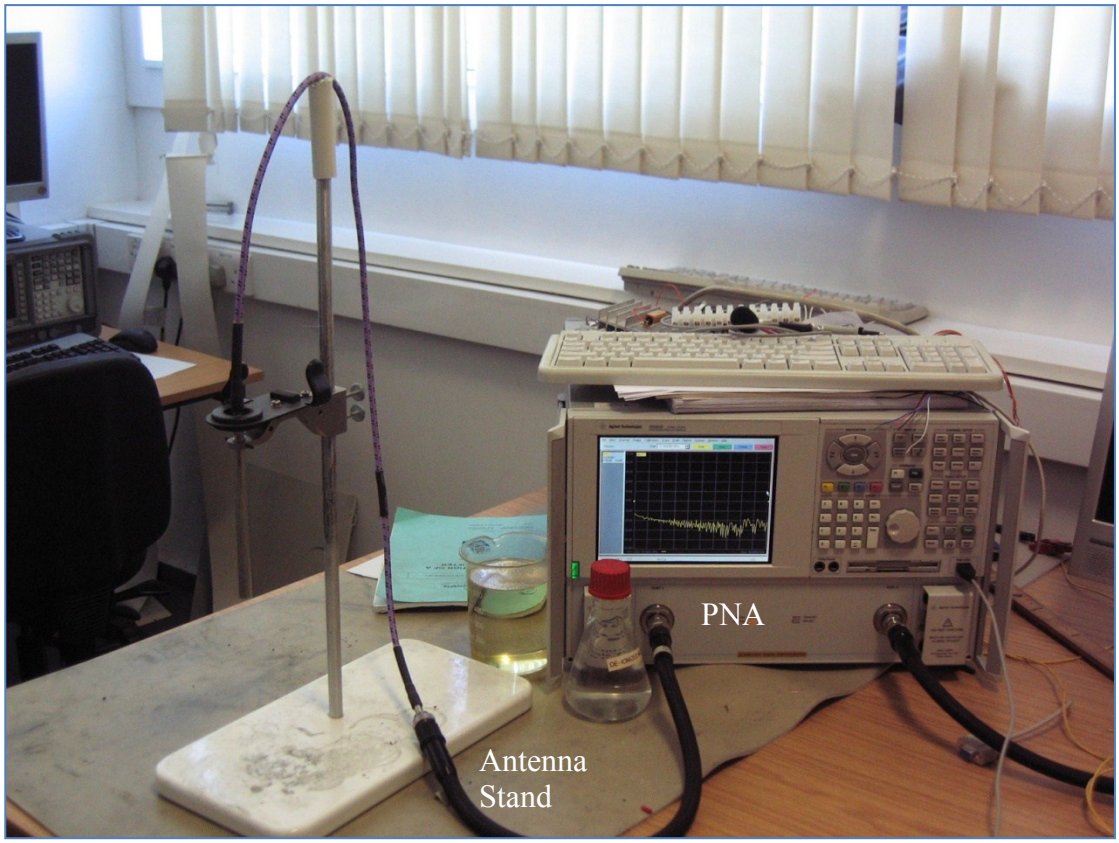

Figure 4-7 S-Parameter measurement system setup

Since the research involves identifying the antenna characteristics of the Monopole, the system setup will be considered as a 1 port network and thereby the only quantity which is of interest is S_{11}. If the value of S_{11} is zero then it indicates that all the power is reflected from the Monopole and thereby none is radiated. One the other hand when S_{11} is -10 dB the total power reflected will be 10% of the input power which implies the rest of power is radiated or dissipated and thus the Monopole will be a low loss antenna.

Figure 4-7 shows the measurement system involved in measuring the S-Parameters of the Monopole. The Monopole is suspended from the antenna stand and it is connected to the Performance Network Analyser (PNA). The PNA is used to measure the S_{11} and prior to

the measurement the PNA is calibrated to the required frequency of operation. The calibration procedure is performed to eliminate all sources of systematic errors inherent in the PNA measurement system. Calibration is generally performed using the mechanical calibration kit. The calibration kit consists of four basic standard types that are used for PNA, namely Short (zero ohms), Open (infinite ohms), Load (System Impedance) and Thru or Line (no terminal impedance).

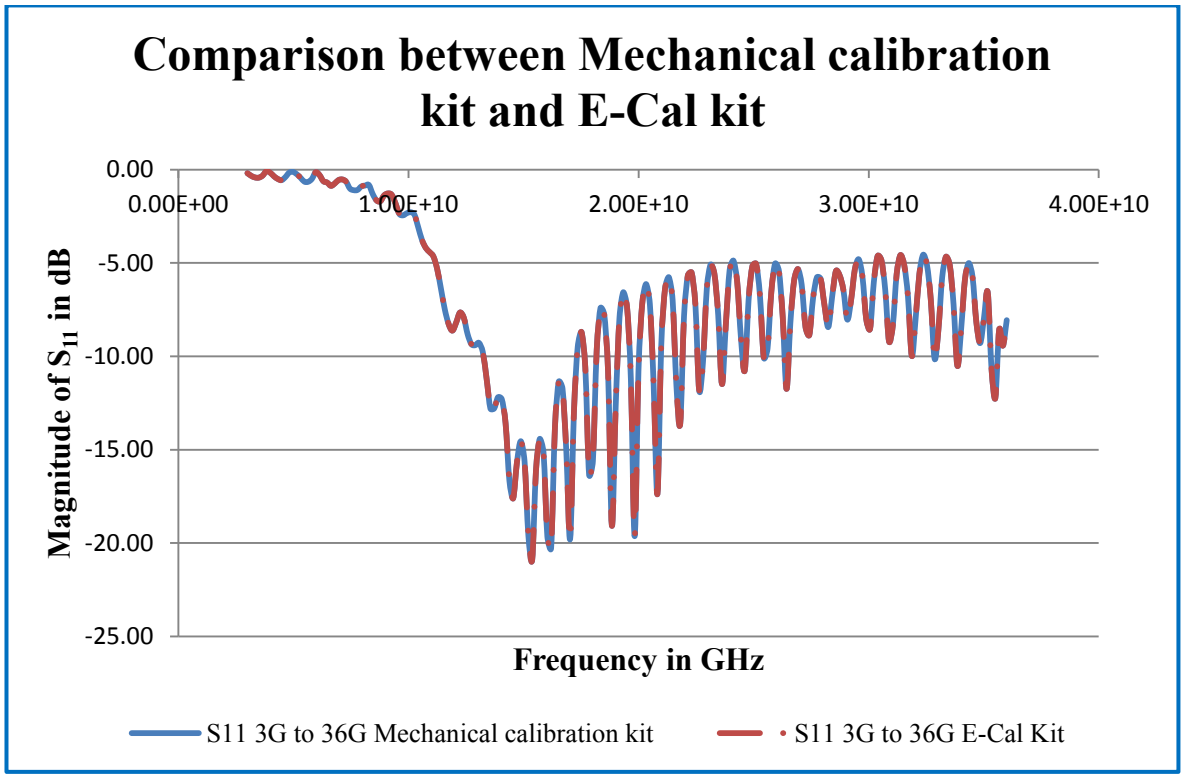

Figure 4-8 Comparison of Mechanical calibration kit and E-Cal Kit

Each of these standards has a predetermined magnitude and phase response as a function of frequency. The reference for error corrected measurements in the PNA is provided by the calibration standards and stored within the PNA. During measurements the analyser measures standards and mathematically compares the results with the ideal models of those

standards and thereby providing error corrections in measurements. In recent years, several PNA manufacturers have developed an electronic calibration kit which performs the same operation as the mechanical calibration kit without the need for the individual standard types. E-Cal is one such calibration kit which is developed for calibrating PNAs. Figure 4-8 shows the S_{11} magnitude measurement of a Monopole antenna operated between 3 and 36 GHz, which has been obtained after calibrating the PNA using mechanical calibration kit and the E-Cal kit. As it can be seen from the figure, both the calibration kits provides exactly the same pattern for the magnitude of S_{11}. The above result has provided confidence in the E-Cal kit and it has been used for all further measurements in this thesis.

4.3.3 Input Impedance Measurement

According to Balanis, input impedance is defined as the "the impedance presented by an antenna at its terminals or the ratio of voltage to current at a pair of terminals or the ratio of the appropriate components of the electric to magnetic fields at a point"[68]. In this section, the input impedance is given as the impedance at the antenna feed. It can be calculated as the ratio of voltage to current at the antenna feed. Direct measurements of input impedance are difficult. Using calibrated PNA it is possible to determine input impedance from the complex reflection coefficient (S_{11}) measurements.

The reflection coefficient is represented by Γ and is a complex quantity which has a real and imaginary part. The reflection coefficient at the input and load can be given as Γ_{in} and Γ_L respectively. In the experimental setup shown in Figure 4-9 the reflection coefficient is

calculated at the load position. Figure 4-9 illustrates the relation between the reflection coefficient at load and the input.

The reflection coefficient at the input position can be calculated using the values of return loss at load using the following expression

$$\Gamma_{in} = \Gamma_L e^{-j2\beta l} \qquad \textbf{4-1}$$

where l is the length of the Monopole and β is the propagation constant and is given as

$$\beta = \frac{2\pi}{\lambda}$$

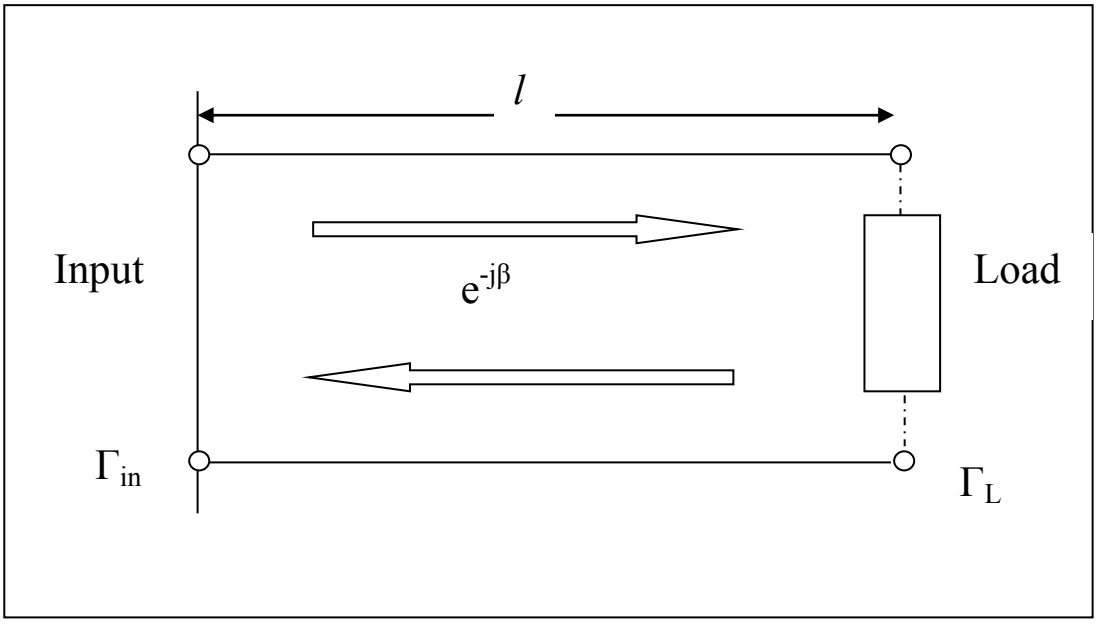

Figure 4-9 Reflection Coefficient Illustration

where λ is the wavelength. Let Γ_{rin} and Γ_{iin} be the real and imaginary parts of Γ_{in}. Then the real part of the input impedance can be calculated using the following expression

$$r = \frac{(1 - {\Gamma_{rin}}^2 - {\Gamma_{iin}}^2)}{(1 - {\Gamma_{rin}}^2) + {\Gamma_{iin}}^2} \quad \textbf{4-2}$$

And the imaginary part can be calculated by

$$x = \frac{2\Gamma_{iin}}{(1 - {\Gamma_{rin}}^2) + {\Gamma_{iin}}^2} \quad \textbf{4-3}$$

So the input impedance can be given as

$$z_{in} = r + jx \quad \textbf{4-4}$$

And if the characteristic impedance Z_0 is known then the normalised impedance can be calculated as

$$Z_{in} = R + jX$$

where

$$R = r.Z_0 \text{ And } X = x.Z_0$$

Thus the input impedance of the Monopole can be obtained using the reflection coefficient values measured experimentally. However equations 4-2 and 4-3 can be transposed to obtain the values of reflection coefficient, given the input impedance of the antenna is known. These interchangeable qualities of the reflection coefficient and input impedance can be used in comparison of results. In the theoretical method the input impedance is predicted, however, in the experimental and simulation techniques the reflection

coefficient is obtained from the measured S-Parameters. Therefore when comparing results for validation purposes, the predicted input impedance is converted to its corresponding reflection coefficient value before comparison. Comparison results of the three techniques are presented in Section 4.5.1.

4.3.4 Radiation Pattern

Figure 4-10 shows the regions around an antenna, where D is the largest dimension of the antenna and λ the wavelength of operation. As can be seen, the regions are classified as the Fresnel region and the Fraunhofer region (far field)[18]. The Fresnel region can be sub-divided into the reactive near field region and the radiating near field region; depending on the distance from the antenna. Mathematical expressions for the region boundaries were formulated based on the dimensions of the antenna and frequency of operation.

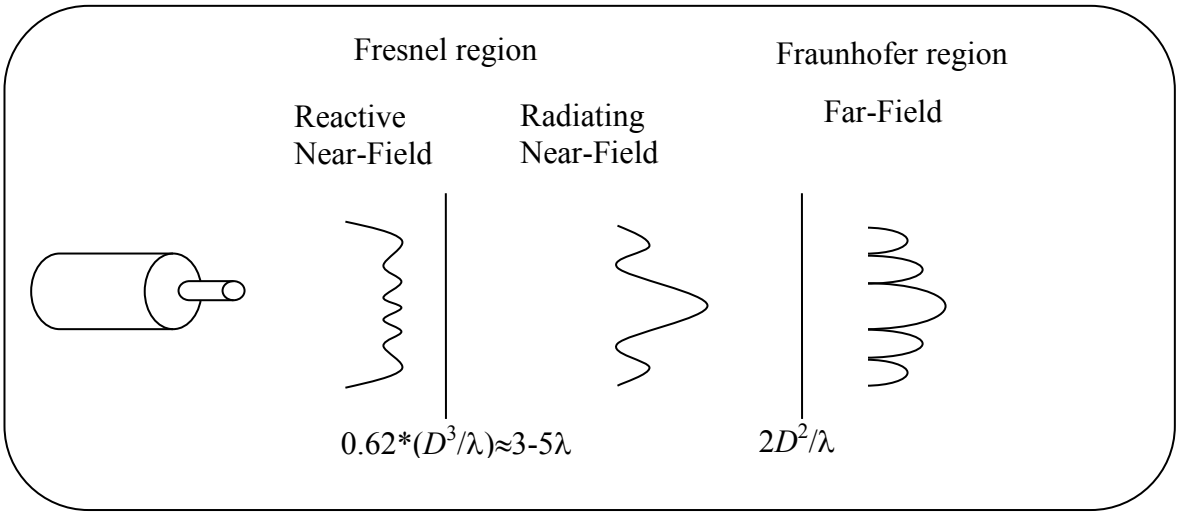

Figure 4-10 Regions of an antenna

The reactive near field extends up to $0.62*(D^3/\lambda)$, which is approximately equal to 3-5λ. And the far field of the antenna starts roughly from $2D^2/\lambda$. So with the information on the antenna's largest dimension and the frequency of operation one can determine the regional boundaries of the antenna fields. These distances can help the designers to understand the behaviour of an antenna at a given distance[80]. Far field radiation pattern is the normal operating region of the antenna hence the measurement of antenna patterns are most commonly associated with obtaining far field patterns. The far field region of an antenna is defined as "that region of the fields of an antenna where the angular field distribution is essentially independent of the distance from the antenna"[18]. Antenna ranges are used in testing and evaluating antennas[71]. IEEE has published a comprehensive list of standard test procedures for antennas[81].

Antenna ranges can be categorised as outdoor and indoor ranges each with its own advantages and limitations. Direct measurements on a far field test range are the simplest way of obtaining the far field radiation pattern of an antenna. The distance between the antenna under test and the receiving antenna should be at least the distance of $2D^2/\lambda$ in order to be in the far field region as given in Figure 4-10. In this measurement system the far field radiation distance has been calculated as 0.8m. Relative power measurements are recorded as the antenna under test is rotated about its axis[71].

Indoor anechoic environments are developed to provide a controlled environment, shielded from outside sources and to minimise electromagnetic interferences. Currently there are two basic types of anechoic chamber designs: the rectangular chamber and the tapered chamber[82]. Tapered chambers are only used when absorbers' performances are not very

good. For this research purpose an indoor rectangular anechoic chamber is used and the frequency of the operation is usually varied between 8.5 and 12.5 GHz.

The inner walls of the anechoic chamber are lined with high quality RF absorber material in order to minimise the reflected energy. Figure 4-5 shows the rectangular anechoic chamber used in the radiation pattern measurement of the Monopole. The surface of a constant radius sphere is used to measure the radiation pattern of any given antenna. Spherical coordinate system (r, θ, and φ) shown in Figure 4-11 helps us identify any given position on the sphere, and because the radius distance r is a fixed quantity, we only need the other two coordinates (θ, φ) to identify a position.

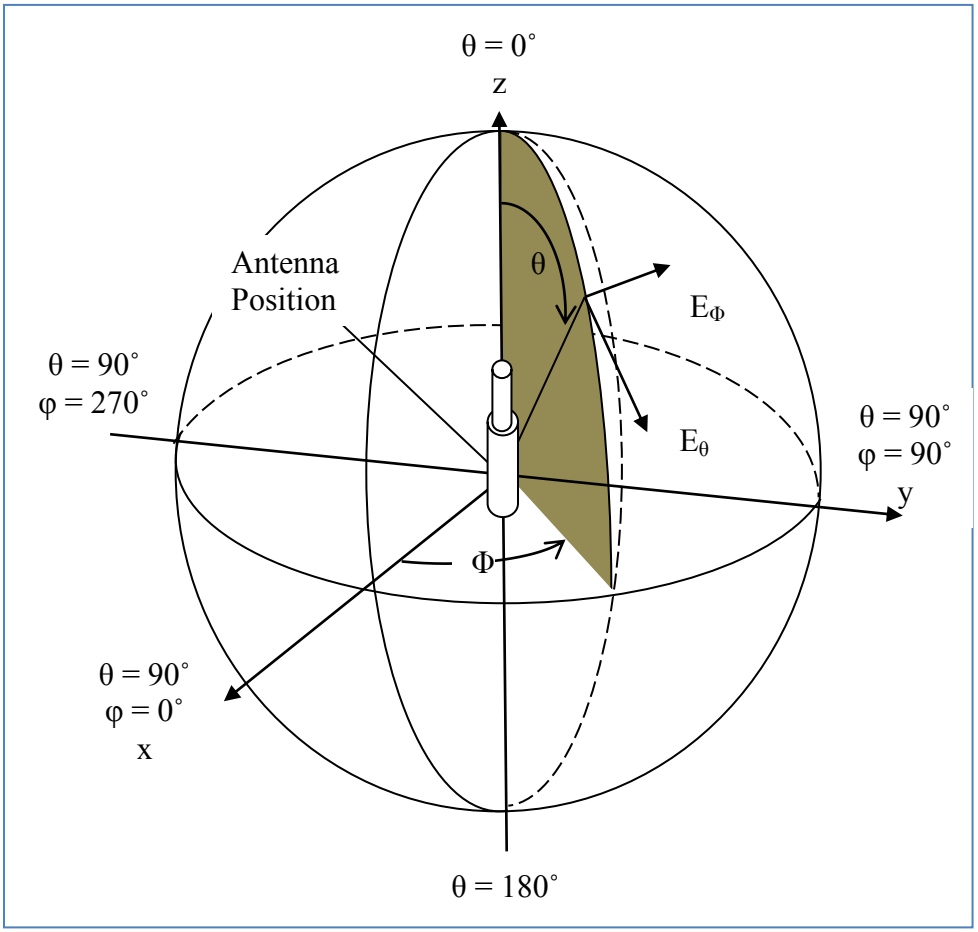

Figure 4-11 Spherical coordinate system

According to Balanis, “A representation of the radiation characteristics of the radiator as a function of θ and φ for constant radial distance and frequency is defined as the pattern of the antenna”[71] . Although an antenna pattern is a three dimensional quantity, a minimum of two two-dimensional patterns is usually obtained to represent orthogonal *E* and *H* planes. These two dimensional patterns are also called cuts, and they are obtained by fixing φ and varying θ between 0˚ and 180˚ and reversing them by have θ fixed and varying φ between 0 and 2π. These cuts are commonly referred to as elevation and azimuth patterns respectively.

4.4 FDTD Simulation and Advantages

Finite Difference Time Domain (FDTD) is a common modelling technique to solve Maxwell’s equations as a function of time in discrete time steps at discrete points in space. Since it is a time domain method, solutions obtained through this method can be used to cover a wide frequency range in a single simulation iteration. Kang Yee introduced this FDTD space grid time stepping algorithm in 1966[83]. Since then the FDTD has been developed into a popular numerical modelling method for solving scientific problems, ranging from electromagnetic wave interactions through microwave to biophotonics[84, 85]. Electromagnetic simulation software called Concerto V7 is used in this research to predict the antenna fields using the Quickwave simulator which runs the FDTD algorithm[86].

The advantages of FDTD include a simple and versatile modelling technique to solve Maxwell’s equation, robust numerical algorithms, ability to adapt any geometries and a

good scalability of computing resources as a function of simulation to volume size. Because of its ability to cover simple simulation iteration over a range of frequencies this method is useful for applications where resonant frequency is not known or broadband results are desired. Since this method calculates the E and H fields directly within the computational space it helps in presenting the results in electromagnetic displays and also no conversion algorithms are needed to convert from E to H field or vice versa. This method also allows the user to specify the materials within the computational domain, which means that this simulation can be used to predict fields from an antenna within media other than freespace.

4.4.1 Simulation Parameters and Procedures

Table 3 shows the flowchart with the stages of the simulation procedure involved in using this computational software package to predict the fields of the Monopole. Preprocessing is the first stage which encompasses the generation of a suitable model and setting global conditions. Frequency of operation, boundary conditions and specifying the materials are the global conditions which are set in this stage. Depending on the specific geometry under consideration, this task may be highly automated or may require many hours of human input and verification. The software comes with an in-house modeller which helps with the antenna design. The Monopole is designed to the same specifications as the antenna that was made for experimental measurements, which allows comparison of the results from two methods. Refer to Table 2 for the list of the parameters of the Monopole.

Preprocessing	
Set Global Conditions	Construct Model
Analysis	
Set Mesh Conditions	Simulate Model
Postprocessing	
Obtaining Results	

Table 3 Flowchart of the Simulation Process

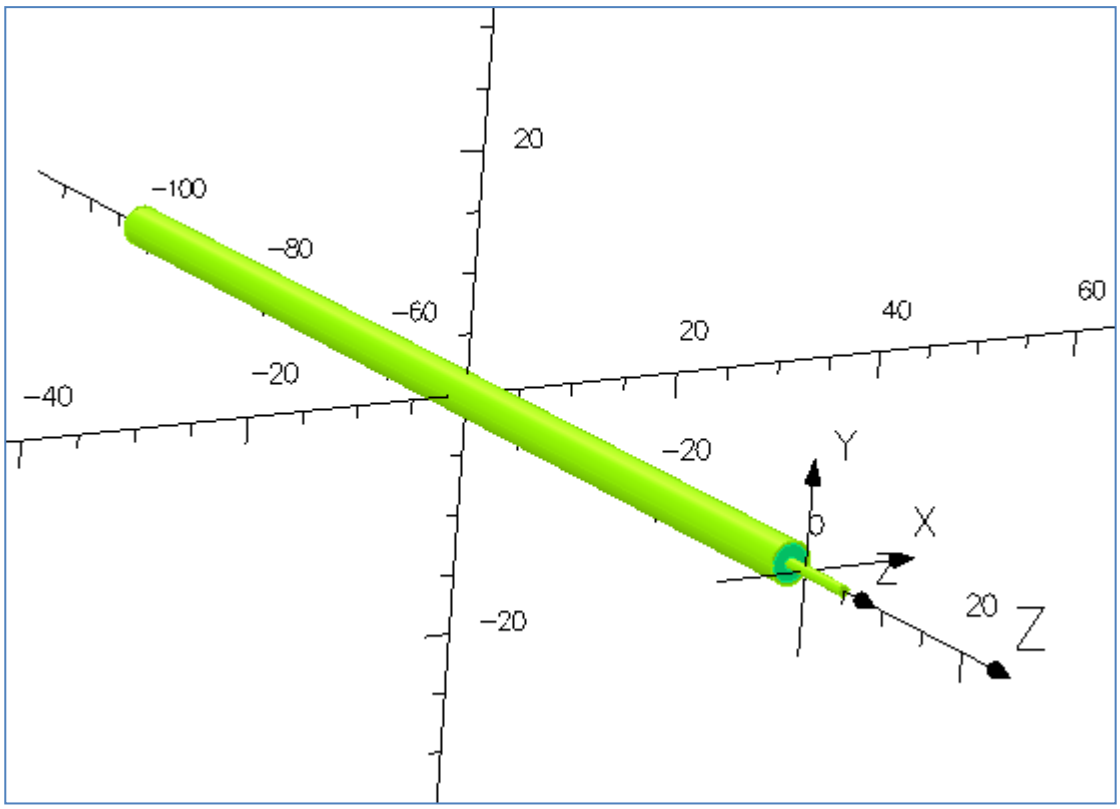

Figure 4-12 Monopole designed in the modeller

Figure 4-12 shows the Monopole designed using the modeller. As an aid to visualisation, the preprocessing stage is a data file containing the model in a form that is directly compatible with the main analysis routines.

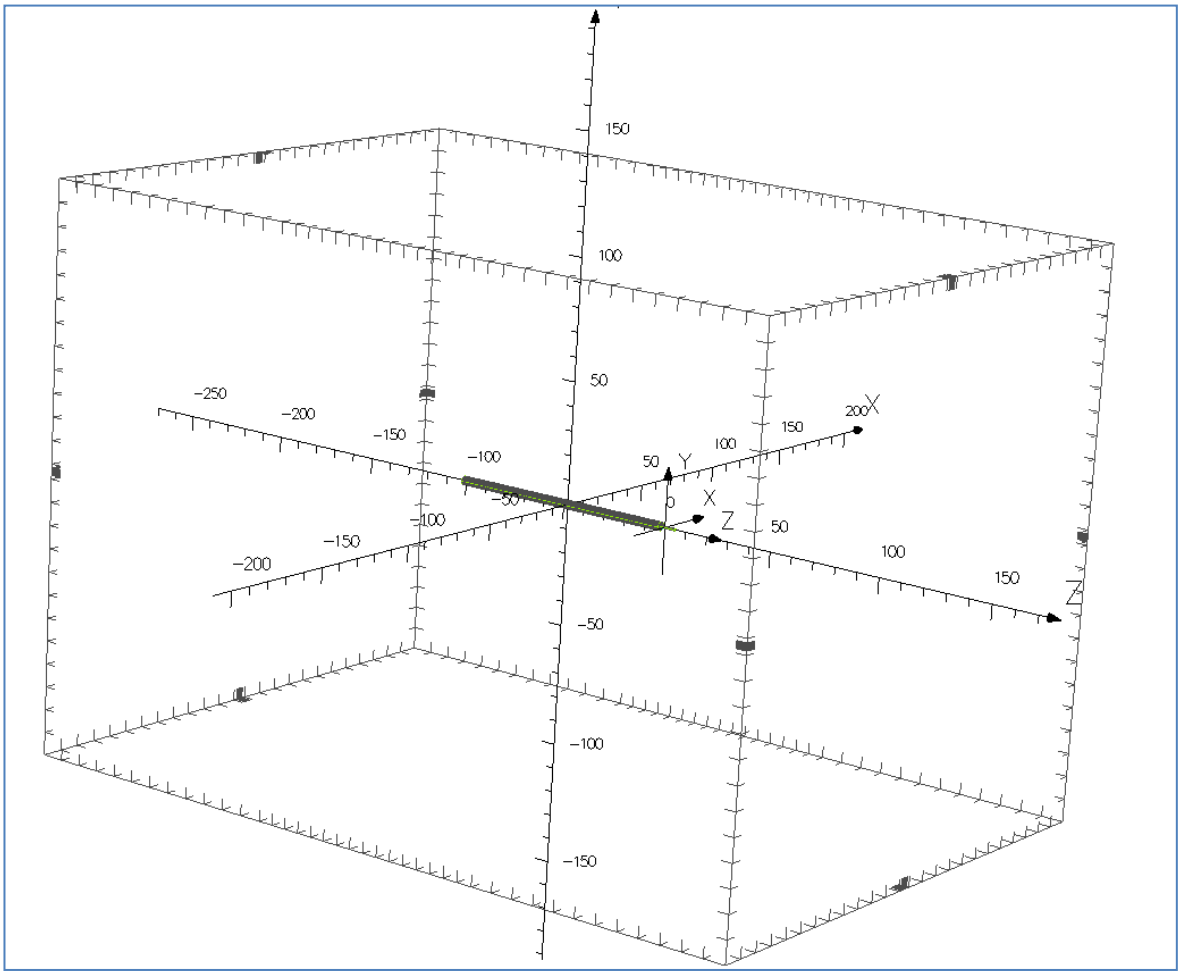

Figure 4-13 Monopole model within a mesh

Analysis is the second stage of the process. Once the Monopole is designed, the model is simulated within a perfectly matched layer (PML) mesh, absorbing boundary conditions to truncate the computational space at a finite distance without creating any reflections. This is also the stage where the mesh conditions are specified. The cells in the mesh have to be smaller than the smallest wavelength and the smallest feature in the model[87, 88]. Figure

4-13 shows the Monopole with the PML mesh. Once the mesh is in place the model is ready to proceed to the mathematical part of the analysis stage.

Analysis primarily consists of the creation and solution of a matrix equation. The analysis stage is computationally intensive but requires little human input or effort. Specialised calculations such as the scattering cross section computation may also be performed in the analysis stage. The output for the analysis stage consists of all numerical results arranged in data files in a fashion that may not be particularly convenient for interpretation. These results are collected and reorganised in the postprocessing stage.

Postprocessing is the final stage of the simulation procedure. Once the simulation process is completed the postprocessing stage helps the user to display the outcome of the simulation. Multiple windows displaying results for S-Parameters and field distributions can be created. This stage includes the generation of graphs, contour plots, colour plots, and colour pictures in order to permit the user to visualise and interpret the numerical results. The results of the Monopole obtained using the concerto simulation software are listed in the following section.

4.4.2 Simulated Results in Freespace

The result extraction phase starts after the model has been designed to specification in the geometric modeller. Once the model is ready and finalised, a series of analysis criteria are checked and inputted into the analysis option. Firstly it is the model excitation; the input and output of energy in models can be defined at ports. Ports are surfaces at which the

electromagnetic field of a particular mode enters or leaves the model. In the Monopole model the feed port is chosen as the dielectric face of the Monopole end and is given as a TEM (Transverse ElectroMagnetic).

Secondly, the analysis option allows the user to determine the frequency limits and the mesh size. Because of the FDTD simulation the software allows us to determine the frequency band for the simulation. The lower limit of the frequency band is chosen as 8.5 GHz and the upper limit as 12.5 GHz. This enables the results obtained from the single simulation iteration to yield results for every 0.5 GHz between 8.5 and 12.5 GHz. The frequency is chosen in accordance with the frequency of operation of the experimental setup where the receiving Horn antenna has the limitation of working in the X band (8.5 to 12.5 GHz).

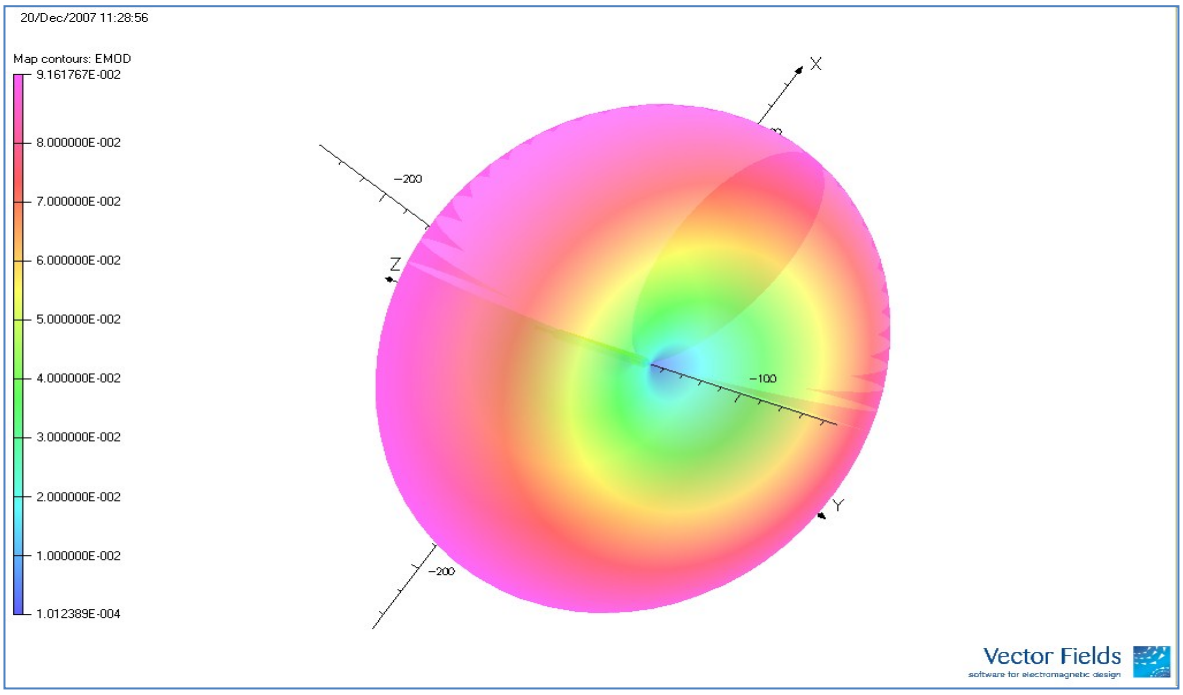

Figure 4-14 3D Representation of the Monopole radiation pattern

Thirdly the antenna material property; the Monopole is modelled exactly the same as the Monopole made with the semi rigid cable. So the antenna has two different materials: the outer cover of the antenna and the innermost wire (Monopole) are chosen as the Metal PEC (perfect electric conductor); the thin layer in between the two metal conductors is chosen as the dielectric layer with permittivity of 2.1, the same as that of the PTFE layer in the semi rigid cable.

Finally, choosing the background material; this determines the workplace around which the Monopole is placed. This option is particularly useful when analysing the Monopole within materials other freespace, as it enables the user to simulate the model in user-defined background material. Initially for the Monopole analysis the background material is chosen as air. Figure 4-14 shows the 3D representation of the radiation pattern of the Monopole. With respect to the Z-axis, the radiation pattern exhibits a doughnut shape, which, when looked at from the +Z or –Z axis (Top View), represents the omnidirectional pattern of the Monopole.

4.5 Discussion of Agreement between New Mathematical Model with Experimental and Simulation Results in Freespace

In Chapter 3, a new mathematical model and its ability to predict input impedance and far field radiation patterns was presented. In this section the validity of the new model is checked by comparing the results obtained against commercial 3D simulation software and experimental results. The comparison of the results obtained using the predicted, experimental and simulation methods are divided into two parts. Firstly, a comparison of

the S-Parameters characteristics using all three methods and, secondly, a comparison of the Monopole radiation patterns with respect to both elevation and azimuth cuts.

4.5.1 S-Parameter/Input Impedance

The S_{11} magnitudes obtained from the three methods are shown in Figure 4-15. All three graphs show a good correlation between the methods. From the figure it can be seen that the Monopole has values lower than -10 dB from 10 to 11 GHz. Generally values lower than -10 dB are desirable for S_{11} as this indicates that the percentage of power reflected is below 10%.

Results	Minimum dB @ Frequency		-10 dB Bandwidth		
			Frequency		Bandwidth
			Minimum	Maximum	
Theoretical	-21 dB	10.5 GHz	10.05 GHz	11 GHz	0.95 GHz
Simulated	-29.5 dB	10.5 GHz	10.1 GHz	11 GHz	0.9 GHz
Experimental	-25 dB	10.5 GHz	10 GHz	11 GHz	1 GHz

Table 4: Monopole bandwidth properties in Freespace at 10.5 GHz

The -10 dB bandwidth calculated using all three techniques is about 1 GHz. The lowest value of return loss obtained at 10.5 GHz is -21 dB for theoretical, -25 dB for experimental and -29.5 dB for simulated results. The reason for this behaviour around this particular

frequency can be attributed to the relation between the frequency of operation and length of the antenna. The Monopole used in simulation is 7 mm, which is approximately a quarter wavelengths at 10.5 GHz. At this length of the Monopole the antenna structure is matched efficiently and at resonant, hence the low values of return loss around this frequency. Therefore the power transmitted through this antenna will be at its maximum (minimum loss) at 10.5 GHz.

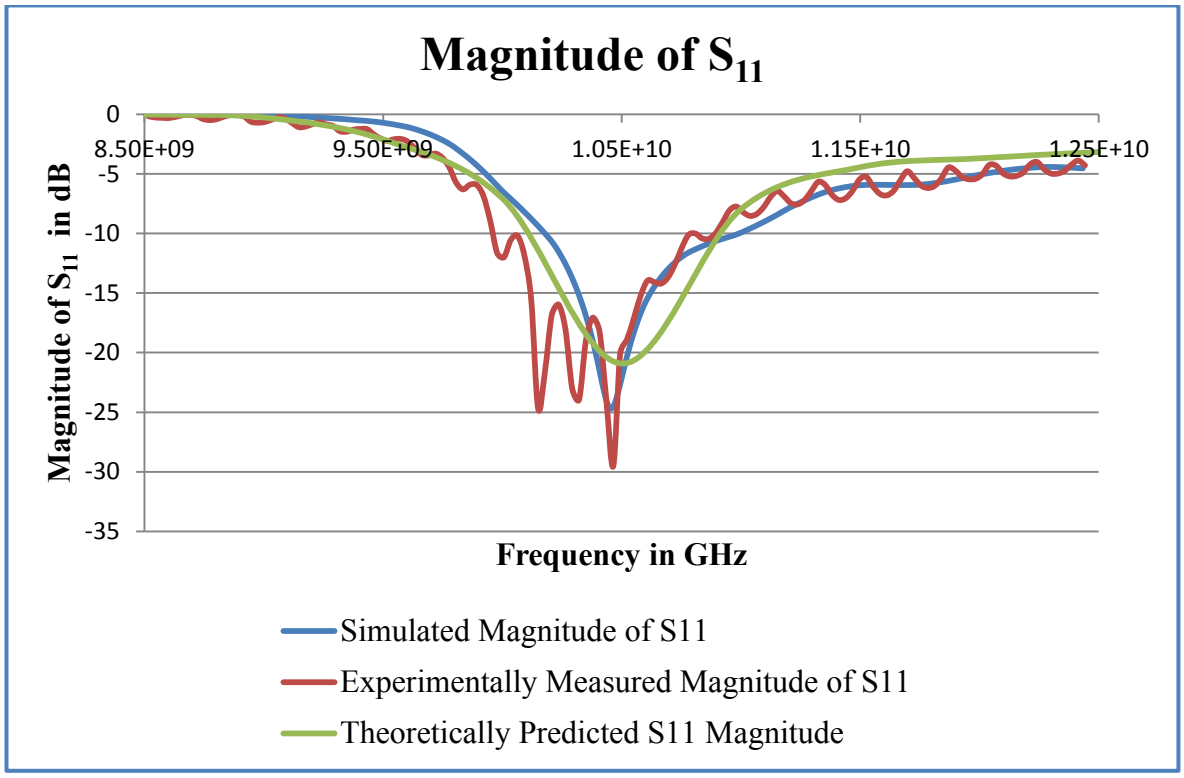

Figure 4-15 Comparison of S_{11} Magnitude

The S_{11} magnitude obtained through the experimental measurement presented in Figure 4-15 shows ripples occurring at 150 MHz intervals. This is due to the experimental setup; the wavelength at which the ripples are occurring at around 1.2 m which is the total distance of the microwave cable of dielectric constant 2.3 used in the S-Parameter

measurement. Thereby the ripples in the graph are due to the reflection of the standing wave ratio within the cable, and thus contributing to the occurrence of lowest value for S_{11} magnitude at frequencies 10 and 10.25 GHz. These reflections can be minimised by accounting for the cable losses in the calibration process. However due to the nature and frequency of the measurements and the usage of different media in the experimental setup, it is not always possible to account for the cable losses in the calibration procedure. Table 4 summarises the bandwidth properties of the Monopole in freespace at 10.5 GHz.

4.5.2 Radiation Patterns

For a Monopole antenna, the azimuth pattern is expected to be omnidirectional i.e., the antenna looks same from all directions and the elevation pattern should follow a $cos\ \theta$ pattern and the 3D pattern is doughnut shaped. The azimuth and elevation patterns of the Monopole obtained from the three methods are shown in Figure 4-16 and Figure 4-18. All three techniques show a very good agreement in both azimuth and elevation patterns. Firstly, considering the azimuth pattern over the angle range between 30˚ and 350˚, the variation between all three methods is less than 0.1 dB. The experimental method is seen to deviate from the simulated and theoretical method as the pattern angle ranges between 350˚ and 30˚. The maximum variation between the experimental method and the other two methods at this range is around 1.5 dB.

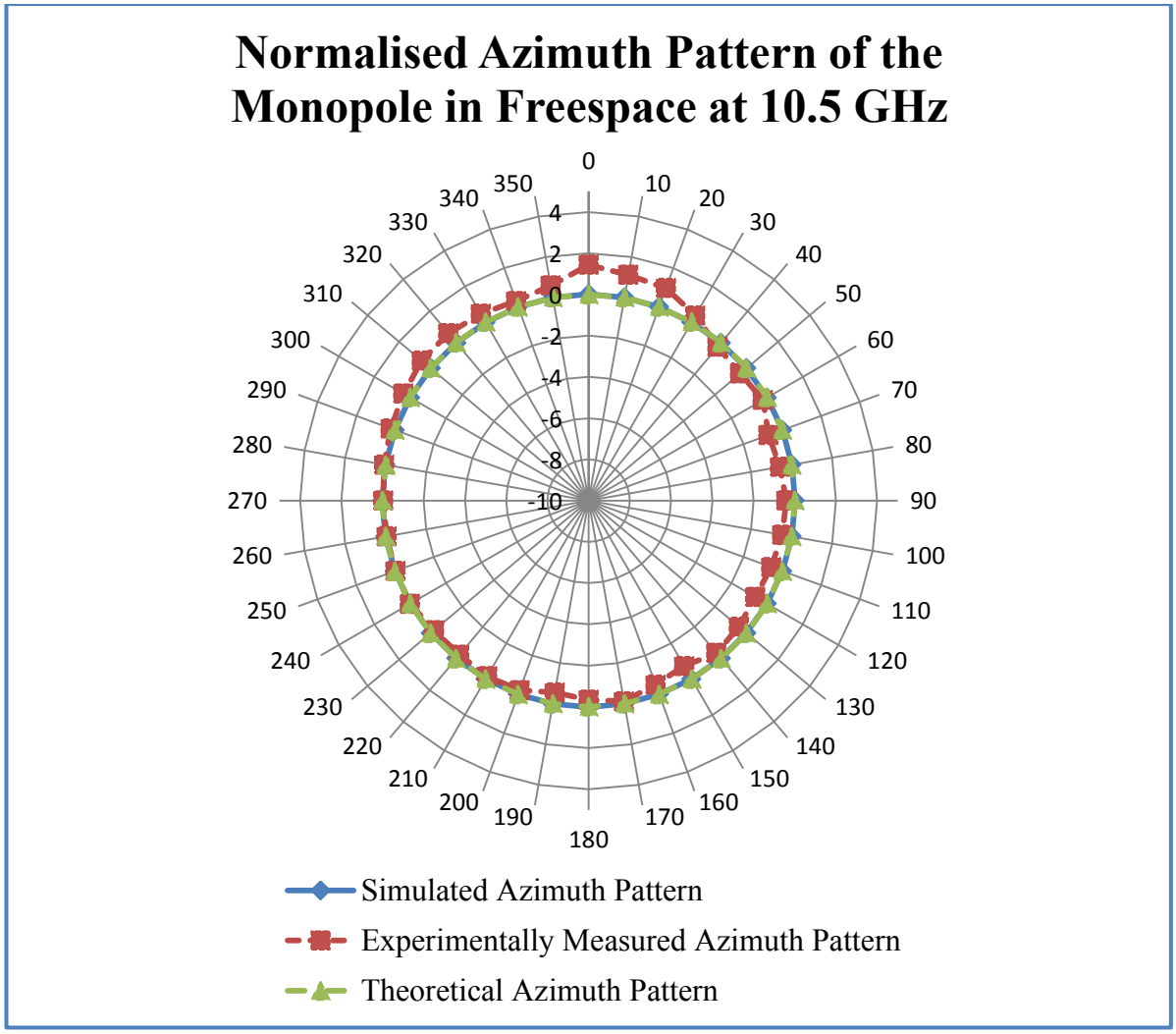

Figure 4-16 Comparison of Monopole azimuth pattern obtained from theoretical, simulated and experimental methods.

The reason for this deviation in the experimental method can be attributed to the antenna shape irregularity. The Monopole used for the experimental procedure is made from semi rigid cables. The antenna itself is made by striping the outer conductor from the inner conductor and this process can leave uneven surfaces on the face of the Monopole, which give rise to the variation shown in Figure 4-17. Figure 4-17 shows the experimental azimuth pattern at different starting angles. As you can see the deviation in azimuth pattern

caused by the antenna irregularity is consistent as we make measurements rotated at every 90˚.

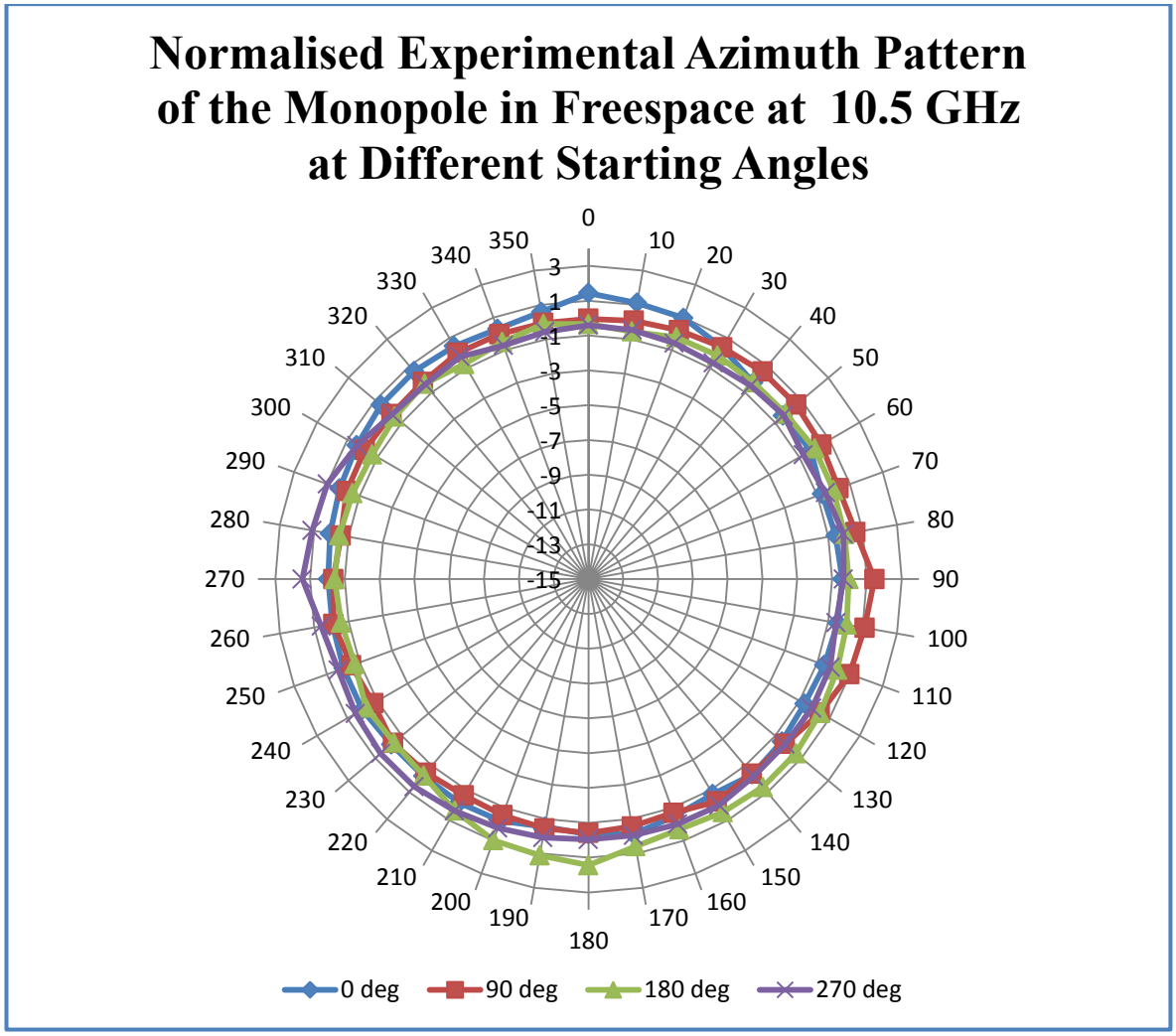

Figure 4-17 Normalised Experimental Azimuth Pattern at Different Starting Angles

When the variation between the elevation patterns from the three methods is considered, the general shape of the pattern obtained from the three methods shows good agreement. However, over the angle ranges 10˚ to 170˚ and 190˚ to 350˚, the variation between these methods exceeds 7 dB. Simulated and experimental results are generally close over the ranges 10 to 150 and 210 to 350 with a variation of less than ± 2 dB. The anticipated

discrepancies close to the nulls are due to the practical imperfections in antennas. The reasons for these different variations are now addressed below.

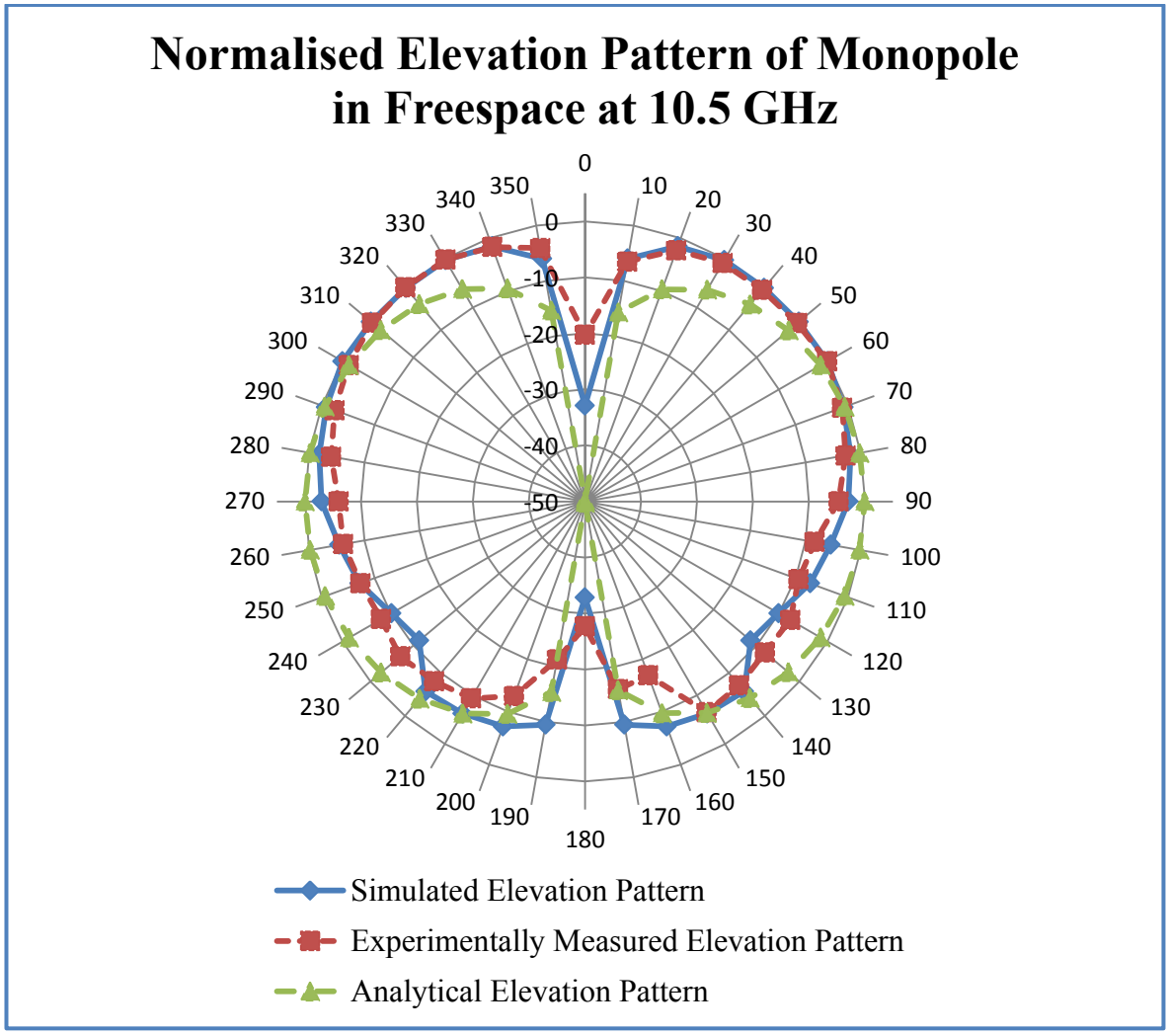

Figure 4-18 Comparison of Monopole elevation pattern obtained from theoretical, simulated and experimental methods.

The difference in the analytical results compared to the experimental and simulated results can be attributed to the way the analytical results were predicted. During the prediction the Monopole is considered solely as an ideal antenna with no outer conductors, which implies that we are predicting the field of an ideal Monopole. However, this is not the case of the

experimental or simulated antenna, as they are modelled from a semi rigid cable, which includes the outer conductor and the dielectric layer around it. This difference in the Monopole setup can be used to explain the variation between the predicted and the other two methods.

Both the simulated and the experimental methods have been able to produce consistent radiation pattern results in close agreement of within ± 2 dB of each other and with the predicted theoretical results. It is especially encouraging that when using the novel mathematical model the antenna fields have been predicted to the same degree of accuracy as that of the results obtained from experimental and simulated over the valid angle, without the need for the mathematically complex Pocklington integral equation.

These results have verified the use of the new model in freespace, the remaining sections in this chapter consider the extension of this new model to be used in more complex permittivities, such as vegetable oil and water. The ability of the methods to correctly predict the antenna characteristics under these lossy conditions will be the key to achieving this.

4.6 Lossy Media Introduction and Properties

Lossy media are used in microwave based medical imaging applications to reduce the reflection at the air-skin interface. Antennas involved in these imaging applications need to work efficiently under these lossy media. In the past, different lossy media have been used in various medical imaging applications. Meaney et al. have used solutions such as saline

and glycerine in their work on microwave imaging of breasts[5]. Bindu et al. have used corn syrup as the lossy medium in their research on active microwave imaging of breast cancer detection[61]. Smith et al., have used vegetable oil as the lossy medium in their research on breast cancer detection using microwave holography[44].

The Monopole in lossy media is very different from the corresponding analysis of a Monopole in freespace. The traditional Pocklington integral equations used to determine the input impedance and the radiation pattern of the Monopole become complex and tedious to solve for lossy media. The normal concepts of input impedance and radiation pattern are also affected by the nature of the lossy media. For example, the radiated fields of the Monopole in a lossy media tend to dissipate in the immediate vicinity of the Monopole; this has implications on how the radiated field propagates and on the measurement of those fields. Moore published the failures of standard antenna techniques when the antennas are in lossy media[89].In his work Moore presented the fundamentals of waves in lossy media and concluded that the effect of the lossy media on a standard antenna can be fully understood only after studying the properties of the lossy media itself. In this research the two lossy medium chosen are vegetable oil and water. In this section the two lossy medium and their properties are explained alongside the reasons behind their selection.

4.6.1 Vegetable Oil

Vegetable oil as a lossy media has been of interest to many researchers involved in imaging applications[9, 22]. One of the reasons behind this interest is the unique properties

of the vegetable oil. The dielectric permittivity and the conductivity variations of the vegetable oil over the frequency range of 500 MHz and 3 GHz are shown in Figure 4-19 and Figure 4-20.

The dielectric permittivity ε_r' for the vegetable oil varied between 2.55 and 2.76 over the specified frequency range. And the conductivity σ varies between 0.01 and 0.04 S/m. The dissipated power loss within the vegetable oil is calculated using the following equations.

The complex permittivity of the vegetable oil can be expressed as

$$\varepsilon_r = \varepsilon_r' - j\varepsilon_r'' \quad \textbf{4-5}$$

Where ε_r' is the dielectric permittivity and ε_r'' is the dielectric loss of the vegetable oil. The loss tangent of the media is calculated using the expression

$$\tan\delta = \frac{\varepsilon_r''}{\varepsilon_r'} \quad \textbf{4-6}$$

Now the propagation constant *k* is also a complex quantity, which is given as

$$k = \sqrt{j\omega\mu_0(\sigma + j\omega\varepsilon)} \quad \textbf{4-7}$$

Where ω is the angular frequency and σ is the conductivity of the media and given as

$$\sigma = \omega\varepsilon_0\varepsilon_r'' \quad \textbf{4-8}$$

And the propagation constant can also represented as

$$k = \alpha + j\beta \quad \textbf{4-9}$$

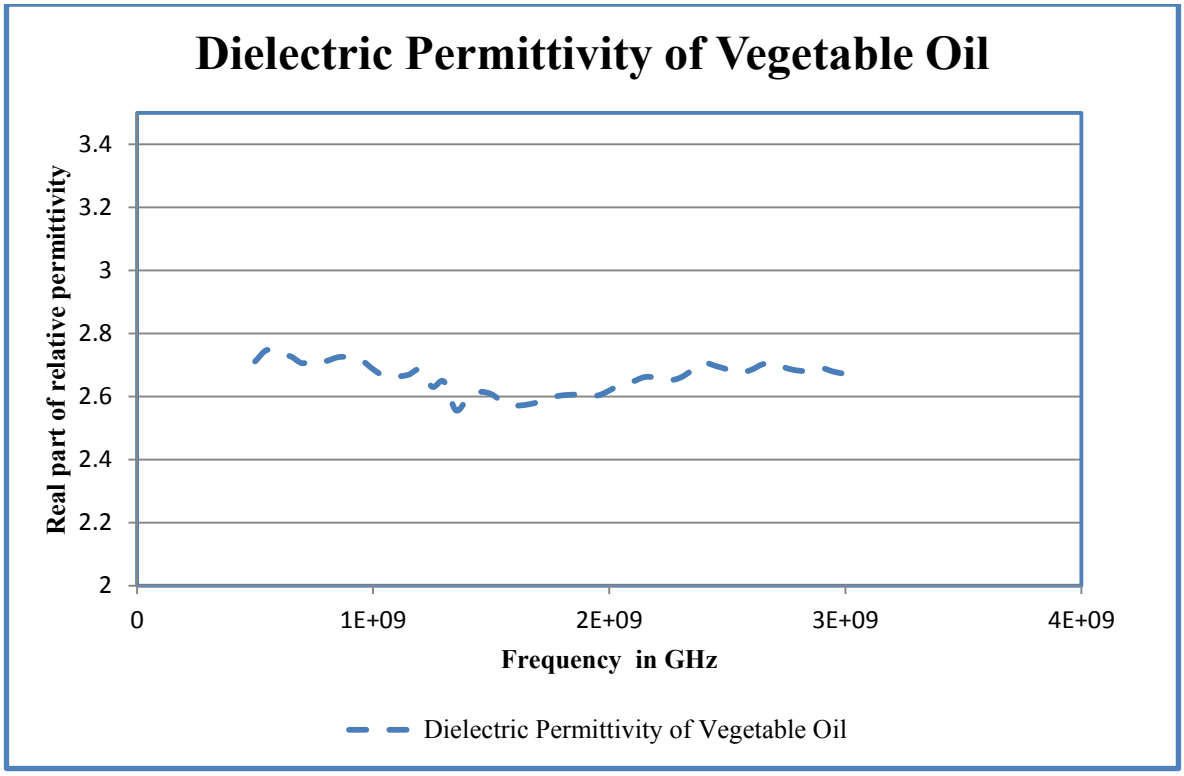

Figure 4-19 Dielectric permittivity of Vegetable Oil

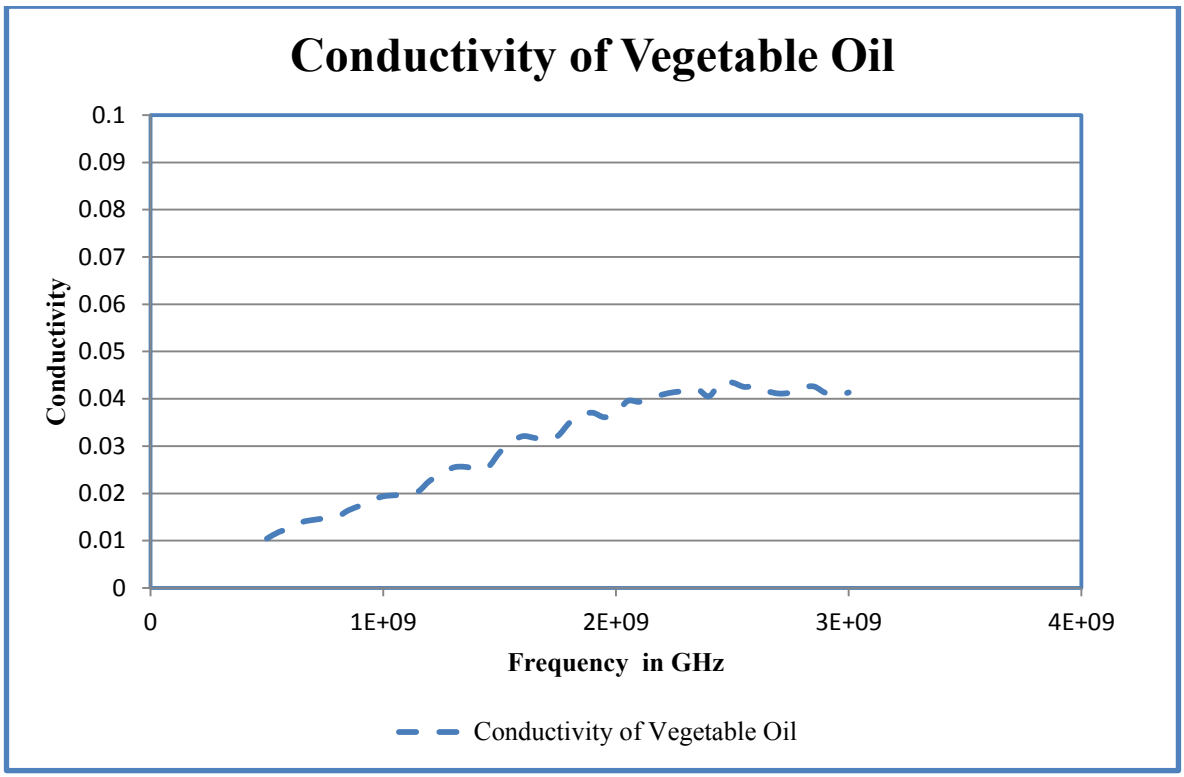

Figure 4-20 Conductivity of Vegetable Oil

Where α represents the attenuation factor and β the phase factor, and they can be calculated by substituting the equations 4-5, 4-6 and 4-8 in equation 4-7 and simplifying, giving

$$\alpha = \omega\sqrt{\mu_0\varepsilon_0\varepsilon_r'(\sqrt{(1+\tan^2\delta)-1}} \qquad \textbf{4-10}$$

And

$$\beta = \omega\sqrt{\mu_0\varepsilon_0\varepsilon_r'(\sqrt{(1+\tan^2\delta)+1}} \qquad \textbf{4-11}$$

If the wave travels in +z direction, then the decaying envelope of the wave is given by $e^{-\alpha z}$, and the sinusoidal nature of the wave with the phase factor of βz is given as $e^{-j\beta z}$ [61]. The dissipative loss for the vegetable oil can be given as

$$Dissipative\ loss = 20\ \log_{10} e^{\alpha z}$$

Figure 4-21 shows the graphs of the dissipative loss of the vegetable oil over the distances of 10 cm and 15 cm in +z direction. As it is shown, over the specified frequency range the dissipative loss of the vegetable oil with z at 10 cm varies between 1.46 and 6.11 dB, indicating a slow rate of increase in dissipative loss with increase in frequency and distance. This is the reason why many researchers choose vegetable oil as a lossy media in their research on medical imaging applications. Because of the popularity of vegetable oil as a lossy media, it has been chosen as one of the lossy media to be used in this research to predict the characteristics of the Monopole within a low loss medium. Also, this provides the opportunity to progress from a freespace environment without loss to vegetable oil, which offers low loss surroundings and thereby improved matching.

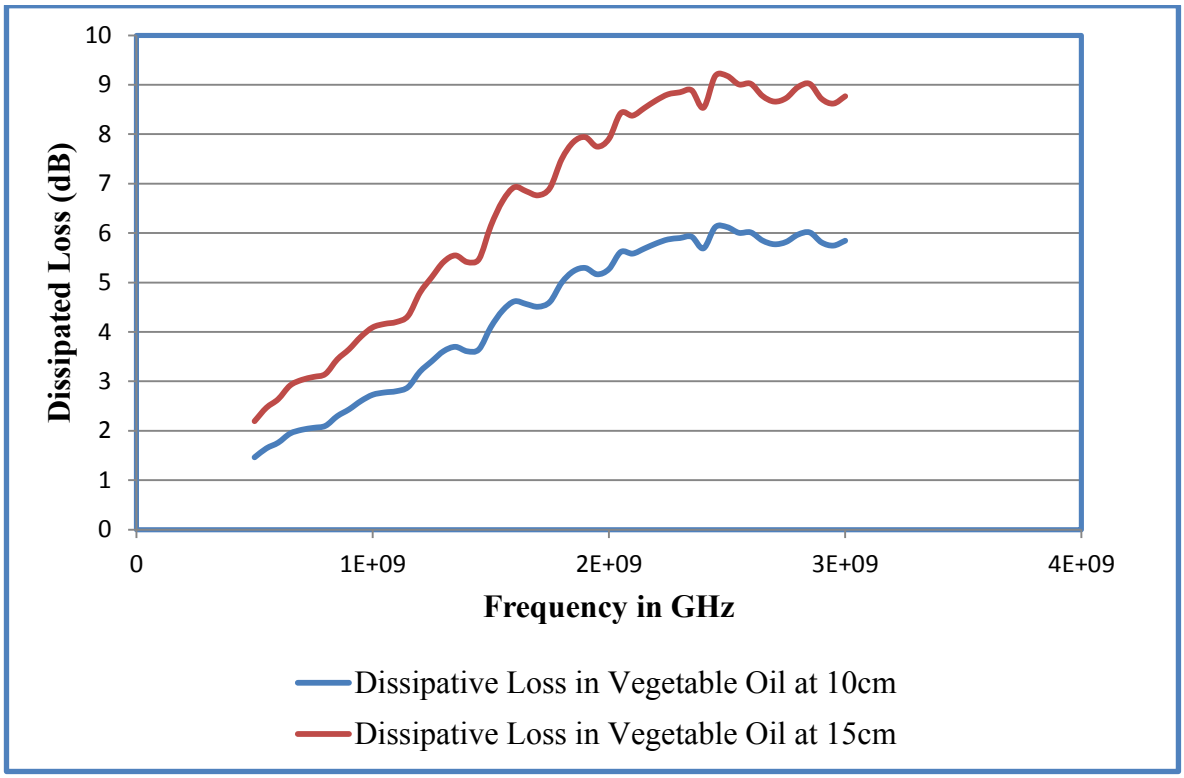

Figure 4-21 Dissipated Loss in Vegetable Oil

4.6.2 Water

Water has been used in many imaging applications worldwide for very simple reasons; it is cheap and readily available[5, 77]. But its simplicity comes with price of it being a high loss medium. The dielectric properties of water are presented in Figure 4-22 and Figure 4-23. The dielectric permittivity ε_r' of the water over the frequency range of 500 MHz and 3 GHz varies between 76.78 and 79.91. The conductivity σ over the range varies between 0.1 and 2.07 S/m. These properties obtained are similar to the water properties reported in Foti's work[77].

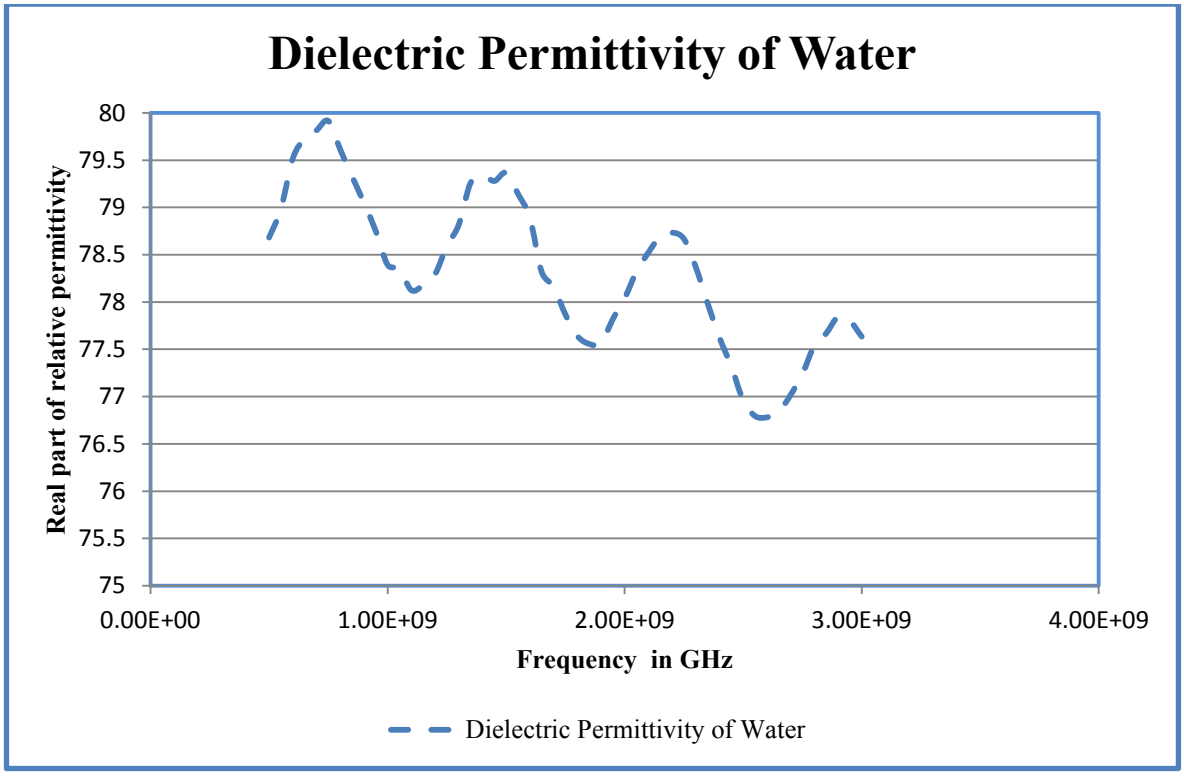

Figure 4-22 Dielectric Permittivity of Water

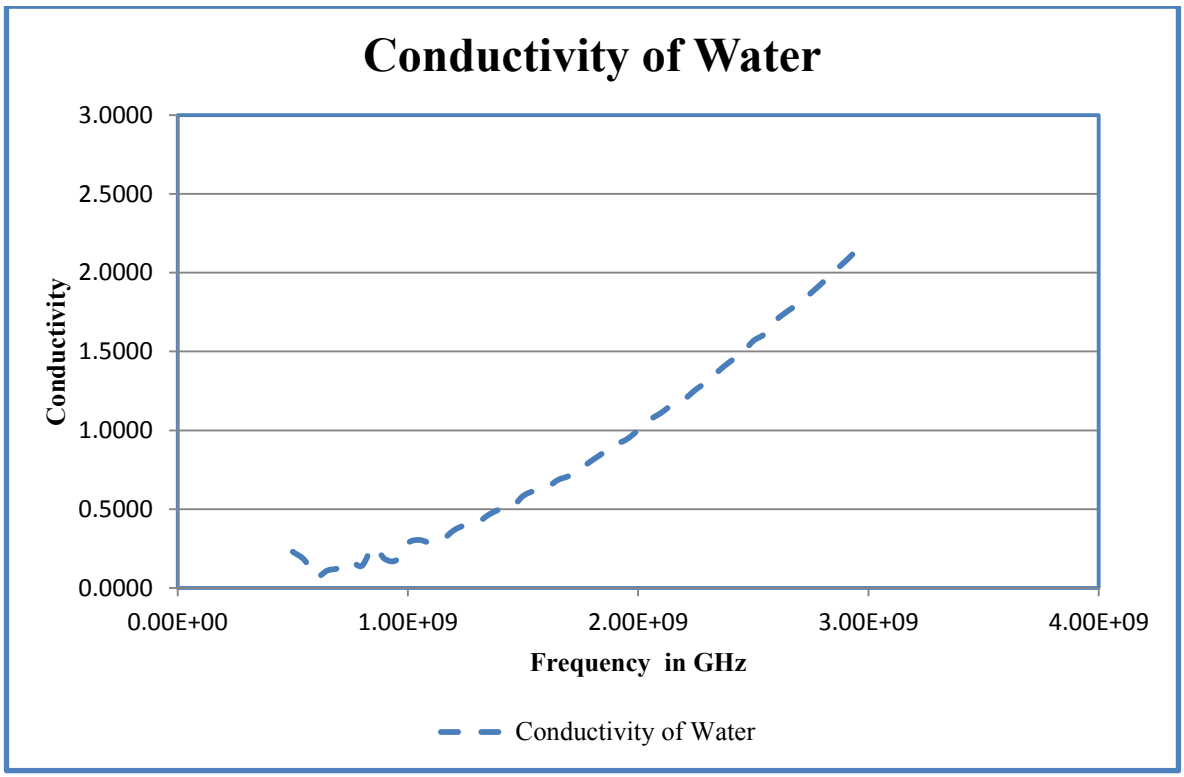

Figure 4-23 Conductivity of Water

Figure 4-24 shows the dissipative loss of tap water at 10 cm and 15 cm. The dissipative loss is calculated in the same way as vegetable oil. However, because of the higher conductivity values the dissipated loss of water at z at 10 cm is very high in comparison with vegetable oil. The dissipative loss at 10 cm varies between 1.67 and 54.24 dB, and if the distance is increased to 15 cm then the loss varies from 2.41 and 81.36 dB over the frequency range of 0.5 to 3.5 GHz. This result for dissipative loss for water confirms the reported theory that the rate of increase of dissipative loss versus frequency and distance is much higher[61]. Thus water is chosen as the lossy medium with high loss to test the new model ability to predict the Monopole characteristics within a higher loss environment.

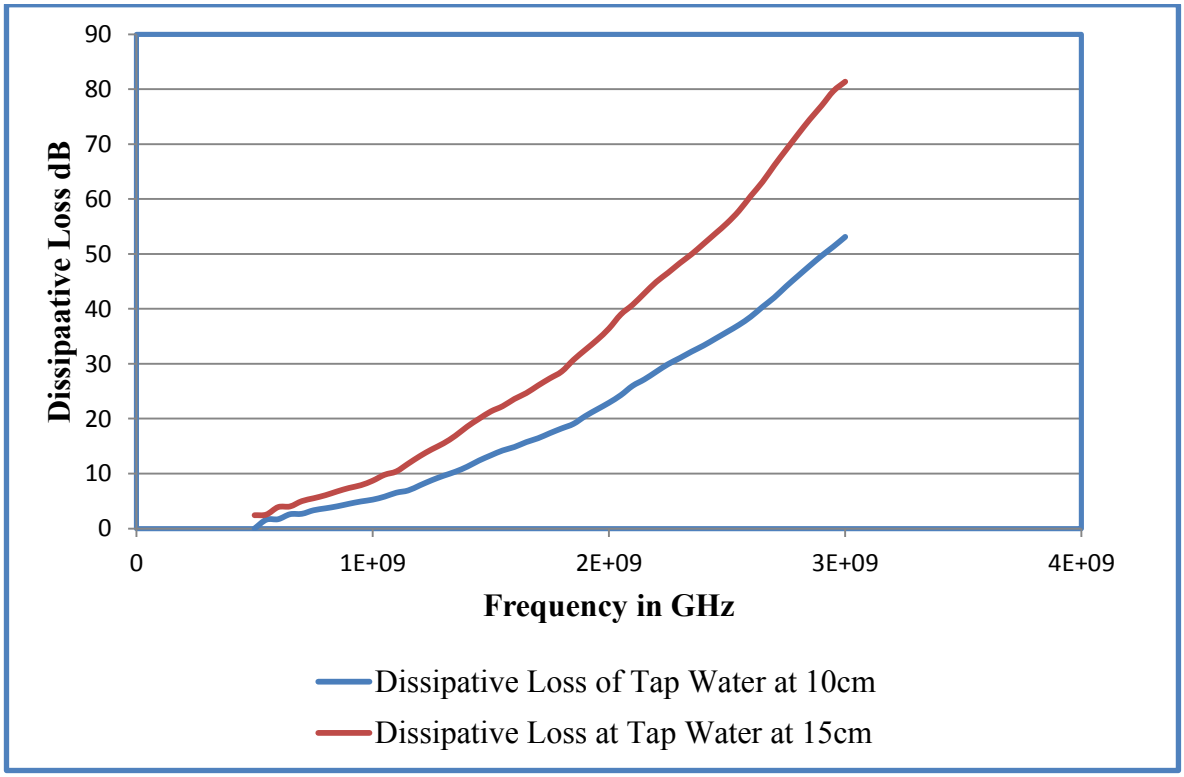

Figure 4-24 Dissipative Loss in Tap Water

4.7 Modification of Setup for Lossy Media Measurements

4.7.1 Predicted Antenna Characteristics

In Chapter 3 a new mathematical model was proposed to predict the current across the Monopole. The new model decreases the computational time as it depends on only three parameters; initial current I_0, damping coefficient α and radial parameter τ. The expression for the new model is given below in 4-12

$$I(z) = I_0 e^{-\alpha z} \sin(k(l-z)) + f(z,\tau) \qquad \textbf{4-12}$$

It was also shown that the first part of this expression accounts for the damping in the current distribution curve and thus characterises the effect of the surrounding medium on the wire. In the freespace results presented in Section 4.5, the damping coefficient α is set to be zero, and varying this parameter α depending on the surrounding medium makes the new mathematical model suitable for applications involving complex dielectric media such as medical imaging applications.

The conductivity of the vegetable oil at 1 GHz is given as 0.019 S/m (refer to Section 4.6.1). This value is substituted in the above expression for the damping coefficient α for the current prediction using the new model. In a similar fashion, the predicted results for the Monopole in water are calculated using the expression in equation 4-12. The conductivity of the water at 1 GHz is given as 0.176 S/m (refer Section 4.6.1). This value is substituted in the above expression for damping coefficient α for the current prediction using the new model.

4.7.2 Experimental Arrangement for Lossy Media Measurements

Earlier in the chapter, the experimental arrangement of the Monopole measurement system in freespace was presented. Figure 4-2 and Figure 4-6 showed the anechoic chamber arrangements for azimuth and elevation pattern measurements in freespace. However, for lossy media measurements the anechoic chamber arrangements cannot be adapted.

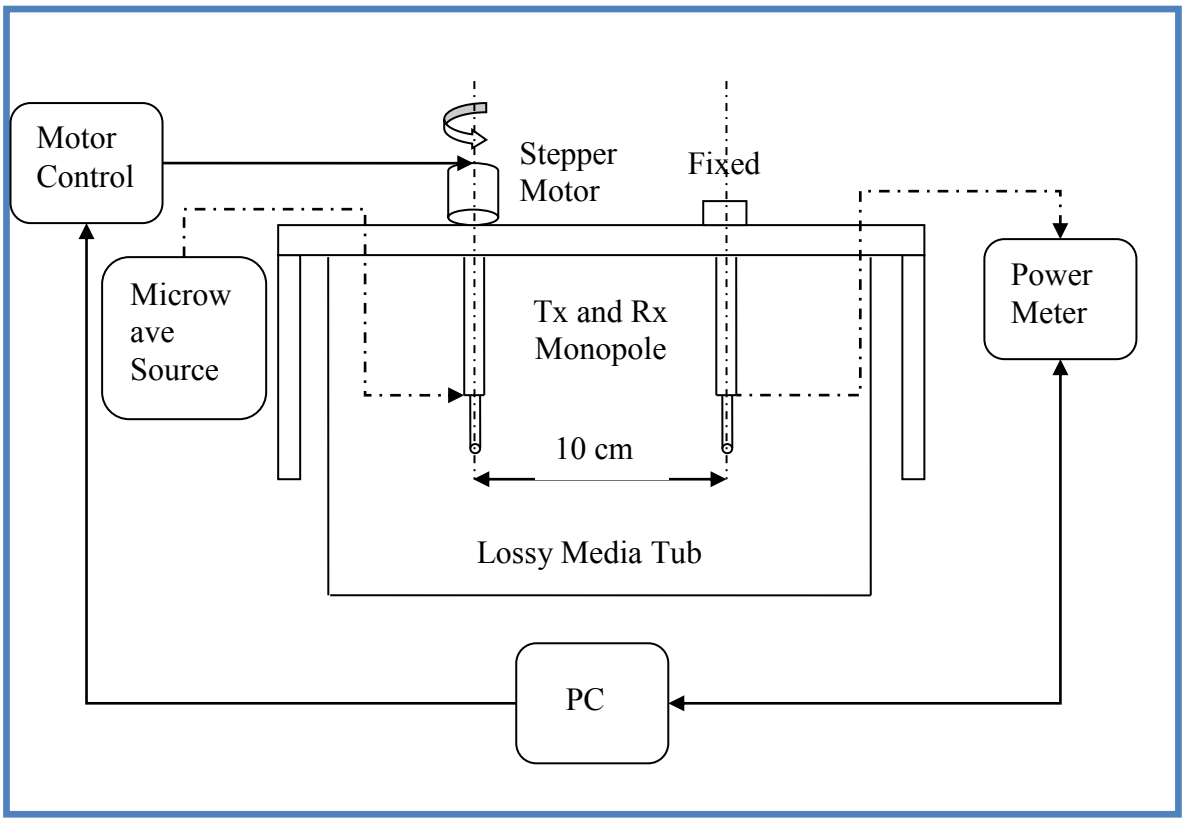

Figure 4-25 Experimental arrangement of the Monopole measurement systems in Lossy Media

Figure 4-25 shows the experimental arrangement of the Monopole measurement system in lossy media. The antenna arrangement shown is for measuring azimuth pattern; this will be changed for elevation measurements (refer Figure 4-4). Table 5 lists the various parameters and specifications involved in the experimental measurements of the Monopole in lossy

media. The experimental arrangement is used for two different dielectric media; vegetable oil and water.

Parameter	Specification
Transmitting Antenna	Monopole (Semi rigid cable)
Receiving Antenna	Monopole (Semi rigid cable)
Distance between antennas	10 cm
Frequency of operation	1 GHz
Lossy media	Vegetable Oil/ Water
Dielectric permittivity of vegetable oil ε_r'	2.86
Conductivity of vegetable oil σ (S/m)	0.019
Dielectric permittivity of water ε_r'	78.39
Conductivity of water σ (S/m)	0.176

Table 5: Lossy media experimental arrangement parameters

In terms of the S-Parameter measurement in lossy media, Figure 4-7 shows the measurement system involved in measuring the S-Parameters of the Monopole. The same measurement system is used to measure the S-Parameters in lossy media. The Monopole is suspended from the antenna holder into a tube of the lossy medium. The other end of the suspended antenna is connected to the PNA which helps to measure the S_{11} in the same

way as the freespace measurements. PNA is calibrated using E-Cal kit before the measurements to ensure the accuracy of the results.

4.7.3 Simulation Arrangements for Lossy Media Measurements

In Section 4.4 the simulation software used in this research was detailed and the steps involved in obtaining the antenna characteristics of the Monopole were discussed. For freespace simulation the background material chosen, in which the Monopole will be simulated, is air. However, for simulation within vegetable oil the software has the provision to change the background material to reflect a workspace with the same properties as vegetable oil. The dielectric permittivity of the workspace is chosen as 2.68 and the conductivity is kept at 0.019 S/m.

For water measurements, the background material is changed to reflect a workspace with the same properties as water. The dielectric permittivity of the workspace is chosen as 78.3 and the conductivity is kept at 0.176 S/m. Because of the advantages of the FDTD simulation, with a single iteration results can be obtained over a specified frequency span. The frequency span is chosen between 0.5 and 3 GHz. This range is chosen so that the results can be validated easily by comparing them with the experimental and predicted results.

4.8 Discussion of Theoretical, Experimental and Simulation Results in Vegetable Oil

The new mathematical model presented in Chapter 3 is extended to predict Monopole input impedance and radiation pattern in a lossy medium environment. Vegetable oil and water are the two lossy media which are considered for this research as they represent media of low loss and high loss conductivity respectively. The validity of the results obtained using the new model is compared with commercial 3D simulation software and experimentally measured results.

4.8.1 S-Parameter/Input Impedance

Figure 4-26 shows the magnitude of S_{11} in vegetable oil at 1 GHz using the new model, simulated and experimental methods. The return loss values for the theoretical method are obtained by converting the input impedance predicted using the expression in Section 4.3.3. The curves for all three methods follow a similar path and they all have the lowest values for S_{11} magnitude at 1 GHz. The -20 dB bandwidth for the three methods is 0.5 GHz and the variation in the bandwidth of the Monopole for values under -20 dB calculated using all three methods is less than 0.05 GHz. The azimuth and elevation patterns of the Monopole obtained from the three methods are shown in Figure 4-27 and Figure 4-28. Table 6 summarises the bandwidth properties of the Monopole in vegetable oil at 1 GHz.

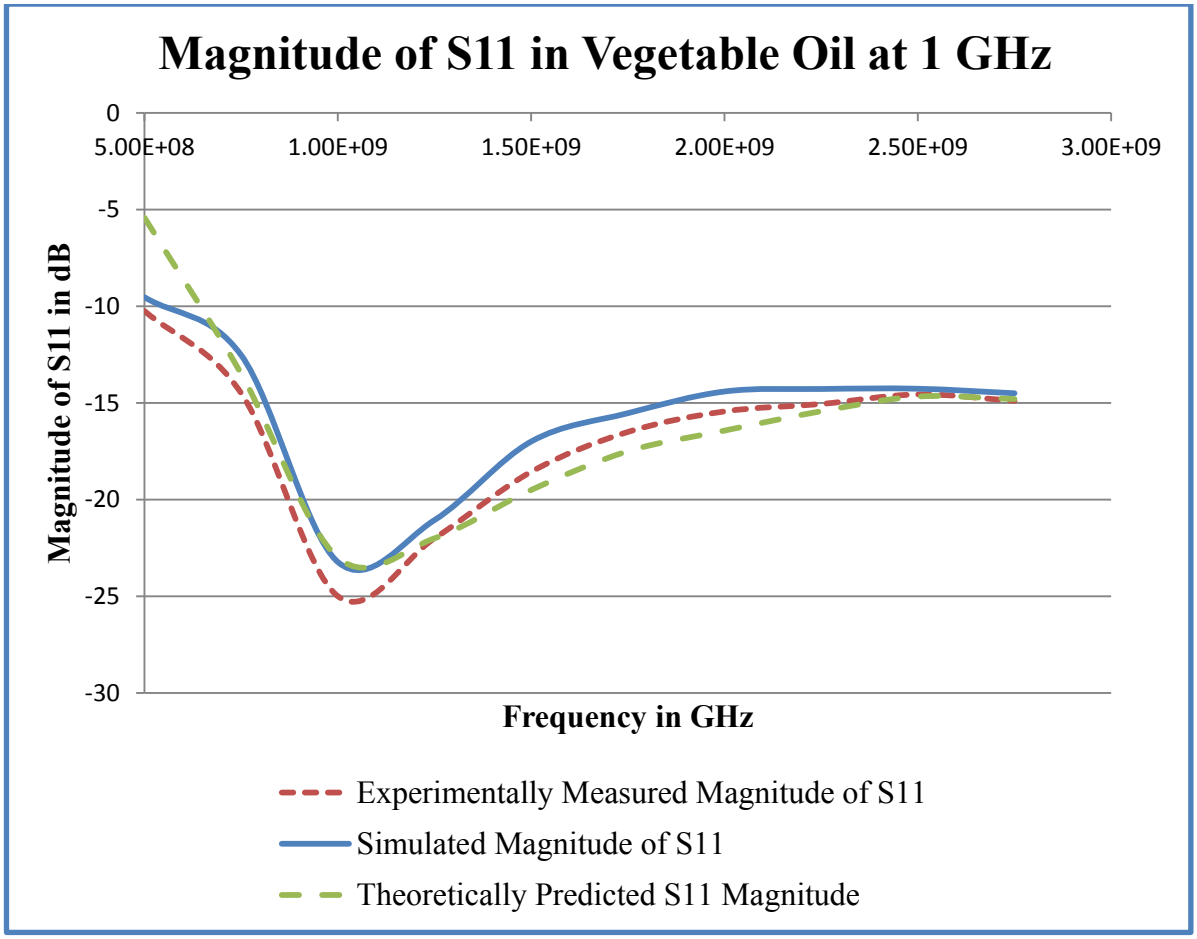

Figure 4-26 Comparison of S_{11} Magnitude in Vegetable Oil

Results	Minimum dB @ Frequency		-20 dB Bandwidth		
			Frequency		Bandwidth
			Minimum	Maximum	
Theoretical	-23 dB	1 GHz	0.9 GHz	1.4 GHz	0.5 GHz
Simulated	-23 dB	1 GHz	0.9 GHz	1.35 GHz	0.45 GHz
Experimental	-25 dB	1 GHz	0.875 GHz	1.4 GHz	0.55 GHz

Table 6: Monopole bandwidth properties in Vegetable Oil at 1 GHz

4.8.2 Radiation Patterns

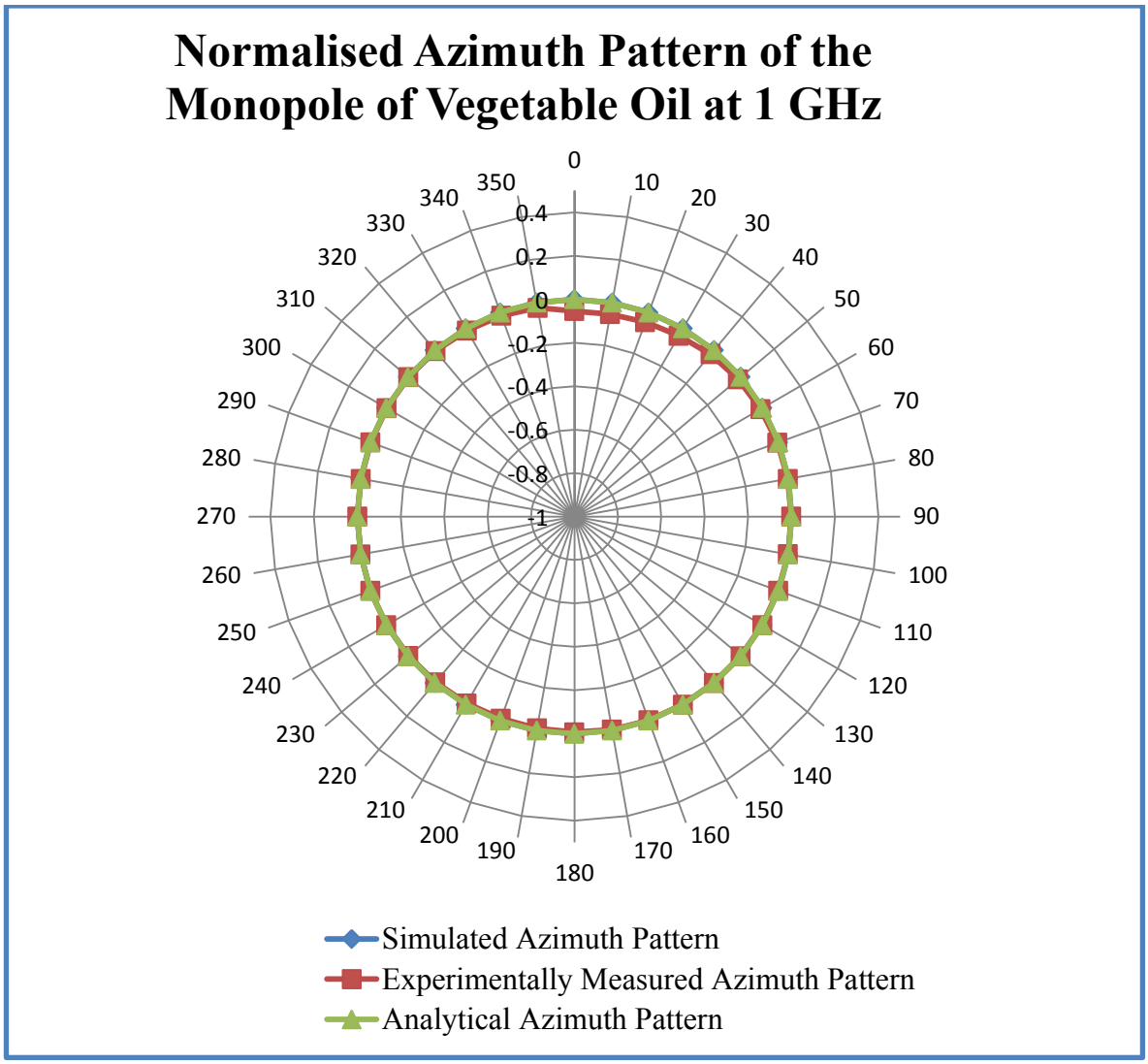

Figure 4-27 Comparison of Normalised Azimuth Pattern in Vegetable Oil

Figure 4-27 and Figure 4-28 show the normalised azimuth and elevation pattern of the Monopole in vegetable oil at 1 GHz respectively. The Monopole radiation pattern looks the same from all directions in azimuth cut, i.e., it is an omnidirectional pattern along the z axis. Considering the azimuth pattern over the angle range of 40˚ to 350˚, the variation between all three methods is less than 0.05 dB. The experimental method is seen to deviate

from the simulated and theoretical methods as the pattern angle ranges between 350˚ and 40˚.

The maximum variation between the experimental methods and the other two methods at this range is 0.05 dB. The reason for this deviation in the experimental method can be attributed to the antenna shape irregularity, the same as in Section 4.5.2. The Monopole used for the experimental procedure is made from semi rigid cables. The antenna itself is made by stripping the outer conductor from the inner conductor using a pipe cutter and this process can leave uneven surfaces on the face of the Monopole, which can give rise to the variation shown in Figure 4-27.

The normalised values obtained for angles 0˚ and 180˚ in the elevation pattern are the lowest; this can be explained by the radiated power of the antenna reaching its minimum at the antenna axis and attaining its maximum values horizontal to the antenna position, thereby exhibiting $cos\ \theta$ radiation pattern. When the variation between the elevation patterns from the three methods is considered, the general shape of the pattern obtained from the three methods is the same as the $cos\ \theta$ pattern. The variations between the three methods over the nulls are considerably higher, as anticipated, because of the practical imperfection of the antenna. The simulated and experimental methods follow each other very closely over the range with a variation of less than 2 dB. However, over the angle range 150˚ to 210˚ the variation between these methods exceeds 5 dB. The reasons for these different variations are now addressed below.

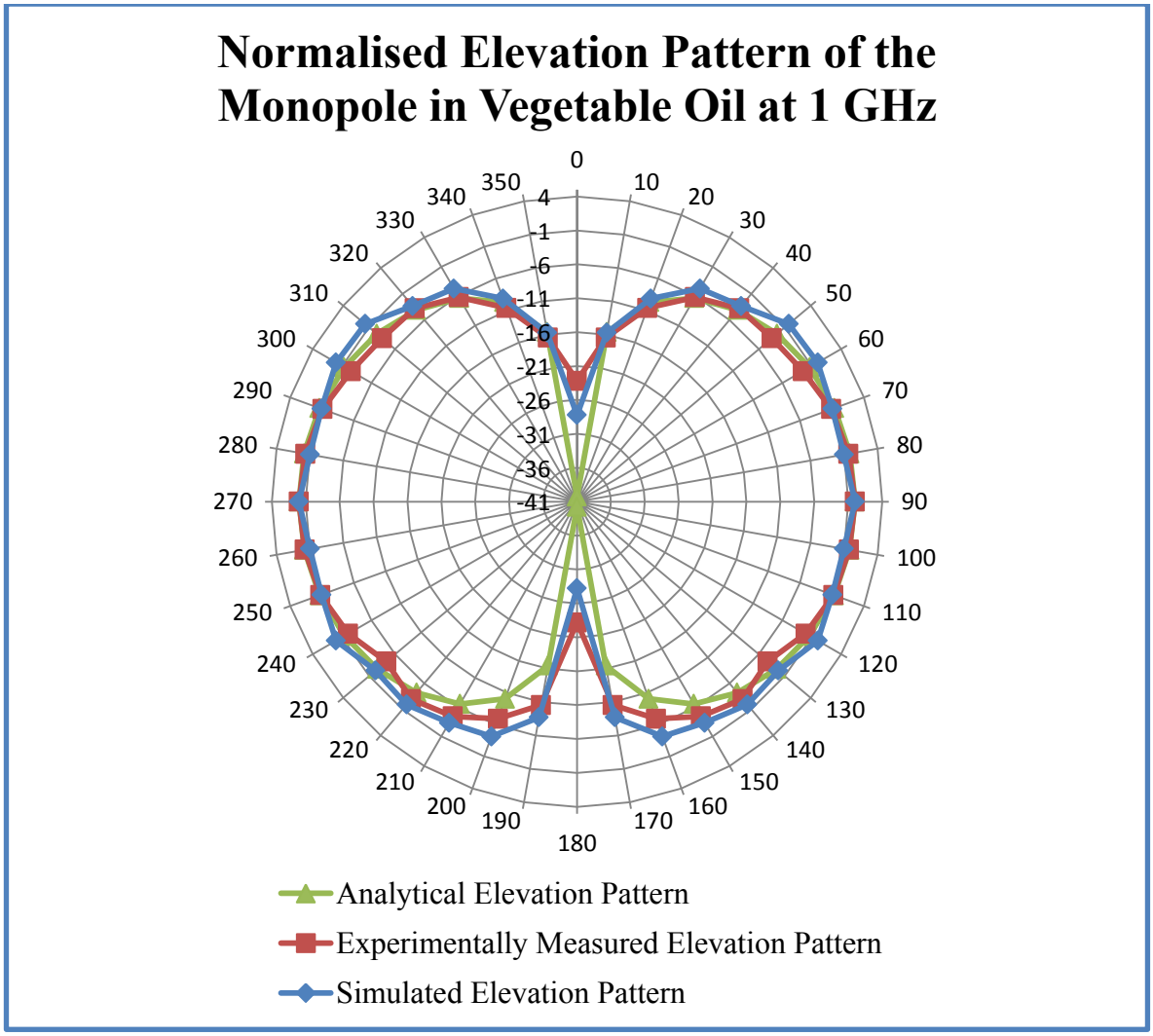

Figure 4-28 Comparison of Normalised Elevation Pattern in Vegetable Oil

The difference in the predicted results compared to the experimental and simulated results can be attributed to the way the analytical results were predicted. During the theoretical analysis the Monopole is considered solely as a wire antenna with no outer conductors, which implies that the predicted field is of an ideal Monopole. However, this is not the case with the experimental and simulated antenna, as they are modelled from a semi rigid cable, which includes the outer conductor and the dielectric layer around it. This difference in the Monopole setup can be used to explain the variation between the predicted and the other two methods. Both the simulated and the experimental methods have been able to

produce consistent radiation pattern results in close agreement of ± 0.1% with each other and with the predicted theoretical results. It is especially encouraging that when using the novel mathematical model within a vegetable oil environment, the antenna fields have been predicted to the same degree of accuracy as that of the results obtained from experimental and simulated over the valid angles.

4.9 Discussion of Theoretical, Experimental and Simulation Results in Water

In this section, the validity of the results obtained using the new model in water is compared against commercial 3D simulation software and experimentally measured results.

4.9.1 S-Parameter / Input Impedance

Figure 4-29 shows the magnitude of S_{11} in water at 1 GHz using the new model, simulated and experimental methods. Similar to freespace and vegetable oil, the return loss values in water predicted by the theoretical method is obtained by converting the input impedance using the expression in Section 4.3.3. The curves for all three methods follow a similar path and they all have the lowest values for S_{11} magnitude at around 1 GHz. The variation in the bandwidth of the Monopole for values under -15 dB calculated using all three methods is 0.025 GHz. Table 7 summarises the bandwidth properties of the Monopole in water at 1 GHz.

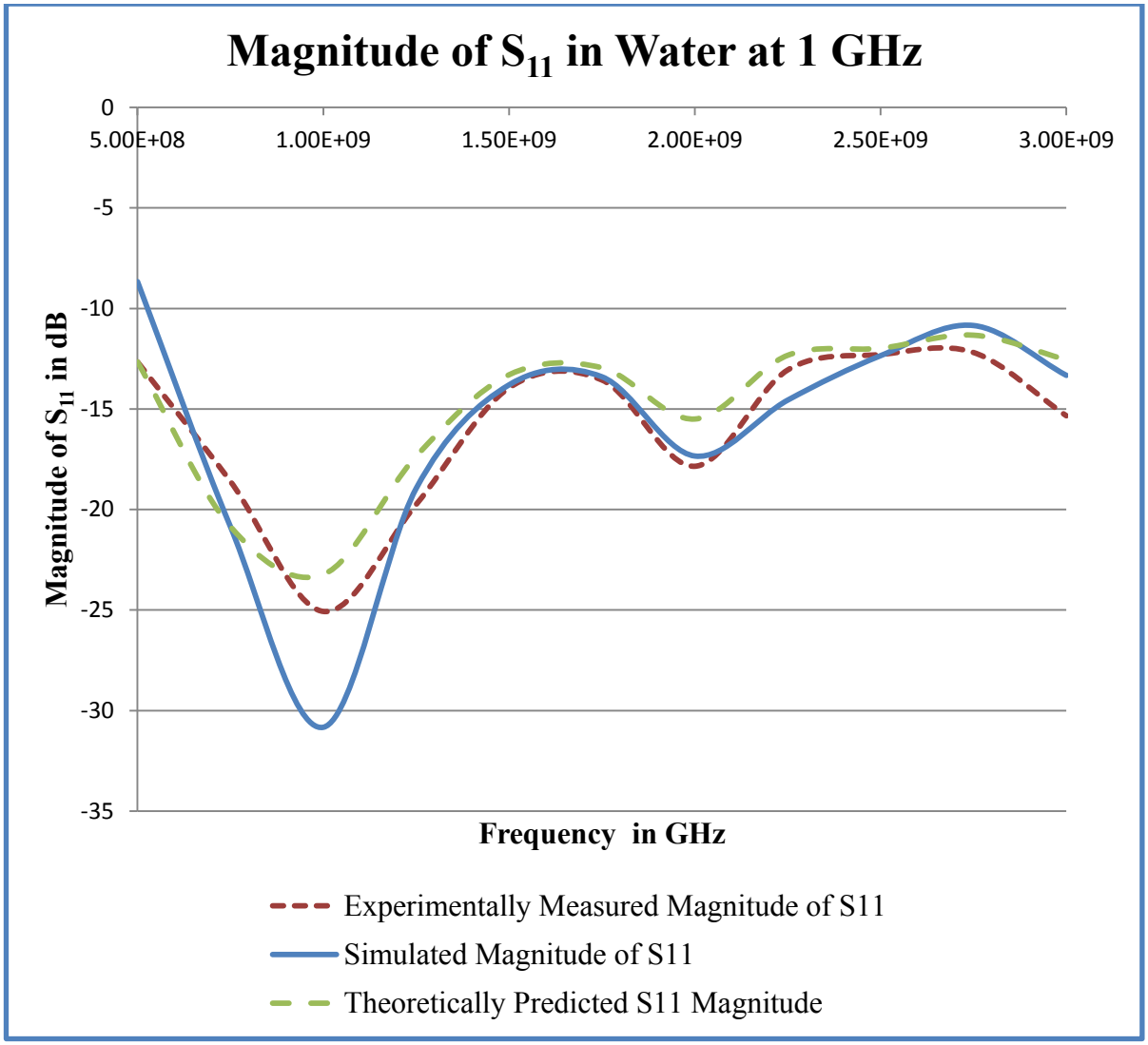

Figure 4-29 Comparison of S_{11} Magnitude in Water

Results	Minimum dB @ Frequency		-15dB Bandwidth		
			Frequency		Bandwidth
			Minimum	Maximum	
Theoretical	-23 dB	0.97 GHz	0.55 GHz	1.35 GHz	0.8 GHz
Simulated	-31 dB	1 GHz	0.6 GHz	1.4 GHz	0.8 GHz
Experimental	-25 dB	1 GHz	0.575 GHz	1.4 GHz	0.825 GHz

Table 7: Monopole bandwidth properties in water at 1 GHz

4.9.2 Radiation Patterns

The azimuth and elevation patterns of the Monopole obtained from the three methods are shown in Figure 4-30 and Figure 4-31. As expected, the Monopole azimuth pattern exhibits an omnidirectional pattern along the z axis, i.e., the antenna radiation pattern looks the same from all directions.

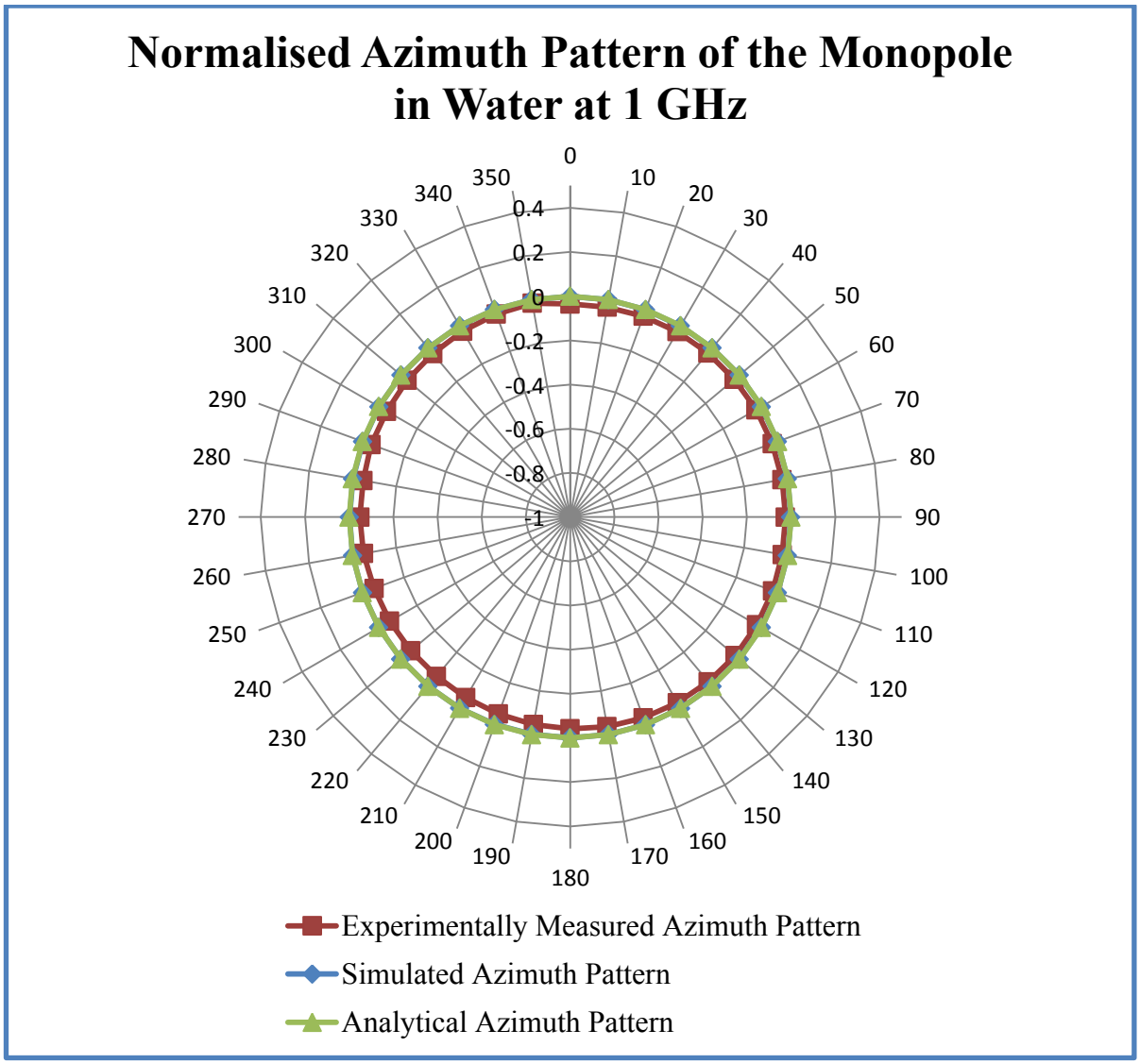

Figure 4-30 Comparison of normalised azimuth pattern in water

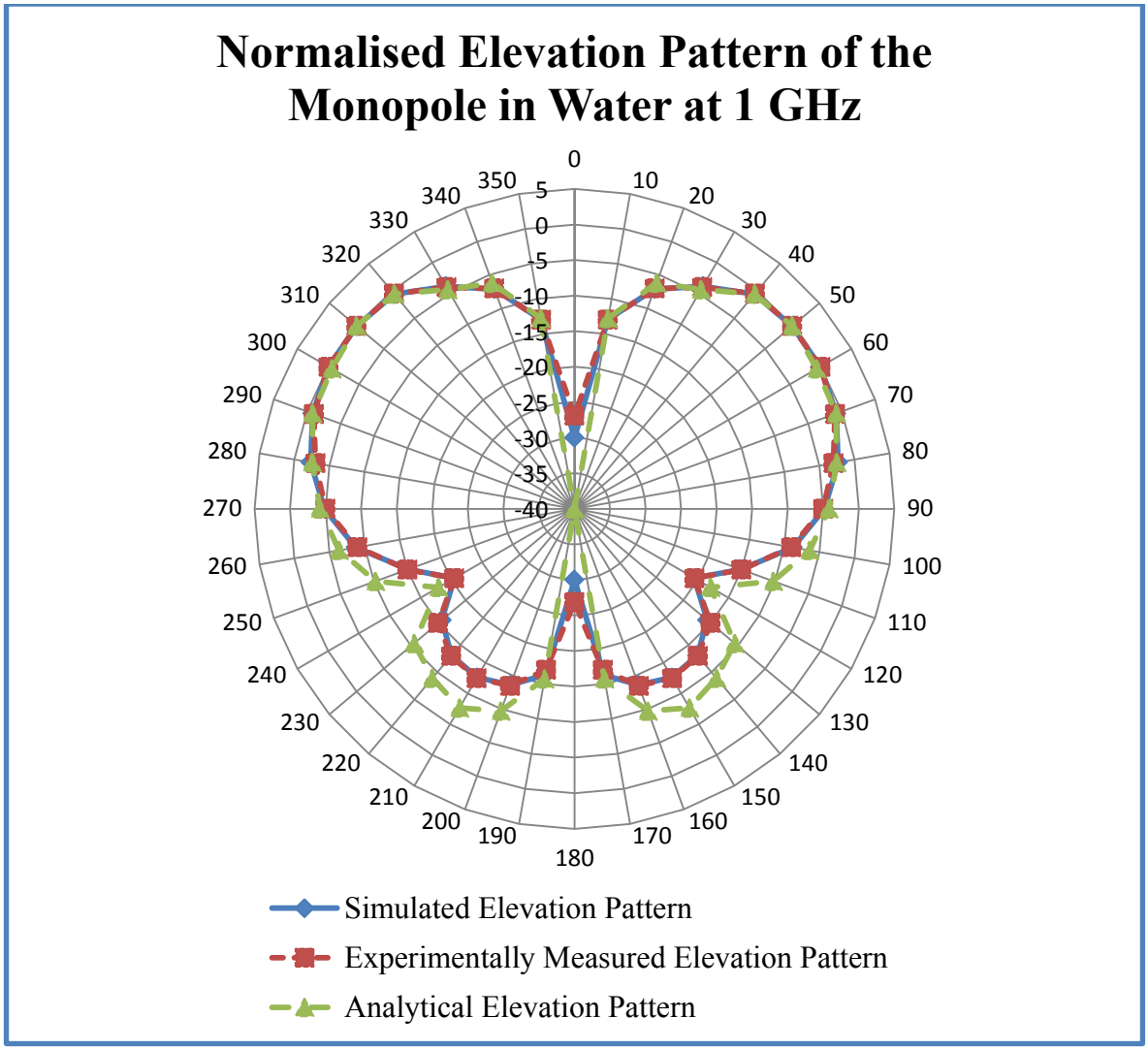

Figure 4-31 Comparison of normalised elevation pattern in water

Considering the azimuth pattern over the angle range between 330˚ and 160˚, the variation between all three methods is less than 0.05 dB. The experimental method is seen to deviate from the simulated and theoretical methods as the pattern angle ranges between 160˚ and 330˚. The maximum variation between the experimental methods and the other two methods at this range is 0.05 dB. This behaviour in the experimental method can be attributed to the antenna shape irregularity the same as in Section 4.5.2. The Monopole used for the experimental procedure is made from semi rigid cables. The antenna itself is made by stripping the outer conductor from the inner conductor using a pipe cutter and this

process can leave uneven surfaces on the face of the Monopole, which can give rise to the variation shown in Figure 4-30.

However, in water with ε_r' of 78.3 and conductivity σ of 0.176 S/m the elevation pattern shows the appearance of an additional lobe along with the main lobe, so the 3D patterns of the Monopole in water is not a *cos* θ pattern. The separation between the lobes occurs at angles 120˚ and 240˚. When the variation between the elevation patterns from the three methods is considered, the general shape of the pattern obtained from the three methods follows the same pattern which shows an appearance of a side lobe along with the main lobe. The variations between the three methods over the angles 0˚ and 180˚ is considerably higher as the simulation and theoretical methods give out very low dB values which are simply beyond the measurement limitation of the experimental setup. The simulated and experimental methods follow each other very closely over the range with a variation of less than 0.1 dB.

Results for the new model agree well with simulation results over the full angular range. All 3 models agree closely on the direction of the maxima, main lobe, nulls and side lobe. However, over the angle ranges 90˚ and 270˚, the analytical values depart from experimental and simulation values by up to 5 dB. The reasons for these different variations are now addressed below.

The difference in the predicted results compared to the experimental and simulated results can be attributed to the way the analytical results were predicted. During the prediction the Monopole is considered solely as the wire antenna with no outer conductors, which implies

that we are predicting the field of an ideal Monopole. An ideal antenna doesn't consider the diffraction from the edges of the antenna. However, this is not the case of the experimental or simulated antenna, as they are modelled from a semi rigid cable, which includes the outer conductor and the dielectric layer around it. This difference in the Monopole setup can be used to explain the variation between the predicted and the other two methods.

Both the simulated and the experimental methods have been able to produce consistent radiation pattern results in close agreement with each other and with the predicted theoretical results. It is especially encouraging that when using the novel mathematical model within a water environment, the antenna fields have been predicted to the same degree of accuracy as that of the results obtained from experimental and simulated, which clearly identifies the appearance of the side lobe along with the main lobe.

4.10 Summary

This chapter has focussed on the development of the Monopole measurement system for freespace measurements and complex permittivities. The new model is validated by comparing the results obtained by the new methods with the results from Tsai's experiment in Section 4.2. The result comparison show good correlation between the two graphs which validates the new model in measuring the antenna characteristics. The characteristics of the Monopole are studied using two different quantities; input impedance and radiation patterns. Subsections in 4.2 are used to explain the different parameters required in measuring return loss and radiation patterns experimentally. The challenge facing the

measurement of input impedance is listed and its relation with return loss is detailed in Section 4.3.3. The spherical coordinate system and the two dimensional cuts of the radiation pattern are explained in Section 4.3.4.

Section 4.4 defines the electromagnetic software used in the simulated method. The FDTD technique is used to simulate the Monopole model. The parameters and procedures involved in the simulation methods are detailed in Section 4.4.1. Also in this section the advantages of the FDTD simulation are listed and its potential to be used in complex workspace such as lossy media is discussed.

An evaluation of the results obtained from all three methods; theoretical, simulation and experimental, is carried out in Section 4.5. Comparison of the return loss shows very good correlation between all three methods and the variation in the bandwidth is less than 0.1%. The radiation pattern results are compared as two dimensional cuts corresponding to azimuth and elevation planes. In both planes all three methods show a very high degree of agreement of less than ± 2 dB between the graphs and the causes for variation at certain angles are explained in Section 4.5.2.

From Section 4.6 this chapter focuses on the extension of the new mathematical model developed to predict the Monopole measurements in lossy media environments. Vegetable oil and water are the two lossy media considered for this research. Vegetable oil and water are chosen for this investigation as they exhibit properties of low and high conductivities respectively. The results presented are validated by comparing them with simulated and experimental methods.

Section 4.7.2 details the experimental arrangement required for Monopole measurement in lossy media along with the parameters and specification required in antenna measurements. The simulation results are obtained from the FDTD simulation after changing the background material of the workspace to that of the vegetable oil ($\varepsilon_r' = 2.68$ and $\sigma = 0.019$ S/m) from freespace. In Section 4.8.2, the results are compared with the predicted and experimental results. It can be seen that the variation among the three methods is 0.05 dB in azimuth pattern and less than 2 dB at most angles in the elevation pattern

The simulation results for the water measurements are obtained after changing the background material from vegetable oil to water. In Section 4.9 the results for the Monopole in water of ε_r' 78.3 and conductivity σ of 0.176 S/m from all three methods are compared. It shows the variation among the three methods in azimuth plane is 0.05 dB and it is especially encouraging that the novel mathematical model accurately predicts the direction of maximum radiation, nulls and exact position of the side lobe in the elevation pattern. Thus the new mathematical model is used to predict the Monopole characteristics in freespace and lossy media environment and this has been validated by results from simulation and experimental procedures.

Chapter 5 Conclusions and Further Work

In this chapter, all the important findings of this research work have been merged, clearly defining the output gained as the result of the work and to show how the aims and objectives outlined in the introduction are addressed. In the second section of this chapter, a discussion is provided on the potential path for future scope of this work and the various practical applications of this proposed model are also presented.

5.1 Conclusions

The intention behind this research work was derived from the desire to help microwave engineers in the medical field to comprehend antenna characteristics in lossy media, which will enable them to develop more clinically viable systems for medical applications. More specifically, the objectives were focussed on understanding the challenges of microwave medical imaging and the theoretical basis behind the characteristics of the microwave antennas in those environments. The research began with the analysis of the patented synthetic reference beam holography technique for medical applications. Initial research on breast phantoms and animal tissues were carried out using this technique. Promising results were obtained and the need to move towards a clinically viable system was presented. During this phase of the research, the limitations of the patented technique were identified and this led to the change in direction of the focus of the initial research proposal and therefore the new aim of this research work.

The aim of this research is to develop a more efficient new model to predict antenna performance in freespace and lossy media, as the Method of Moment technique requires extensive computational time. Theoretical calculations of the antenna characteristic of a microwave antenna using the traditional approach involving Pocklington Integral Equation and Method of Moment analysis are studied. Steps involved in calculating the radiation pattern and input impedance of a microwave antenna using the above methods are explained and presented in Chapter 3. Section 3.3.2 details the limitation of this traditional approached and leads on to the need for a novel mathematical model to eliminate the computationally intensive techniques involved in these methods. A novel mathematical model to theoretically predict the characteristics of a microwave antenna is developed in Section 3.4. The adaptability of this approach to different lengths of Monopole is presented. The validation of this model is carried out by comparing the results obtained from the new mathematical model with that of a published result.

The advantages of utilizing this new mathematical model to predict antenna characteristics are two-fold. Firstly, the ability to predict the radiation pattern and input impedance of a Monopole accurately, without the need for complex mathematical processes. The Method of Moment technique involves the use of basis function to predict the antenna characteristics. The accuracy of the predicted results depends on the amount of the basis functions involved. However, as the number of basis functions increases the computational time to predict the results using this traditional method increases by N^2. This relation between the accuracy of the results and basis functions is eliminated in the new model as its accuracy does not depend of the number of basis function involved, which in turn reduces the computational time.

Secondly, the new model only depends on three parameters; the initial current I_0, α the damping coefficient and τ the wire radius parameter. This allows the new model to be easier to calculate and predict the current across the wire in comparison with the traditional approaches. This also allows the new model to be used in applications involving lossy media like medical imaging application. The dielectric constant of a lossy medium is complex in comparison to that of freespace. In the traditional method this increases the computational time from $N \times N$ to $(N \times N)^2$. However the new model only needs to adjust the damping coefficient in order to accommodate the complex dielectric constant. This makes the new model very effective in predicting the current across the wire in applications involving lossy medium. This advantage of the new model has led to the development of predicting the Monopole characteristics in different dielectric media such as vegetable oil and water.

The experimental procedure used for data collection in dielectric media, is one of the new systems developed during the course of this research work. The new system allows the measurements of antenna characteristics such as radiation patterns, input impedance and return loss. It also has provisions to measure the dielectric properties of the lossy media. Vegetable oil and water are chosen for this investigation as they exhibit properties of low and high conductivities respectively. The main aim behind the development and implementation of the novel mathematical model was to avoid complex traditional approaches in predicting antenna characteristics in various dielectric media. To validate that the proposed model and system could be used to replace the traditional approaches it was necessary to show that the same level of accuracy and information could be attained. It has been shown through analytical prediction that the two methods provide equivalent results. The comparisons provided in Chapter 4 between the radiation patterns and input

impedance attained from experimental and simulation provided confirmation of the predicted results in freespace, vegetable oil and water.

In conclusion, a novel mathematical model has been developed and its ability to predict the antenna characteristics of a Monopole has been observed. It has also been shown that from the three parameters of the new model it is possible to obtain the Monopole characteristics in lossy media surroundings. Verification of this was made by comparing the results obtained using this model with that of the traditional approaches and also with the results obtained from experimental and simulation procedures. The verification process confirmed the ability of the novel model to predict accurately the Monopole characteristics. The further development of the prediction in dielectric media increases the versatility of the new model leading to the successful culmination of the initial research aim and objectives.

5.2 Further Work

The results presented throughout this thesis and the positive conclusions they have allowed to be drawn, regarding the capabilities of this novel method, have highlighted the importance and the value of this work. The novel method and the experimental system were constructed to understand the characteristics of a single Monopole and its suitability for medical imaging applications. As a direct result of the work on understanding the characteristics of microwave antenna in lossy media using the new model, four areas have been identified as the means of future work.

The first area of further work lies in expanding the existing system to an array based model which will increase the wideband capabilities of the measurement system to be used in medical imaging. The second area involves further development and refining of the new model using interpolation techniques so that the current across the wire can be predicted for any length of wire. The third and fourth area of future work are based on adopting the new method for investigation of microwave antennas in security and subsea engineering.

5.2.1 Microwave Medical Imaging

Microwave Medical Imaging is an area of much interest to microwave engineers and medical practitioners because microwaves are a non-ionising form of radiation and pose no health risk to human tissue cells when used within reasonable power levels. Due to its relatively small wavelength they can maintain sufficient image resolution while reducing the risk of exposure to radiation when compared to X-rays. The area of early breast cancer detection is of particular interest for two reasons: firstly, the dielectric properties of a malignant tumour even in the early stages are significantly different to those of normal tissues and therefore microwave medical imaging may provide an earlier detection of such tumours[18]. Secondly the human breast is one of the most easily accessible organs of the human body. The relatively low conductivity of fatty tissues and the location of breast lesions with these regions allow microwaves to penetrate to sufficient depths to be scattered from breast lesions and be detected. Having the patient lie in prone position[5] makes the reach of the breast more accessible and makes it easier to perform tests and also this way of imaging is more comfortable for the patient than X-ray mammography.

The key aspect of this microwave medical imaging is the resolution obtained using these methods. The accuracy in imaging cell structure is important as this provides vital information to the medical practitioners to understand the shape of the tumours and thereby the necessary diagnosis. One way to improve the resolution of the microwave medical imaging system is to increase the wideband capabilities of the microwave antenna used. One way of achieving wideband characteristics is by using an adaptive antenna array system. The array system will have a row of Monopoles which will be controlled by RF switch matrix. The novel mathematical model helps to characterise a single Monopole in lossy medium. This model can be expanded to understand the characteristics of the antenna array and to see the effect of the array system on each of the Monopole characteristics.

Figure 5-1 Clinical prototype of electronically switched Monopole array system by Meaney

The array system will be electronically switched thereby increasing the time taken to perform the scan of the breast. This antenna array system will also help to overcome another challenge faced by medical practitioners involved in breast cancer detection which is locating the malignant breast tissue. Current mammogram standards require biopsy to identify the cancer cells. The wideband capabilities of this proposed system will help to present the results in 3D, so that medical practitioners can identify the location of the malignant tissue (whether it is close to chest or nipple) without the need for a biopsy. A clinical prototype of the electronically switched array based system was developed by Meaney[5]. Figure 5-1 shows the prototype model and the future work of this research will be to develop a similar system which takes into account the mutual coupling between the Monopoles used in the array system.

5.2.2 Further Development of New Model

The result section in this thesis has clearly demonstrated the ability of the new model to predict antenna characteristics in lossy media and the advantages in comparison with the traditional methods with respect to the processing time. However, in order to utilise this new model in more complex and sophisticated applications, the model needs to have the capabilities to predict the antenna characteristics irrespective of the antenna length. One area of future work can be carried out in developing the new model further. The current expression of the new model is given as

$$I(z) = I_0 e^{-\alpha z} \sin(k(l-z)) + f(z,\tau)$$

Where the final part of the expression *f (z,τ)* is given as

$$f(z,\tau) = \begin{cases} d_0 + \frac{\tau}{4}\sin\big(2k(l-z)\big)\,, & for\ l = (2w+1)\,\frac{\lambda}{4} \\ d_0 + 2\tau\sin\big(2k(l-z)\big)\,, & for\ l = 2w(\lambda/4) \end{cases}$$

In the above expression the length *l* of the Monopole antenna is taken into consideration as a multiple of wavelength *λ*. Although this assumption holds true for most applications, in order to make the model more robust and efficient it is important to develop it further so that it accounts for antenna lengths in between the multiples of *λ/2* and *λ/4*. This refinement of the new model can be performed using interpolation techniques. Also expanding the new model to incorporate the theory of mutual coupling in antenna array will be advantageous in applications requiring wideband capabilities.

5.2.3 Security Applications

Figure 5-2 shows the image obtained from microwave imaging of a covered hand gun cut-out. The image proves the ability of the Synthetic reference beam holography technique to be used in security applications[90]. The new refined model can be used to improve the microwave techniques for security applications. Although the image in Figure 5-2 can be used to show the overall structure of the gun, the image quality needs to be improved in order to achieve accurate imaging of the trigger area of the gun. Understanding the mutual

coupling between Monopoles in arrays can be used to provide wideband capabilities which can be used to obtain images of high accuracy and resolution.

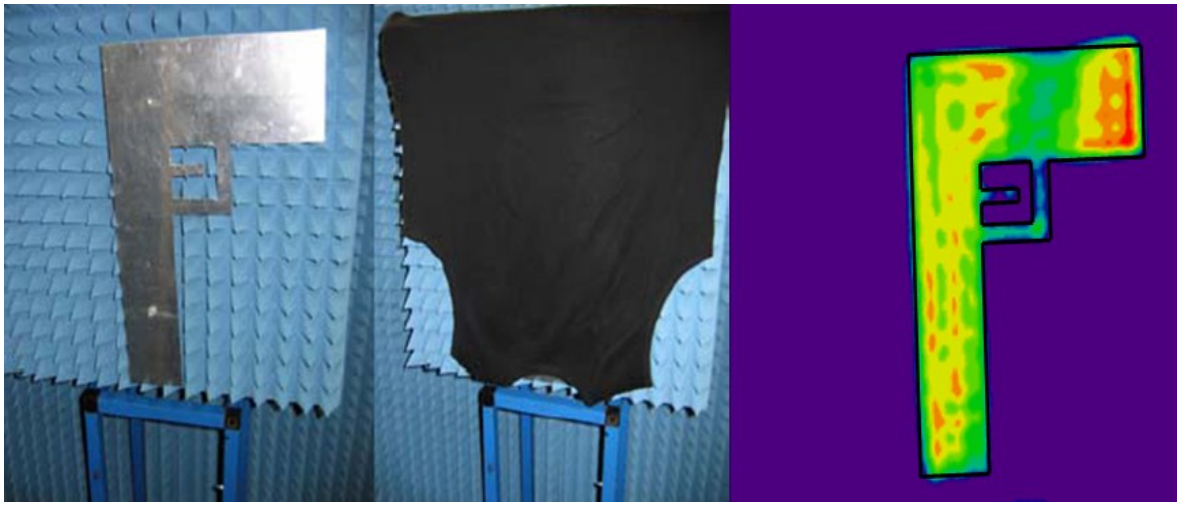

Figure 5-2 Security applications - Image of a covered Hand gun cut-out

Also the new model is not restricted to one particular microwave imaging system. In Manchester Metropolitan University, a Home Office funded research is carried out in detecting concealed weapons using Late Time Response (LTR) signature. This security imaging research is developed as an alternative to the metal detector at airports and event and conference venues. One of the key features of the LTR technique is the use of low frequency microwave antennas and their ability to effectively transmit and receive responses from concealed foreign objects. The new model outlined in this thesis together with the refinement addressed in the previous section can be extended to be used in this particular security application.

5.2.4 Subsea Engineering

Underwater communication is a rapidly growing field of applied research and engineering. The need for underwater communication exists in applications such as off-shore oil and gas industry, seismic analysis and drilling, pollution monitoring in environmental systems and communication between submarines[91-94]. Underwater communication in each of these applications involves transmitting and receiving antennas or antenna array systems. One of the lossy media used in the analysis of the new mathematical model on Monopole is water. The model predicted the antenna characteristics within water. This ability of this model could be utilised in research involving antennas in subsea engineering.

Modification to the existing model has to be made on two accounts in order to effectively use this model in subsea engineering: Firstly the frequencies of operation of most of these applications are strictly stipulated by the governing body of the respective industry. In the current setup the new mathematical model is operated between 1 and 12.5 GHz. It is essential to understand the appropriate frequency spectrum for each of these applications and to modify the new model to reflect the change in frequency; Secondly, the saline nature of the lossy media in underwater communication needs to be considered. The three different media used in this research are freespace, vegetable oil and water. On expanding the new approach to underwater communication it is essential to modify the setup to account for the saline nature of the sea water in order to effectively predict the antenna characteristics.

Appendix I: Method of Moment

The general approach to convert integral equations to a discrete matrix equation is known as Method of Moments (MOM). The specific discretization places a limit on the accuracy of a numerical result for a fixed number of basis and testing functions and determines whether or not the numerical result will converge to the exact solution as the number of basis and testing functions is increased. In order to explain the discretization process involved in MOM we introduce Inner Product Spaces[76].

Inner Product Spaces

Consider an equation of the form $Lf = g$, where L is a continuous linear operator such as the integral operators. The function f is the unknown to be determined, and g represents a known excitation. If a unique solution exists, it is given by $f = L^{-1} g$, where L^{-1} is inverse operator. In practice, we are usually not able to determine L^{-1} and resort to numerical solutions. The linear L maps functions in its domain (such as the unknown f) to functions in its range (such as the excitation g). As a general rule, the domain and range are different linear spaces.

It is convenient to introduce the notion of an inner product, which is a scalar quantity denoted ‹*a, b*› satisfying the following properties:

$$\langle a, b\rangle = \langle b, a\rangle^*$$

$$\langle \alpha a, \beta b + c\rangle = \alpha^* \beta \langle a, b\rangle + \alpha^* \langle a, c\rangle$$

$$\langle a, a\rangle > 0, if\ a \neq 0$$

$$\langle a, a\rangle = 0, if\ a = 0$$

Where *a, b*, and *c* are functions and α and β are scalars. Complex conjugation is denoted using a dagger (*). Any inner product satisfying these properties can be used to define a natural norm

$$\|a\| = \sqrt{\langle a, a \rangle}$$

And the associated metric

$$d(a, b) = \|a - b\|$$

The metric provides us with the notion of "distance" between two functions. Two functions *a* and *b* in an inner product space are said to be *orthogonal,* if

$$\langle a, b \rangle = 0$$

In a similar fashion, functions B_n in an inner product space from an orthogonal set if

$$\langle B_m, B_n \rangle = 0\,, \qquad m \neq n$$

The set B_n is said to be complete if the zero function is the only function in the inner product space orthogonal to each member of the set. A set B_n that is both complete and orthogonal is said to be a basis and can be used to represent any function *f* in the inner product space in the sense that

$$\left\| f - \sum \alpha_n B_n \right\| = 0$$

where the α_n are scalar coefficients and given as

$$\alpha_n = \frac{\langle B_n, f \rangle}{\langle B_n, B_n \rangle} \qquad \textbf{I-1}$$

In practice, we are forced to project the functions of interest onto a finite dimensional subspace of the original inner product space. In the subspace, the basis is truncated to the form $B_1, B_2, \ldots B_N$, and the representation is given by

$$f \cong f^N = \sum_{n=1}^{N} \alpha_n \beta_n \qquad \textbf{I-2}$$

The scalar coefficients $\alpha_1, \alpha_2 \ldots \alpha_N$ are selected to minimise the distance between the function f and the representation f^N. The error

$$d(f, f^N) = \|f - f^N\|$$

Is minimised when the coefficients are chosen to make the error orthogonal to the N-dimensional basis, that is

$$\langle B_n, f - f^N \rangle = 0 \, , n = 1,2 \ldots N$$

This is known as an orthogonal projection. Because of the orthogonality of the basis functions, the coefficients are the same in the subspace as in the original inner product space. Therefore, the orthogonal projection (the best representation as measured by the metric) is realised using coefficients from equation I-1

Now consider the equation $Lf = g$. The solution is represented in the N-dimensional subspace of the original domain of L, and its general form is given in equation I-2. The best approximation is obtained when the coefficients from equation I-1 are employed. Unfortunately, since f is not known, the coefficients α_n cannot be determined directly from equation I-1. On the other hand, quantities defined on the range of the linear operator L are known and might be more convenient to work with. If the set T_m forms a basis for the

range space operator L, any function in the range may be represented in the N- dimensional subspace spanned $T_1, T_2 \ldots T_N$ *according to*

$$g \cong g^N = \sum_{m=1}^{N} \beta_m T_m \qquad \textbf{I-3}$$

The projection that minimises the error d (g, g^N) employs coefficients

$$\beta_m = \frac{\langle T_m, g \rangle}{\langle T_m, T_m \rangle}$$

If g is a known function, the coefficients β_m are readily determined, in a similar fashion, the function LB_n can be represented by

$$LB_n \cong \sum_{m=1}^{N} l_{mn} T_m$$

Where the coefficients l_{mn} that minimise the error

$$\left\| LB_n - \sum_{m=1}^{N} l_{mn} T_m \right\|$$

Are given by

$$l_{mn} = \frac{\langle T_m, LB_n \rangle}{\langle T_m, T_m \rangle} \qquad \textbf{I-4}$$

The coefficients of equation I-4 achieve an orthogonal projection in the range of the operator and therefore provide the best approximation as measured by the metric. Returning to the approximate solution of the equation $Lf = g$, we represent the unknown

solution f in the form of equation I-2, where α_n are unknowns to be determined. This representation produces a function on the range space having the form

$$Lf^N \cong \sum_{n=1}^{N} \alpha_n LB_n$$

Projecting this function on the N-dimensional subspace spanned by the set $T_1, T_2 \ldots T_N$ yields

$$Lf^N \cong \sum_{n=1}^{N} \sum_{m=1}^{N} l_{mn} \alpha_n T_m$$

where the coefficients l_{mn} are obtained from equation I-4. Equating this representation for Lf^N with the representation from equation I-3 for g^N produces the discrete system of equations

$$\sum_{n=1}^{N} l_{mn} \alpha_n = \beta_m \, , m = 1,2 \ldots N \qquad \textbf{I-5}$$

This system is an $N \times N$ matrix equation that can be solved for the coefficients α_n. The preceding discussion indicated that an approximate solution of the linear equation $Lf = g$ may be obtained in the form

$$f \cong \sum_{n=1}^{N} \alpha_n B_n$$

Where the functions B_n are known as basis functions defined on the domain of L and the scalars α_n are unknown coefficients to be determined. By substituting the above expression into $Lf = g$, and a system of linear equations is obtained by forcing the residual

$$L\left(\sum_{n=1}^{N}\alpha_n B_n\right) - g = \sum_{n=1}^{N}\alpha_n LB_n - g$$

to be orthogonal to a set of testing functions $T_1, T_2 \ldots T_N$. This produces the matrix equation $\mathbf{L}\alpha = \beta$ having entries

$$l_{mn} = \langle T_m, LB_n \rangle \text{ and } \beta_m = \langle T_m, g \rangle$$

The matrix equation $\mathbf{L}\alpha = \beta$ is formally identical to equation I-5, except for the normalisation. Provided the matrix **L** is non singular, the unknown coefficients can be found using standard matrix solution algorithms. Since the system of equations is obtained by forcing the residuals to be orthogonal to the testing functions, this procedure is often given the name weighted-residual method[76]. In electromagnetics, it is also known as Method of Moments.

References

1. **Steinberg, D.B. and M.H. Subbaram, *Microwave Imaging Techniques*1991, New York: John Wiley & Sons, inc.**
2. **Kraus, J.D., *Radio Astronomy*1966, New York: McGraw - Hill Book Company.**
3. **Smith, D. and M. Leach, *3D Imaging of Antenna Fields from Electronically Synthesised Scalar Intensity Patterns.* Asia-Pacific Conference on Applied Electromagnetics, APACE 03, KL, Malaysia, Conf. Publ., 2003. 1: p. 50-53.**
4. **Brett, H., *Microwave Imaging Sensors Datasheet*, in *Roke Manor Research Limited*2006: Romsey, Hampshire.**
5. **Meaney, P.M., et al., *Initial Clinical Experience with Microwave Breast Imaging in woman with normal Mammography.* Acad Radiol: Author Manuscript PMC, 2007. 14(2): p. 207-218.**
6. **Thompson, A.R. Moran, and Swenson, *Interferometry and Synthesis in Radio Astronomy*1896, New York: Wiley & Sons, Inc.**
7. **Steinberg, D.B., *Microwave Imaging with Large Antenna Arrays: Radio Camera Principles and Techniques*1983, New York: Wiley & Sons Inc.**
8. **Ausherman, D.A., et al., *Developments in Radar Imaging.* IEEE Transaction on Aerospace Electronics System, 1984. 20(4): p. 363-398.**
9. **Fdo, M.J., et al., *A Holographic Solution for Concealed Object Detection.* The Mediterranean Journal of Computers and Networks, 2006. 2(4): p. 84-89.**
10. **Smith, D., M. Leach, and A. Sambell, *Microwave Indirect Holographic Imaging using an adaptation of Optical Techniques.* IEEE Microwave and Wireless Components Letters, 2003. 13(9): p. 379-381.**

11. **Smith, D., et al., *Indirect holographic techniques for determining antenna radiation characteristics and imaging aperture fields.* IEEE Antennas & Propagation Magazine, 2007. 37(3).**

12. **Fear, E.C., *Microwave imaging of the Breast.* Technology Cancer Research Treatment, 2005. 4: p. 69-82.**

13. **Fear, E.C., et al., *Enhancing Breast Tumor Detection with near Field Imaging.* IEEE Microwave Magazine, 2002. 2: p. 1527-1542.**

14. **Meaney, P.M., et al., *A Clinical Prototype for Active Microwave Imaging of the Breast.* IEEE Transactions on Microwave Theory and Techniques, 2000. 48(11).**

15. **Fear, E.C., P.M. Meaney, and M.A. Stuchly, *Microwaves for breast cancer detection?* IEEE Potentials, 2003: p. 12 - 18.**

16. **Meaney, P.M., K.D. Paulsen, and J. Chang, *Near-Field Microwave Imaging of Biologically based materials using a Monopole system.* IEEE Transactions on Microwave Theory and Techniques, 1998. 46(1).**

17. **Smith, D., M. Leach, and A. Sambell, *An Indirect Holographic Method for Determining Antenna Radiation Patterns and Imaging Antenna Fields.* IEEE International Symposium on Antenna and Propagation, San Antonio, Texas, 2002.**

18. **Leach, M., *A New Method for Holographic Measurements of Microwave Antenna Radiation Patterns*, in *CEIS*2006, Northumbria University: Newcastle. p. 104-110.**

19. **Leach, M., et al., *Imaging Dielectric Objects Using A Novel Synthetic Off-Axis Holographic Technique.* Microwave and Optical Technology Letters, 2006. 48(10): p. 1957 - 1961.**

20. **Elsdon, M., et al., *Microwave Imaging of Concealed Metal Objects using a Novel Indirect Hologrphic Method.* Microwave and Optical Technology Letters, 2005. 47: p. 536-537.**

21. **Smith, D., et al., *A Microwave Indirect Holographic System for Security and Medical Imaging Applications.* European Conference on Antennas and Propagation, 2006.**

22. **Elsdon, M., et al., *Early Breast Cancer Detection using Indirect Microwave Holography.* European Microwave Conference, Manchester, 2006.**

23. **Smith, D., et al., *A Method for 3D Breast Cancer Imaging using Microwave Holography.* International Symposium on Antennas and Propagation, Singapore, 2006.**

24. **Tsai, L.L., *A Numerical soultion for the Near and Far Field of an Annular Ring of Magnetic Current.* IEEE Transactions on Antennas and Propagation, 1972. AP-20(5): p. 569-576.**

25. **Sill, J.M. and E.C. Fear, *Tissue Sensing Adaptive Radar for Breast Cancer Detection - Experimental Investigation of Simple Tumor Models.* IEEE Transactions on Microwave Theory and Techniques, 2005. 53: p. 3312-3319.**

26. **Fear, E.C., et al., *Confocal Microwave Imaging for breast cancer detection: localization of tumors in three dimensions.* IEEE Transactions on Biomedical Engineering, 2002. 49(812-822).**

27. **Society, A.C., *Cancer Facts & Figures 2005, Atlanta, GA 2005*, 2005.**

28. **Brown, M., *Screening mammography in community practice.* American J. Roentgen, 1995. 165: p. 1373-1377.**

29. **Nass, S.J., C. Henderson, and J.C. Lashof, *Mammography and Beyond: Developing Technologies for the Early Detection of Breast Cancer.* Committee**

on Technologies for the Early Detection of Breast Cancer, Eds., National Cancer Policy Board, Institute of Medicine and Commission on Life Studies, National Research Council, 2001.

30. Huynh, P.T., A.M. Jarolimek, and S. Daye, *The False-Negative Mammogram.* Radiographics, 1998. 18: p. 1137-1154.

31. Fletcher, S.W. and J.G. Elmore, *Mammographic Screening for Breast Cancer.* New England Journal of Medicine, 2003. 37: p. 1672 - 1680.

32. Nilavalan, R., et al., *Numerical Investigation of Breast Tumour Detection using multi static radar.* IEE Electronics Letters, 2003. 39(25).

33. Mehta, T.S., *Current Uses of Ultrasound in the evaluation of the Breast.* Radiologic Clinics of North America, 2003. 41: p. 841-856.

34. Joy et al., J.E., *Saving Women's Lives:Strategies for Improving Breast Cancer Detection and Diagnosis.* Committee on New Appraoches to Early Detection and Diagnosis of Breast Cancer, Institute of Medicince and National Research Council, 2004.

35. Kinkel, K. and N.M. Hylton, *Challenges to Intrepretation of Breast.* MR. JMR, 2001. 13: p. 821-829.

36. Bocquet, B., et al., *Microwave Radiametric Imaging at 3 GHz for the Exploration of Breast Tumors.* IEEE Transactions on Microwave Theory and Techniques, 1990. 38: p. 791-793.

37. Carr, K.L., *Microwave Radiometry: its Importance to the detection of cancer.* IEEE Transactions on Microwave Theory and Techniques, 1989. 37: p. 1862-1869.

38. **Carr, K.L., et al., *Radiometric sensing: An adjuvant to Mammography to determine breast biospy.* IEEE International Symposium on MTT, Dig. , 2000. 2: p. 929-932.**

39. **Mouty, S., et al., *Microwave Radiometric Imaging for the characterisation of breast tumors.* European Physics Journal: Applied Physics, 2000. 10: p. 73-78.**

40. **Kruger, R.A., et al., *Thermoacoustic CT with radio waves: A Medical Imaging Paradigm.* Radiology, 1999. 211: p. 275-278.**

41. **Kruger, R.A., et al., *Thermoacoustic computed tomography of the breast at 434 MHz.* IEEE International Symposium on MTT, Dig., 1999. 2: p. 591-594.**

42. **Wang, L.V., et al., *Microwave Induced acoustic imaging of biological tissue.* Rev.Sci. Instrum., 1999. 70: p. 3744-3748.**

43. **Ku, G. and L.V. Wang, *Scanning Thermoacoustic tomography in biological tissues.* Medical Physics, 2000. 27: p. 1195-1202.**

44. **Smith, D., et al., *Medical Imaging using a Microwave Indirect Holographic Technique.* Mediterranean Microwave Symposium (MMS), Genova, Italy, 2006(w).**

45. **Hagness, S.C., A. Taflove, and J.E. Bridges, *Two dimensional FDTD analysis of pulsed microwave confocal system for breast cancer detection: fixed focus and antenna- array sensors.* IEEE Transactions on Biomedical Engineering, 1998. 45: p. 1470-1479.**

46. **Davis, S.K., et al., *Microwave Imaging via Space-Time Beamforming for Early Detection of Breast Cancer: Beamformer design in the Frequency Domain.* Journal of Electromagnectic Waves and Appl., 2003. 17(2): p. 357-381.**

47. **Hagness, S.C., A. Taflove, and J.E. Bridges, *Three Dimensional FDTD analysis of Pulsed microwave confocal system for breast cancer detection: design of an***

antenna array element. **IEEE Transactions on Antennas and Propagation, 1999. 45: p. 783-791.**

48. Fear, E.C. and J.M. Sill, *Preliminary Investigations of Tissue Sensing Adaptive Radar for Breast Tumor Detection.* Proceedings of the 25th Annual Meeting of the IEEE Engineering in Medicine and Biology Society, 2003: p. 3787 - 3790.

49. Smith, D., et al., *Imaging of dielectric objects from phase patterns reconstructed using indirect holographic intensity patterns.* 9th International Conference on Electromagnetics in Advanced Applications ICEAA 2005, 2005: p. 401-404.

50. Li, X., et al., *Microwave Imaging via Space-Time Beamforming: Experimental Investigation of Tumor Detection in Multilayer Breast Phantoms.* IEEE Transactions on Microwave Theory and Techniques, 2004. 52(8): p. 1856 - 1865.

51. Elsdon, M., et al., *Microwave Holographic Imaging of Breast Cancer.* IEEE International Symposium on Microwave, Antenna, Propagation and EMC Technologies for Wireless Communications, 2007.

52. Meaney, P.M., et al., *An Active Microwave Imaging system of reconstruction of 2-D electrical property distributions.* IEEE Transactions on Biomedical Engineering, 1995. 42: p. 1017-1026.

53. Jofre, L., et al., *Medical Imaging with a microwave tomographic scanner.* IEEE Transactions on Biomedical Engineering, 1990. 37: p. 303-312.

54. Bolomey, J.C., *Recent European developments in active microwave imaging for industrical, scientific and medical applicaitons.* IEEE Transactions on Microwave Theory and Techniques, 1989. 37: p. 2109-2117.

55. Agrawall, N.P., K. Girish, and K.P. Ray, *Wide-Band Planar Monopole Antennas.* IEEE Transactions on Antennas and Propagation, 1998. 46(2).

56. **Liang, J., et al., *Printed circular disc Monopole antenna for ultra-wideband applications.* IEE Electronics Letters, 2004. 40: p. 1246-1247.**

57. **Chen, Z.N., K. Hirasawa, and K. Wu, *A Novel Top Sleeve Monopole in Two Parallel Plates.* IEEE Transactions on Antennas and Propagation, 2001. 49(3): p. 438-443.**

58. **Antonino-Daviu, E., et al., *Wideband Double-Fed Planar Monopole antennas.* IEE Electronics Letters, 2003. 39(23): p. 1635-1636.**

59. **Chen, Z.N., M.Y.W. Chia, and M.J. Ammann, *Optimization and Comparison of Broadband Monopoles.* IEE Proceeding Microwave Antennas Propagation, 2003. 150(6): p. 429-435.**

60. **Bindu, G., et al., *Wideband Bow-tie antenna with Coplanar Stripline Feed.* Microwave and Optical Technology Letters, 2004. 42(3).**

61. **Bindu, G., et al., *Active Microwave Imaging For Breast Cancer Detection.* Progress in Electromagnetics Research 2006. 58: p. 149-169.**

62. **Gibson, P.J., *The Vivaldi Aerial.* 9th European Microwave Conference, Brighton, 1979: p. 101 - 105.**

63. **Langley, J.D.S., P.S. Hall, and P. Newham, *Balanced Antipodal Vivaldi Antenna for wide bandwidth phased arrays.* IEE Proceeding Microwave Antennas Propagation, 1996. 143(2).**

64. **Abbosh, A.M., H.K. Kan, and M.E. Bialkowski, *Design of Compact Ultra Wideband Antipodal Antenna.* Microwave and Optical Technology Letters, 2006. 48(12).**

65. **Walton, K.L. and V.C. Sundberg, *Broadband Ridged Horn Design.* Microwave Journal, 1964: p. 96-101.**

66. **Notras, B.M., C.D. McCarrick, and D.P. Kasilingam, *Two Numerical techniques for analysis of Pyramidal Horn antenna with continous metallic ridges.* Proceedings of IEEE International Symposium Antenna Propagation, Dig., 2001. 2: p. 560-563.**

67. **Rosenbury, E.T., et al., *Low cost compatible wideband antenna*, U.S., Editor 2002: U.S.**

68. **Li, X., et al., *Numerical and Experimental Investigation of an Ultrawideband Ridged Pyramidal Horn Antenna with Curved lauching Plane for Pulse radiation.* IEEE Antennas and Wireless Propagation Letters, 2003. 2.**

69. **Allen, O.E., D.A. Hill, and A.R. Ondrejka, *Time- domain antenna characterization.* IEEE Transactions on Electromagnectic Compatability, 1993. 35: p. 339-345.**

70. **Otto, D.V., *The Admittance of Cylindrical Antennas Driven From a Coaxial Line.* Radio Science, 1967. 2(9): p. 1031 - 1042.**

71. **Balanis, C.A., *Antenna Theory: Analysis and Design Second Edition*1997, New York: John Wiley&Sons, Inc.**

72. **Kraus, J.D., *Electromagnetics*. Fourth ed1991, New York: McGraw-Hill, Inc.**

73. **Burgess, R.E., *Aerial Characteristics.* Wireless Engineering, 1944. 21: p. 154-160.**

74. **Thiele, G.A., *Wire Antennas*, in *Computer Techniques for Electromagnetics*, M. R, Editor 1973, Pergamon: NewYork. p. Chapter 2 p:7-70.**

75. **Lilly, J.D., *Application of the Moment Method to Antenna Analysis*, in *Department of Electrical Engineering*1980, West Virginia University.**

76. **Peterson, A.F., S.L. Ray, and R. Mittra, *Computational Methods for Electromagnetics*1998, Oxford: Oxford University Press.**

77. **Foti, S.J., et al., *A Water-Immersed Microwave Phased Array System for Interrogation of Biological Targets*. Medical Applications of Microwave Imaging, ed. L.E. Larsen and J.H. Jacobi1986, New York: IEEE Press. 148-166.**

78. **Tsai, L.L., *Analysis and Measurement of a dipole antenna mounted symmetrically on a conducting sphere or cylinder*, in *Dept. of Electrical Engineering*1970, Ohio State University: Columbus.**

79. **HP, *S-Parameters Circuit Analysis and Design*, in *Application Note An-95*1968.**

80. **Johnson, R.C., H.A. Ecker, and J.S. Hollis, *Determination of Far-Field Antenna Patterns From Near-Field Measurements.* Proceedings of the IEEE, 1973. 61(12): p. 1668-1692.**

81. ***IEEE Standard Test Procedures For Antennas*1979, New York: IEEE Inc., Wiley.**

82. **Gillette, M.R. and P.R. Wu, *RF Anechoic Chamber Design Using Ray Tracing.* International IEEE/Antenna Propagation Symposium Digest, June 1977: p. 246-252.**

83. **Yee, K.S., *Numerical Solution of Initial Boundary Value Problems Involving Maxwell's Equations in Isotropic Media.* IEEE Transactions on Antennas and Propagation, May 1966. Ap -14(No 3): p. 302-307.**

84. **Taflove, A. and S. Hagness, *Computational Electrodynamics: The Finite-Difference Time-Domain Method*. 3rd ed2005: Artech House Publishing.**

85. **Taflove, A., *Application of the Finite-Difference Time-Domain method to steady state electromagnetic penetration problems.* IEEE Transactions on Electromagnetic Compatability, 1980. 22: p. 191-202.**

86. **Vector Fields, L., *Concerto User Guide*, C.G. Company, Editor 2005: Oxford.**

87. **Berenger, J.P., *A Perfectly Matched Layer for the Absorption of Electromagnetics Waves.* Journal Computational Physics, October 1994. 114: p. 185 - 200.**

88. **Andrew, W.V., C.A. Balanis, and P.A. Tirkas, *A Comparison of the Berenger Perfectly Matched Layer and the Lindman Higher-Order ABC's for the FDTD Method.* IEEE Microwave and Guided Wave Letters, June 1995. 5(No 6): p. 192 - 194.**

89. **Moore, K.R., *Effects of a Surrounding Conducting Medium on Antenna Analysis.* IEEE Transactions on Antennas and Propagation, 1963: p. 216-225.**

90. **Leach, M., et al., *A Modified Holographic Technique for Antenna Measurements and Object Imaging.* Proceedings ISAP 2007, Niigata, Japan, 2007.**

91. **Hyatt, J.L., *Ship-shore communications for the off-shore oil industry.* Radio and Electronic Engineer, 1980. 50(8): p. 381-389.**

92. **Monin, A., *Submarine floating antenna model for LORAN-C signal processing.* Aerospace and Electronic Systems, IEEE Transactions on, 2003. 39(4): p. 1304-1315.**

93. **Kurano, S., T. Ishiwata, and N. Konishi. *The study of the float buoy ranging system for the underwater vehicle*. in *Underwater Technology, 2000. UT 00. Proceedings of the 2000 International Symposium on*. 2000.**

94. **Bayoumi, M.A. *Wireless sensors networks infrastructure for Oil Industry*. in *International Conference on Advanced Technologies for Communications (ATC), 2010*. 2010.**